

Article

Discovery and functional interrogation of SARS-CoV-2 RNA-host protein interactions 文章 SARS-CoV-2 RNA-宿主蛋白相互作用的发现和功能研究

Ryan A.Flynn^{1, 12, 13, 14, 15}✉  Ryan A.Flynn¹¹²¹³¹⁴¹⁵ ... Julia A.Belk^{2, 3, 12} 朱莉娅 A.Belk²³¹² ... YanyanQi³ 燕燕七号 ... YukiYasumoto⁴ YukiYasumoto⁴ ... JinWei^{5, 6} 金威⁵⁶ ... Mia MadelAlfajaro^{5, 6} 米娅·马德尔阿尔法哈罗⁵⁶ ... QuanmingShi⁷ 全名十 ... Maxwell R.Mumbach⁷ 麦克斯韦·R·蒙巴赫⁷ ... AditiLimaye³ AditiLimaye³ ... Peter C.DeWeirdt⁸ 彼得·C·德威特⁸ ... Cameron O.Schmitz^{5, 6} 卡梅伦 O.施密茨⁵⁶ ... Kevin R.Parker⁷ 凯文·R·帕克⁷ ... ElizabethWoo⁹ 伊丽莎白·伍⁹ ... Howard Y.Chang^{7, 10} 霍华德Y.Chang⁷¹⁰ ... Tamas L.Horvath⁴ 塔马斯·L·霍瓦斯⁴ ... Jan E.Carette¹¹ Jan E.Carette¹¹ ... Carolyn R.Bertozzi^{1, 10} 卡罗琳·R·伯托齐¹¹⁰ ... Craig B.Wilen^{5, 6}✉ 克雷格 B.Wilen⁵⁶ ... Ansuman T.Satpathy³✉ 安苏曼T.Satpathy³

<https://doi.org/10.1016/j.cell.2021.03.012> <https://doi.org/10.1016/j.cell.2021.03.012>

Under a Creative Commons license 执照

[open access](#) [Get rights and content](#) 获取权利和内容

Referred to by Emmanuelle V. LeBlanc, Che C. Colpitts

[SARS-CoV-2 RNA: Exclusive friends and common foes SARS-CoV-2 RNA : 唯一的朋友和共同...](#)

Cell, Volume 184, Issue 9, 29 April 2021, Pages 2276-2278

Highlights 强调

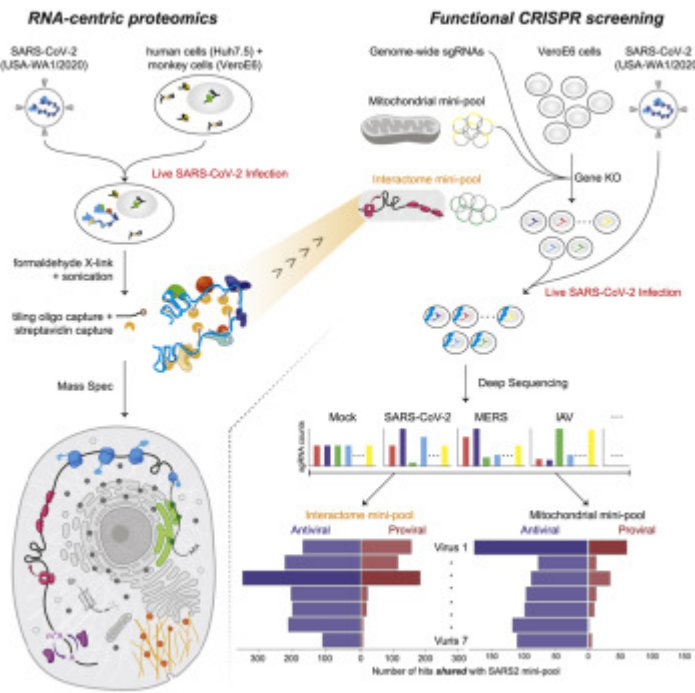
- ChIRP-MS of SARS-CoV-2 RNA identifies viral RNA-host protein interaction networks
- Comparative analysis identifies SARS-specific and multi-viral RNA-protein complexes
- SARS-CoV-2 interactome-focused CRISPR screens reveal a broad antiviral response
- Host mitochondria serve as a general organelle platform for anti-SARS-CoV-2 immunity
- SARS-CoV-2 RNA的ChIRP-MS识别病毒RNA-宿主蛋白相互作用网络 • 比较分析确定了 SARS 特异性和多病毒 RNA-蛋白质复合物 • 以 SARS-CoV-2 相互

Summary 概括

SARS-CoV-2 is the cause of a pandemic with growing global mortality. Using comprehensive identification of RNA-binding proteins by mass spectrometry (ChIRP-MS), we identified 309 host proteins that bind the SARS-CoV-2 RNA during active infection. Integration of this data with ChIRP-MS data from three other RNA viruses defined viral specificity of RNA-host protein interactions. Targeted CRISPR screens revealed that the majority of functional RNA-binding proteins protect the host from virus-induced cell death, and comparative CRISPR screens across seven RNA viruses revealed shared and SARS-specific antiviral factors. Finally, by combining the RNA-centric approach and functional CRISPR screens, we demonstrated a physical and functional connection between SARS-CoV-2 and mitochondria, highlighting this organelle as a general platform for antiviral activity. Altogether, these data provide a comprehensive catalog of functional SARS-CoV-2 RNA-host protein interactions, which may inform studies to understand the host-virus interface and nominate host pathways that could be targeted for therapeutic benefit.

SARS-CoV-2 是导致全球死亡率不断上升的大流行病的原因。使用质谱法 (ChIRP-MS) 对 RNA 结合蛋白的综合鉴定，我们鉴定了 309 种在活动感染期间结合 SARS-CoV-2 RNA 的宿主蛋白。将此数据与来自其他三种 RNA 病毒的 ChIRP-MS 数据整合，定义了 RNA-宿主蛋白相互作用的病毒特异性。靶向 CRISPR 筛选显示，大多数功能性 RNA 结合蛋白保护宿主免受病毒诱导的细胞死亡，7 种 RNA 病毒的比较 CRISPR 筛选显示了共享的和 SARS 特异性抗病毒因子。最后，通过结合以 RNA 为中心的方法和功能性 CRISPR 筛选，我们证明了 SARS-CoV-2 和线粒体之间的物理和功能联系，突出了该细胞器作为抗病毒活性的通用平台。总而言之，这些数据提供了功能性 SARS-CoV-2 RNA-宿主蛋白相互作用的综合目录，这可以为研究提供信息，以了解宿主-病毒界面并指定可以针对治疗益处的宿主途径。

Graphical abstract 图形概要



[Download](#) : [Download high-res image \(195KB\)](#)

[Download](#) : [Download full-size image](#)

下载 : [下载高分辨率图片 \(195KB\)](#) 下载 : [下载全尺寸图片](#)



[Previous article in issue](#) [上一篇文章](#)



[Next article in issue](#) [下一篇文章](#)

Keywords 关键词

ChIRP-MSSARS-CoV-2host-pathogen interactionsRNA virusCRISPRRNA-binding proteinsmitochondria

Introduction 介绍

Despite similarities in replication strategies of their compact genomes, positive single-stranded RNA (ssRNA) viruses cause a remarkable variety of human diseases. Mosquito-borne flaviviruses such as dengue virus and Zika virus cause systemic disease, while human coronaviruses generally cause respiratory symptoms ([Ahlquist, 2006](#); [Carrasco-Hernandez et al., 2017](#)). The recent pandemic emergence of the novel coronavirus severe acute respiratory syndrome coronavirus 2 (SARS-CoV-2), which can cause potentially fatal coronavirus disease 2019 (COVID-19), illustrates the threat to public health posed by RNA viruses. Less than 1 year into the outbreak, more than 103 million people have been infected by SARS-CoV-2, and 2.3 million people have died. The severity of the virus

has caused global economic disruption, and treatment options remain limited, in part due to an incomplete understanding of the molecular determinants of viral pathogenesis.

尽管它们的紧凑基因组的复制策略相似，但阳性单链 RNA (ssRNA) 病毒会导致多种人类疾病。登革热病毒和寨卡病毒等蚊媒黄病毒会引起全身性疾病，而人类冠状病毒通常会引起呼吸道症状 (Ahlquist, 2006 年；Carrasco-Hernandez 等人, 2017 年)。最近出现的新型冠状病毒严重急性呼吸系统综合症冠状病毒 2 (SARS-CoV-2) 可导致潜在的致命冠状病毒病 2019 (COVID-19)，这说明 RNA 病毒对公共健康构成威胁。爆发不到一年，就有超过 1.03 亿人感染了 SARS-CoV-2，230 万人死亡。该病毒的严重性已导致全球经济中断，治疗选择仍然有限，部分原因是对病毒发病机制的分子决定因素的了解不完全。

The process of infecting a host cell is complex, multistep, and often highly virus-specific. Viruses must bind and enter host cells, and once inside the cell, their genetic material leverages and remodels cellular pathways to express, replicate, and produce new infectious virions. RNA viruses deposit large autonomous RNA transcripts into the dense intracellular milieu of the host cells, which eventually generate virally encoded protein products. Together, these RNA and protein species remodel the cell to facilitate the viral life cycle. We and others have demonstrated the utility of functionally exploring how different virally derived molecules hijack the host, in particular in the context of flaviviruses (Li et al., 2020). For example, mapping physical associations between the host and virus at the level of protein-protein interactions (PPIs) have defined key pathways relevant to infection (Eckhardt et al., 2020). In parallel to efforts that focus on viral proteins, a number of groups have taken an RNA-centric view of the host-viral interface to understand how host cells recognize and respond to the RNA genome (Kim et al., 2020a; Lenarcic et al., 2013; Ooi et al., 2019; Phillips et al., 2016; Viktorovskaya et al., 2016). Finally, genetic screening efforts provide another strategy to discover cellular proteins and pathways that are essential for viral replication or that are part of the host innate immune responses (Puschnik et al., 2017; Schoggins and Rice, 2011).

感染宿主细胞的过程是复杂的、多步骤的，并且通常具有高度的病毒特异性。病毒必须结合并进入宿主细胞，一旦进入细胞，它们的遗传物质就会利用和重塑细胞通路来表达、复制和产生新的感染性病毒粒子。RNA 病毒将大型自主 RNA 转录物沉积到宿主细胞的密集细胞内环境中，最终产生病毒编码的蛋白质产物。这些 RNA 和蛋白质种类一起重塑细胞以促进病毒生命周期。我们和其他人已经证明了在功能上探索不同病毒衍生分子如何劫持宿主的效用，特别是在黄病毒的背景下 (Li 等, 2020)。例如，在蛋白质-蛋白质相互作用 (PPI) 水平上绘制宿主和病毒之间的物理关联已经定义了与感染相关的关键途径 (Eckhardt 等, 2020)。与专注于病毒蛋白的工作并行，许多研究小组对宿主 - 病毒界面采取了以 RNA 为中心的观点，以了解宿主细胞如何识别和响应 RNA 基因组 (Kim 等人, 2020a；Lenarcic 等人, 2013；Ooi 等人, 2019 年；Phillips 等人, 2016 年；Viktorovskaya 等人, 2016 年)。最后，基因筛选工作提供了另一种策略来发现病毒复制

所必需的或宿主先天免疫反应的一部分的细胞蛋白和途径 (Puschnik 等 , 2017 ; Schoggins 和 Rice , 2011) 。

While there has been significant past work to understand coronaviruses (Cockrell et al., 2018; Gralinski and Baric, 2015), the emergence of novel strains that are highly transmissible and cause severe disease in humans has underscored the need for further study (Menachery et al., 2015). Recent studies have described SARS-CoV-2-encoded proteins (Kim et al., 2020b) and how these proteins associate with host protein factors (Gordon et al., 2020) or host RNA transcripts (Banerjee et al., 2020); however, there is a gap in understanding the precise host interactions of the SARS-CoV-2 viral RNA (vRNA). To address this gap, we used comprehensive identification of RNA-binding proteins by mass spectrometry (ChIRP-MS), which provides a comprehensive view of the host interactions of vRNAs (Chu et al., 2015). This strategy provided an opportunity to define the shared and SARS-CoV-2-specific host pathways that associate with vRNAs. We combined the RNA-centric approach with genome-wide and focused mini-pool genetic perturbations, which demonstrated that the majority of functional SARS-CoV-2 RNA-binding factors protect the host from virus-induced cell death. Finally, we discovered a physical and functional interaction between SARS-CoV-2 and host mitochondria, particularly as a subcellular platform for antiviral host proteins.

虽然过去在了解冠状病毒方面已经开展了大量工作 (Cockrell 等人 , 2018 年 ; Gralinski 和 Baric , 2015 年) , 但高度传播并导致人类严重疾病的新型毒株的出现强调了进一步研究的必要性 (Menachery 等人 , 2015 年) 。等 , 2015) 。最近的研究描述了 SARS-CoV-2 编码的蛋白质 (Kim 等人 , 2020b) 以及这些蛋白质如何与宿主蛋白因子 (Gordon 等人 , 2020 年) 或宿主 RNA 转录物 (Banerjee 等人 , 2020 年) 相关联 ; 然而 , 在理解 SARS-CoV-2 病毒 RNA (vRNA) 的精确宿主相互作用方面存在差距。为了解决这一差距 , 我们使用质谱法 (ChIRP-MS) 对 RNA 结合蛋白进行了全面鉴定 , 这提供了 vRNA 的宿主相互作用的全面视图 (Chu 等 , 2015) 。该策略为定义与 vRNA 相关的共享和 SARS-CoV-2 特异性宿主途径提供了机会。我们将以 RNA 为中心的方法与全基因组和集中的迷你池遗传扰动相结合 , 这表明大多数功能性 SARS-CoV-2 RNA 结合因子可以保护宿主免受病毒诱导的细胞死亡。最后 , 我们发现了 SARS-CoV-2 与宿主线粒体之间的物理和功能相互作用 , 特别是作为抗病毒宿主蛋白的亚细胞平台。

所以 , 文章的目的 , 就是想研究 病毒的RNA , 是在宿主细胞里面如何产生作用的 ?

Results 结果

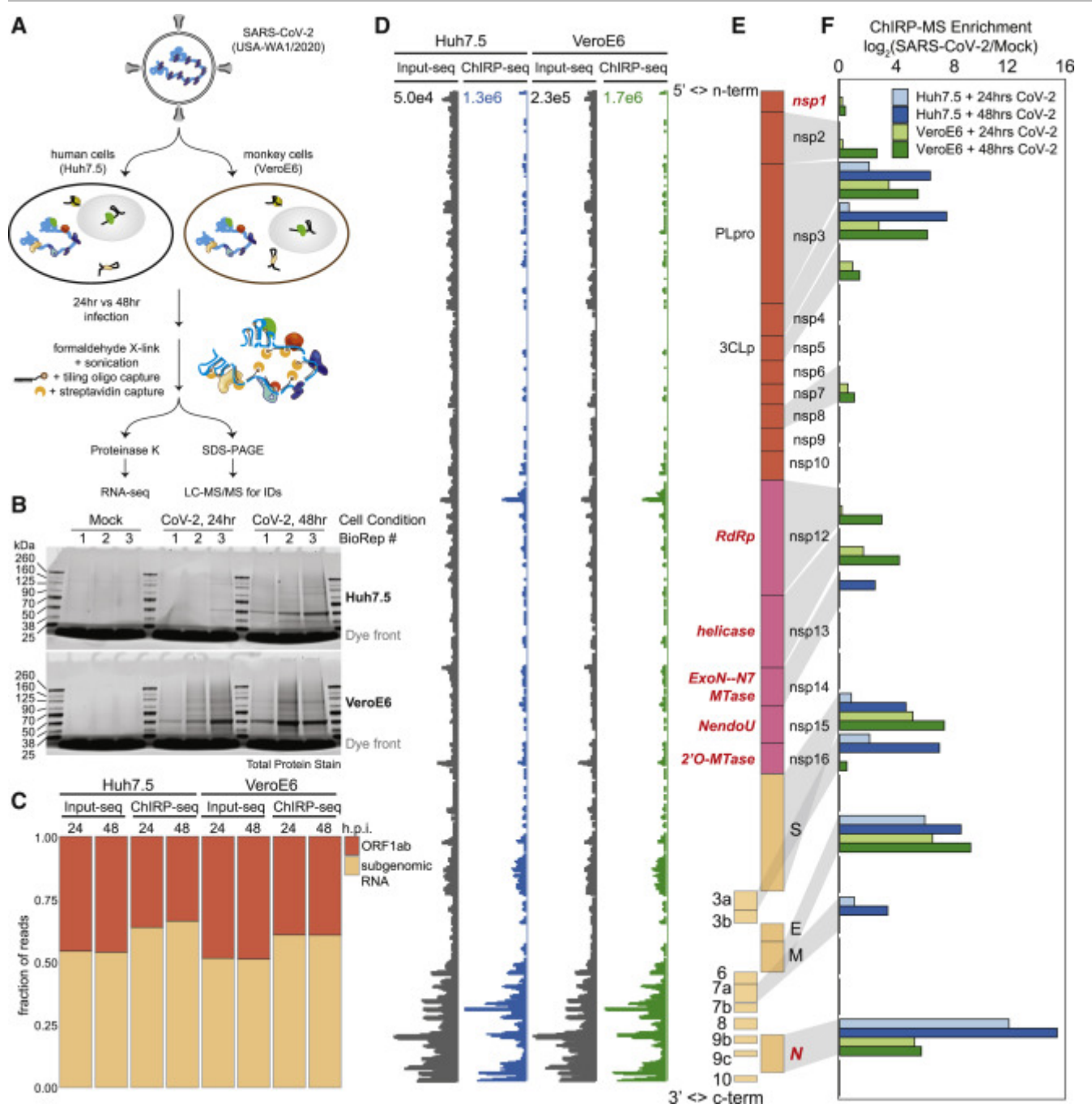
ChIRP-MS of SARS-CoV-2 viral RNA in infected mammalian cells 受感染哺乳动物细胞中 SARS-CoV-2 病毒 RNA 的 ChIRP-MS

To define the host protein interactome of the ~30kb SARS-CoV-2 RNA, we performed ChIRP-MS (Figure 1A). ChIRP-MS is advantageous as a discovery tool because it uses formaldehyde as a crosslinking agent to recover entire protein complexes associated

with cellular RNAs (Chu and Chang, 2018; Chu et al., 2015). We selected two cell lines: Huh7.5, a human hepatocyte cell line that is naturally susceptible to productive infection by SARS-CoV-2, and Vero E6, a monkey kidney cell line that dominates the research space for preparation and propagation of SARS-CoV-2 and other viruses (Harcourt et al., 2020; Zhou et al., 2020). We tiled 108 biotinylated oligonucleotide probes (Table S1) to capture the full-length positive-strand vRNA, which includes subgenomic RNA species that accumulate to higher copy numbers during infection (Kim et al., 2020b). We performed ChIRP-MS experiments at two different time points, 24 and 48 h post infection (h.p.i.), to (1) comprehensively identify all vRNA-binding factors and (2) understand the temporal association of host factors with the vRNA (Figure 1A). From each condition, input and ChIRP-enriched RNA and protein samples were collected for analysis (Figure 1A). Analysis of enriched ChIRP protein samples showed that mock samples had little protein staining, while we observed an infection- and time-dependent increase in total protein recovered after infection of either cell line with SARS-CoV-2 (Figure 1B). The band present in all infected samples at ~50 kDa is consistent with the viral nucleocapsid (N) protein (Figure 1B; Chang et al., 2014). We assessed the technical quality of the ChIRP by analyzing the viral and host RNAs recovered. RNA sequencing from mock samples resulted in negligible mapping to the SARS-CoV-2 genome before or after pull-down, as expected (Figure S1A). In contrast, in SARS-CoV-2 infected cells, we observed 2.7% (Huh7.5, 48 h.p.i.) and 14.4% (Vero E6, 48 h.p.i.) of all reads in total RNA mapping to the viral genomic RNA, which increased to 60% (Huh7.5, 48 h.p.i.) and 68% (Vero E6 48 h.p.i.) after pull-down, demonstrating robust enrichment of vRNA after ChIRP (Figure S1A). Since coronaviruses produce full-length as well as subgenomic RNAs, we next assessed whether ChIRP-MS was biased for the higher molar copy subgenomic RNAs. ChIRP enrichment showed robust coverage of the ORF1a/b region as well as of the subgenomic RNA regions, which was visually and quantitatively similar to the input coverage across Huh7.5 and Vero E6 (Figures 1C–1E). Together these protein- and RNA-level quality controls demonstrate the robust sampling of the entire SARS-CoV-2 positive-strand RNA by the designed ChIRP-MS probes.

为了定义~30kb SARS-CoV-2 RNA 的宿主蛋白相互作用组，我们进行了 ChIRP-MS (图 1A)。ChIRP-MS 作为一种发现工具具有优势，因为它使用甲醛作为交联剂来回收与细胞 RNA 相关的完整蛋白质复合物 (Chu 和 Chang, 2018 年；Chu 等人, 2015 年)。我们选择了两种细胞系：Huh7.5，一种天然易受 SARS-CoV-2 生产性感染的人肝细胞系，以及 Vero E6，一种猴肾细胞系，在制备和传播 SARS 的研究空间中占主导地位。CoV-2 和其他病毒 (Harcourt 等人, 2020 年；Zhou 等人, 2020 年)。我们平铺了 108 个生物素化寡核苷酸探针 (表 S1) 以捕获全长正链 vRNA，其中包括在感染期间积累到更高拷贝数的亚基因组 RNA 种类 (Kim 等人, 2020b)。我们在感染后 24 小时和 48 小时 (hpi) 两个不同时间点进行了 ChIRP-MS 实验，以 (1) 全面识别所有 vRNA 结合因子和 (2) 了解宿主因子与 vRNA 的时间关联 (图 1A)。从每个条件中，收集输入和富含 ChIRP 的 RNA 和蛋白质样品进行分析 (图 1A)。对富集的 ChIRP 蛋白样本的分析表明，模拟样

本几乎没有蛋白染色，而我们观察到在感染 SARS-CoV-2 任一细胞系后恢复的总蛋白呈感染和时间依赖性增加（图 1B）。所有感染样本中存在的约 50 kDa 条带与病毒核衣壳（N）蛋白一致（图 1B；Chang 等人，2014）。我们通过分析回收的病毒和宿主 RNA 来评估 ChIRP 的技术质量。正如预期的那样，来自模拟样本的 RNA 测序导致在下拉之前或之后与 SARS-CoV-2 基因组的映射可以忽略不计（图 S1A）。相比之下，在 SARS-CoV-2 感染的细胞中，我们观察到 2.7% (Huh7.5, 48 hpi) 和 14.4% (Vero E6, 48 hpi) 的总 RNA 映射到病毒基因组 RNA，增加到下拉后 60% (Huh7.5, 48 hpi) 和 68% (Vero E6 48 hpi)，表明 ChIRP 后 vRNA 的富集（图 S1A）。由于冠状病毒产生全长以及亚基因组 RNA，我们接下来评估了 ChIRP-MS 是否偏向于更高摩尔拷贝的亚基因组 RNA。ChIRP 富集显示 ORF1a/b 区域以及亚基因组 RNA 区域的强大覆盖，这在视觉上和数量上与 Huh7.5 和 Vero E6 的输入覆盖率相似（图 1C-1E）。这些蛋白质和 RNA 水平的质量控制共同证明了设计的 ChIRP-MS 探针对整个 SARS-CoV-2 正链 RNA 的可靠采样。



[Download : Download high-res image \(906KB\)](#) 下载 : 下载高分辨率图像 (906KB)

[Download : Download full-size image](#) 下载 : 下载全尺寸图片

Figure 1. ChIRP-MS identifies host and viral proteins associated with the SARS-CoV-2 RNA genome in infected cells

图 1. ChIRP-MS 识别受感染细胞中与 SARS-CoV-2 RNA 基因组相关的宿主和病毒蛋白

(A) Schematic of the ChIRP-MS protocol.

(A) ChIRP-MS 协议的示意图。

(B) SDS-PAGE analysis of total protein samples enriched using SARS-CoV-2 targeting biotinylated oligonucleotides from mock (uninfected) cells or cells infected for 24 or 48 h with SARS-CoV-2.

(B) 使用 SARS-CoV-2 靶向来自模拟 (未感染) 细胞或用 SARS-CoV-2 感染 24 或 48 小时的细胞的生物素化寡核苷酸富集的总蛋白样品的 SDS-PAGE 分析。

(C) Quantification of the percentage of reads mapping to SARS-CoV-2 gRNA (ORF1a/b) versus the subgenomic RNA before and after pull-down.

(C) 量化映射到 SARS-CoV-2 gRNA (ORF1a/b) 的读数与下拉前后的亚基因组 RNA 的百分比。

(D) RNA-seq coverage of the SARS-CoV-2 genome before and after pull-down.

(D) 下拉前后 SARS-CoV-2 基因组的 RNA-seq 覆盖率。

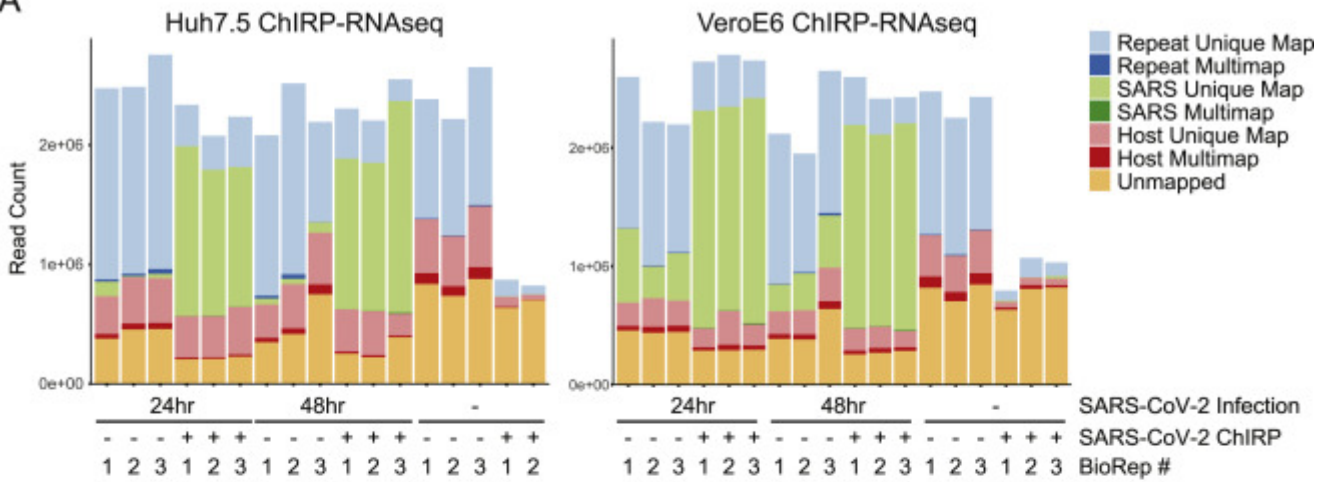
(E) Structure of the SARS-CoV-2 genome.

(E) SARS-CoV-2 基因组的结构。

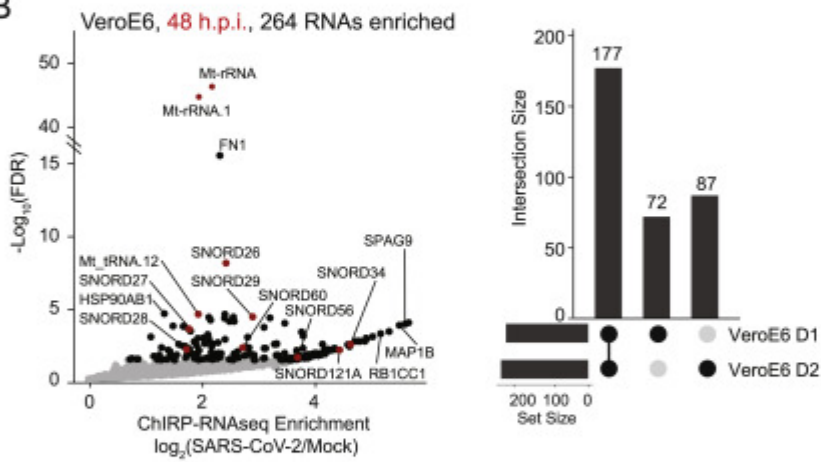
(F) ChIRP-MS enrichment of each viral protein in Huh7.5 and Vero E6 cells at the indicated time points.

(F) 在指定时间点 Huh7.5 和 Vero E6 细胞中每种病毒蛋白的 ChIRP-MS 富集。

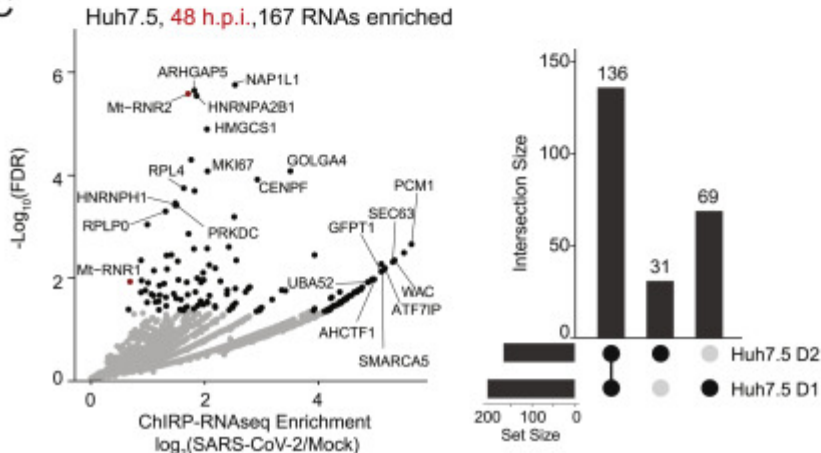
A



B



C



Download : Download high-res image (756KB) 下载 : 下载高分辨率图像 (756KB)

Download : Download full-size image 下载 : 下载全尺寸图片

Figure S1. SARS-CoV-2 ChIRP-RNA-seq in Huh7.5 and Vero E6 cells, related to Figure 1
图 S1。Huh7.5 和 Vero E6 细胞中的 SARS-CoV-2 ChIRP-RNA-seq，与图 1 相关

(A) Host and viral RNA-seq alignment statistics for all samples across Huh7.5 (left) and VeroE6 (right) cell lines.

(A) Huh7.5 (左) 和 VeroE6 (右) 细胞系中所有样本的宿主和病毒 RNA-seq 比对统计数据。

(B) Enriched host RNAs after viral RNA pulldown in VeroE6 cell line 48 h.p.i. (left) and conservation across time points (right).

(B) 在 VeroE6 细胞系 48 hpi 中病毒 RNA 下拉后富集的宿主 RNA。 (左) 和跨时间点的保护 (右)。

(C) Enriched host RNAs after viral RNA pulldown in Huh7.5 cell line 48 h.p.i. (left) and comparison across time points (right).

(C) 在 Huh7.5 细胞系 48 h.p.i. 中病毒 RNA 下拉后富集的宿主 RNA。 (左) 和跨时间点的比较 (右) 。

SARS-CoV-2 encodes 16 nonstructural proteins, 4 structural proteins, and 6 accessory proteins (Finkel et al., 2020) (Figure 1E). We observed that 13 of 26 viral proteins were reproducibly enriched, including RNA-binding viral proteins. In the subgenomic RNA region, the major viral proteins conserved across cell types were N, M, and S, while ORF3a and 7a were selectively enriched from infected Huh7.5 cells (Figure 1F). Within the larger ORF1a/b, nsp3 and nsp4 were enriched in both cell lines; however, we saw stronger association of the known RNA-binding proteins (RBPs, names in red in Figure 1E) in Vero E6 cells (Figure 1F). The robust enrichment of specific ORF1a/b-encoded proteins provides strong evidence that the ChIRP-MS approach samples interactions across the entire length of the genomic RNA. However, species, cell type, and sex of organism differences between Vero E6 and Huh7.5 may underlie differences in overall interactomes. For example, Vero E6 cells support higher SARS-CoV-2 replication and viral egress, while replication in Huh7.5 cells reaches lower peak levels with delayed kinetics (Harcourt et al., 2020). Nonetheless, viral protein enrichments were specific and reproducible, and the common features of these cell lines enabled us to define a core SARS-CoV-2 RNA-associated proteome.

SARS-CoV-2 编码 16 种非结构蛋白、4 种结构蛋白和 6 种辅助蛋白 (Finkel 等人 , 2020) (图 1E)。我们观察到 26 种病毒蛋白中有 13 种被可重复地富集，包括结合 RNA 的病毒蛋白。在亚基因组 RNA 区域，跨细胞类型保守的主要病毒蛋白是 N 、 M 和 S ，而 ORF3a 和 7a 是从受感染的 Huh7.5 细胞中选择性富集的 (图 1F)。在较大的 ORF1a/b 中，两种细胞系中都富含 nsp3 和 nsp4 ；然而，我们在 Vero E6 细胞 (图 1F) 中看到了已知 RNA 结合蛋白 (RBP , 图 1E 中的红色名称) 的更强关联。特定 ORF1a/b 编码蛋白的大量富集提供了强有力的证据，证明 ChIRP-MS 方法对整个基因组 RNA 长度的相互作用进行采样。然而， Vero E6 和 Huh7.5 之间的物种、细胞类型和生物体性别差异可能是整体相互作用组差异的基础。例如， Vero E6 细胞支持更高的 SARS-CoV-2 复制和病毒流出，而 Huh7.5 细胞中的复制达到较低的峰值水平，具有延迟的动力学 (Harcourt 等 , 2020)。尽管如此，病毒蛋白富集是特异性和可重复的，这些细胞系的共同特征使我们能够定义一个核心的 SARS-CoV-2 RNA 相关蛋白质组。

A comprehensive atlas of host-factors that interact with the SARS-CoV-2 genomic RNA 与 SARS-CoV-2 基因组 RNA 相互作用的宿主因素的综合图谱

To define the host-derived interacting proteins of the SARS-CoV-2 RNA, we searched the ChIRP-MS data against a database of known monkey or human proteins. Comparing SARS-CoV-2-infected to mock (uninfected) cells, we defined high-confidence interactomes in each condition (FDR ≤ 0.05 , LFC > 0 ; Figures 2A and 2B). A total of 163

(Vero E6) and 229 (Huh7.5) host factors were bound to the SARS-CoV-2 RNA (Table S2). Analysis of the factors enriched at 24 versus 48 h.p.i revealed that most factors enriched in Vero E6 cells were invariant between the two time points (Figure 2C, left), while the Huh7.5 interactome evolved more dramatically over this period, with 48 h.p.i. showing an expanded set of interacting proteins (Figure 2C, middle). We repeated the same analysis on the ChIRP RNA sequencing (ChIRP-RNA-seq; Figures S1B and S1C), which is discussed in more detail below. We next compared the associated host factors across cell lines and found a core set of 83 factors co-bound in both cell lines, totaling 309 host factors aggregated across the two cell lines (Figure 2C, right). Given the more complete proteome reference, we focused our subsequent analysis on the human dataset.

为了定义 SARS-CoV-2 RNA 的宿主衍生相互作用蛋白，我们针对已知猴子或人类蛋白质的数据库搜索了 ChIRP-MS 数据。将感染 SARS-CoV-2 的细胞与模拟（未感染）细胞进行比较，我们定义了每种条件下的高置信度相互作用组（ $FDR \leq 0.05$, $LFC > 0$ ；图 2A 和 2B）。共有 163 个（Vero E6）和 229 个（Huh7.5）宿主因子与 SARS-CoV-2 RNA 结合（表 S2）。对 24 和 48 hpi 富集的因子的分析表明，在 Vero E6 细胞中富集的大多数因子在两个时间点之间是不变的（图 2C，左），而 Huh7.5 相互作用组在此期间进化得更为显著，48 hpi 显示一组扩展的相互作用蛋白质（图 2C，中间）。我们对 ChIRP RNA 测序（ChIRP-RNA-seq；图 S1B 和 S1C）重复了相同的分析，下面将对此进行更详细的讨论。我们接下来比较了跨细胞系的相关宿主因子，发现在两种细胞系中共结合了 83 个核心因子，总共有 309 个宿主因子在两种细胞系中聚合（图 2C，右）。鉴于更完整的蛋白质组参考，我们将后续分析重点放在了人类数据集上。

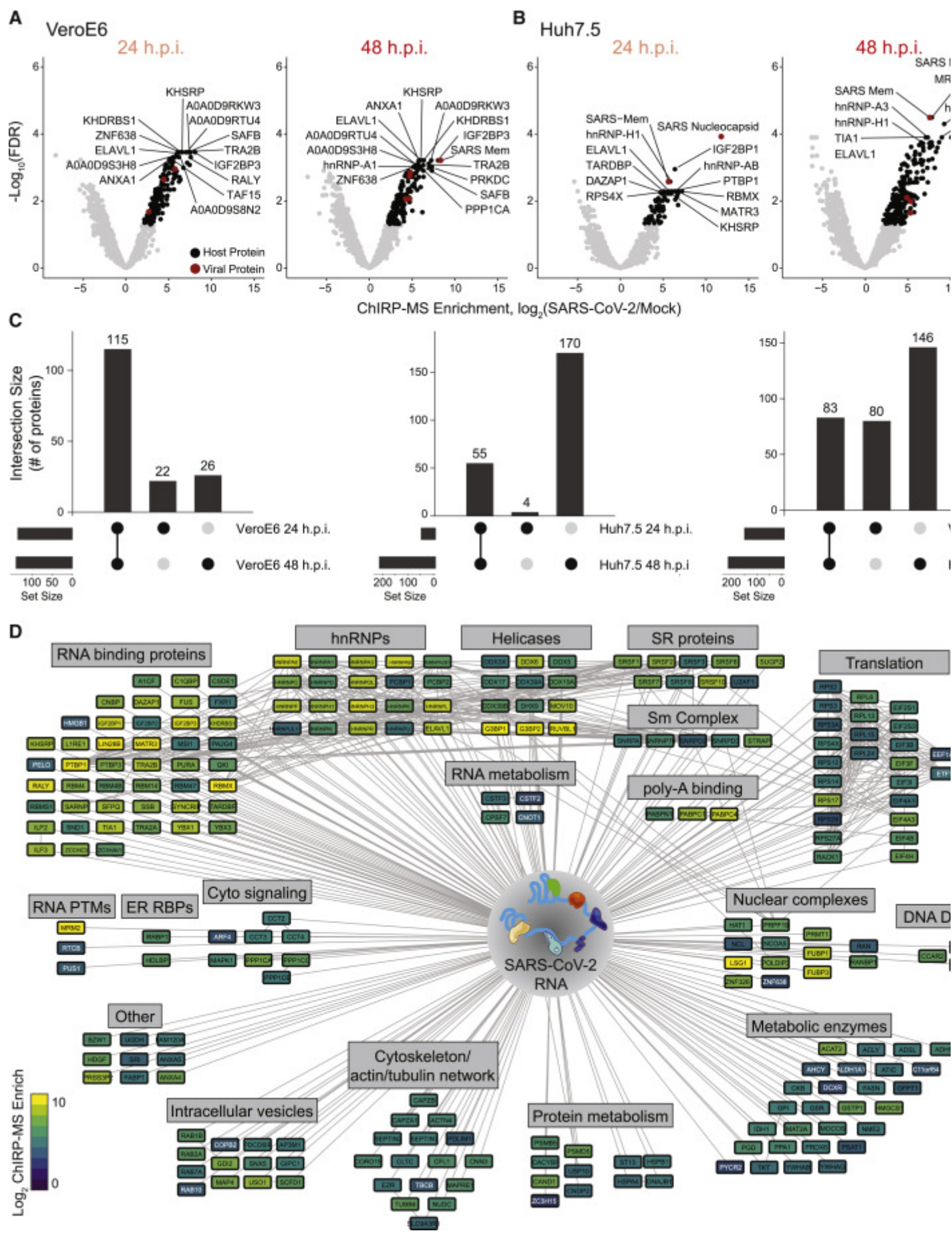


Figure 2. Changes in the SARS-CoV-2-associated proteome across time points and cell lines
图 2. SARS-CoV-2 相关蛋白质组在不同时间点和细胞系的变化

(A and B) ChIRP-MS results in Vero E6 (A) or Huh7.5 (B) cells after viral RNA pull-down at 24 and 48 h.p.i. Significantly enriched proteins indicated in black (host proteins) or red (viral proteins). (A 和 B) ChIRP-MS 在 24 和 48 hpi 病毒 RNA 下拉后产生 Vero E6 (A) 或 Huh7.5 (B) 细胞。显着富集的蛋白质以黑色（宿主蛋白）或红色（病毒蛋白）表示。

(C) Conservation of enriched proteins between time points (left, middle) and cell lines (right). (C) 时间点（左、中）和细胞系（右）之间富集蛋白质的保存。

(D) Cytoscape network representation of the SARS-CoV-2-associated human proteome. Colors indicate ChIRP enrichment in Huh7.5 cells 48 h.p.i.

(D) SARS-CoV-2 相关人类蛋白质组的 Cytoscape 网络表示。颜色表示 Huh7.5 细胞 48 h.p.i. 中的 ChIRP 富集。

We visualized the high-confidence human interactome using Cytoscape (Shannon et al., 2003), where each node represents a protein significantly enriched in the Huh7.5 ChIRP-MS dataset, and nodes are connected if there is a previously described PPI (Figure 2D). Structuring this network by broad functional categories demonstrated the diversity of host proteins associated with the vRNA, spanning generic RNA adaptor proteins, RNA helicases, RNA processing enzymes, and RNA modification enzymes (Figure 2D). We also noted a set of relatively unexpected pathways including metabolic enzymes, intracellular vesicle proteins, cytosolic signaling, cytoskeleton, and intracellular trafficking proteins (Figure 2D). We next compared these results between 24 and 48 h.p.i. and found that a set of RBPs were strongly bound early in infection, suggesting that these RBPs may be important for the earliest steps of detection or replication of the vRNA (Figure S2A). Comparing the Vero E6 and Huh7.5 interactomes revealed that the binding of core RBPs was highly conserved across cell lines, as were other categories such as nuclear complexes, poly-A binding proteins, and serine/arginine-rich splicing factors (Figure S2B). We next compared the ChIRP-MS results to a set of host factors identified by vRNA pull-down after UV-C crosslinking (RNA antisense purification MS [RAP-MS]; Schmidt et al., 2021) and found that the majority of RAP-MS factors (30/47, 64%) were also enriched in the ChIRP-MS dataset (Figures S3A and S3B). However, ChIRP-MS enriched an additional 199 proteins that were not identified as significant in the UV-C dataset. The increased scope, but high specificity, of ChIRP-enriched factors is consistent with prior reports (Chu et al., 2015; Ooi et al., 2019) and is due to crosslinking differences between formaldehyde and UV-C. We confirmed this finding by comparing enrichments of each method within the combined high-confidence interactomes (FDR ≤ 0.05 , average LFC ≥ 0 ; Figure S3D, left) and expanded interactomes (average LFC ≥ 1 ; Figure S3D, right). Finally, we compared the ChIRP-MS data to the host-viral protein-protein interactome (PPI; Gordon et al., 2020). We found that only 11/332 host factors (3.3%) from the PPI study overlapped with the ChIRP-MS network (Figures S3A and S3C), demonstrating that SARS-CoV-2 RNA and proteins largely interact with distinct protein complexes inside of

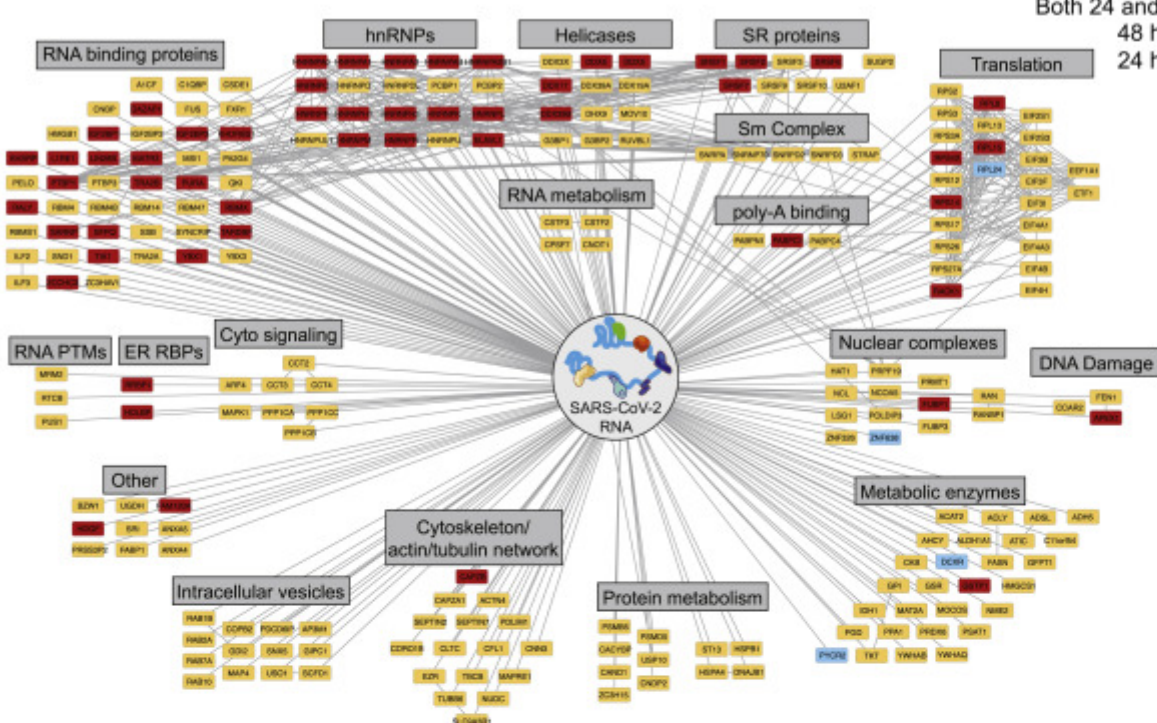
the cell. However, of the 11 host factors that bind both vRNA and viral proteins, RAB2A, RAB7A, and RAB10 have been validated as functional in SARS-CoV-2 infection (Hoffmann et al., 2021). Together, these comparisons highlight the orthogonality of an RNA-centric approach to PPI-based studies and the power of ChIRP-MS to discover large complexes associated with vRNAs during infection.

我们使用 Cytoscape (Shannon et al., 2003) 可视化了高可信度的人类交互组，其中每个节点代表 Huh7.5 ChIRP-MS 数据集中显着富集的一种蛋白质，如果存在先前描述的 PPI，则连接节点（图 2D）。通过广泛的功能类别构建该网络证明了与 vRNA 相关的宿主蛋白的多样性，涵盖通用 RNA 衔接蛋白、RNA 解旋酶、RNA 加工酶和 RNA 修饰酶（图 2D）。我们还注意到一组相对意外的途径，包括代谢酶、细胞内囊泡蛋白、细胞质信号、细胞骨架和细胞内运输蛋白（图 2D）。我们接下来在 24 和 48 hpi 之间比较了这些结果。并发现一组 RBP 在感染早期被强烈结合，这表明这些 RBP 可能对 vRNA 检测或复制的最早步骤很重要（图 S2A）。比较 Vero E6 和 Huh7.5 相互作用组显示，核心 RBP 的结合在细胞系中高度保守，其他类别如核复合物、poly-A 结合蛋白和富含丝氨酸/精氨酸的剪接因子也是如此（图 S2B）。我们接下来将 ChIRP-MS 结果与 UV-C 交联后通过 vRNA pull-down 鉴定的一组宿主因子进行比较（RNA 反义纯化 MS [RAP-MS]；Schmidt 等人，2021）并发现大多数 RAP-MS 因子（30/47, 64%）在 ChIRP-MS 数据集中也得到了丰富（图 S3A 和 S3B）。然而，ChIRP-MS 富集了另外 199 种蛋白质，这些蛋白质在 UV-C 数据集中没有被确定为重要的。ChIRP 富集因子的范围增加但特异性高，这与之前的报告一致（Chu 等人，2015 年；Ooi 等人，2019 年），这是由于甲醛和 UV-C 之间的交联差异所致。我们通过比较组合高置信度交互组（ $FDR \leq 0.05$ ，平均 $LFC \geq 0$ ；图 S3D，左）和扩展交互组（平均 $LFC \geq 1$ ；图 S3D，右）中每种方法的富集证实了这一发现。最后，我们将 ChIRP-MS 数据与宿主-病毒蛋白质-蛋白质相互作用组（PPI；Gordon 等，2020）进行了比较。我们发现 PPI 研究中只有 11/332 个宿主因子（3.3%）与 ChIRP-MS 网络重叠（图 S3A 和 S3C），表明 SARS-CoV-2 RNA 和蛋白质在很大程度上与不同的蛋白质复合物相互作用。细胞。然而，在结合 vRNA 和病毒蛋白的 11 种宿主因子中，RAB2A、RAB7A 和 RAB10 已被证实在 SARS-CoV-2 感染中起作用（Hoffmann 等，2021）。总之，这些比较突出了以 RNA 为中心的方法对基于 PPI 的研究的正交性，以及 ChIRP-MS 在感染期间发现与 vRNA 相关的大型复合物的能力。

A

Presence in the Huh7.5 High Confidence Interactome

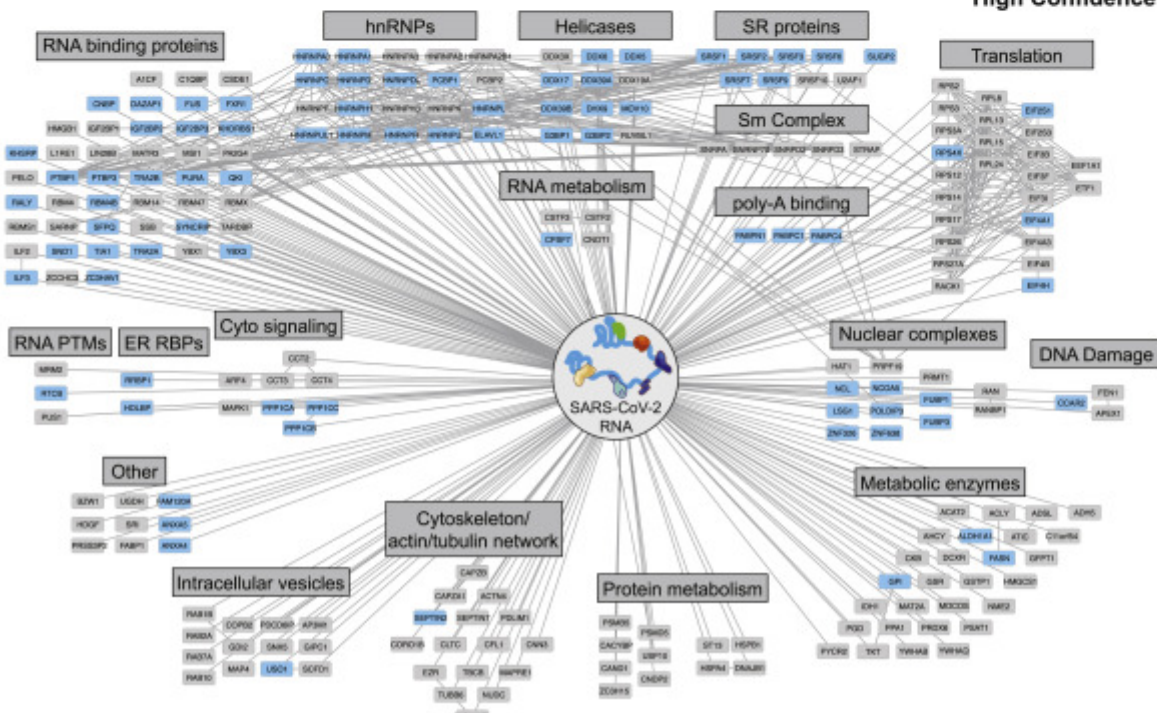
Both 24 and 48 h.p.i. █
48 h.p.i. only █
24 h.p.i. only █



B

Presence in the VeroE6 High Confidence Interactome

Yes █
No █



Download : Download high-res image (2MB) 下载 : 下载高分辨率图像 (2MB)

Download : Download full-size image 下载 : 下载全尺寸图片

Figure S2. SARS-CoV-2 ChIRP-MS across infection times and between cell types, related to Figure 2

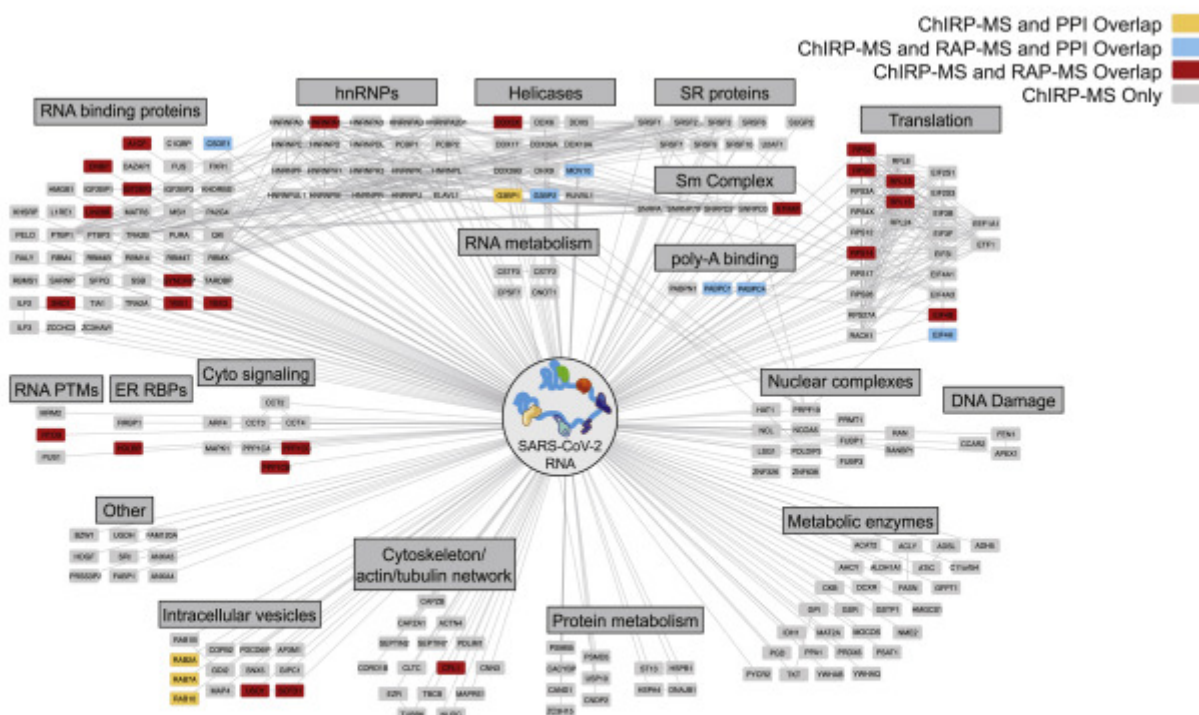
图 S2。SARS-CoV-2 ChIRP-MS 跨越感染时间和细胞类型，与图 2 相关

(A) High-confidence SARS-CoV-2 human interactome network colored by time point (24 h.p.i., 48 h.p.i., or both).

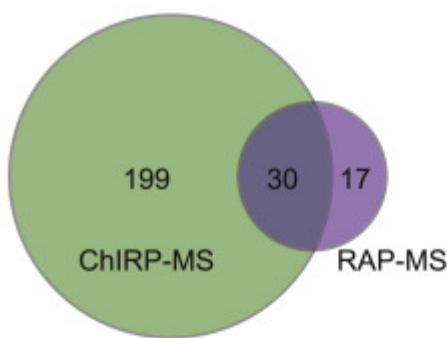
(A) 按时间点 (24 h.p.i.、48 h.p.i.，或两者) 着色的高置信度 SARS-CoV-2 人类相互作用组网络。

(B) High-confidence SARS-CoV-2 human interactome network colored by cell line conservation.
(B) 通过细胞系保护着色的高可信度 SARS-CoV-2 人类相互作用组网络。

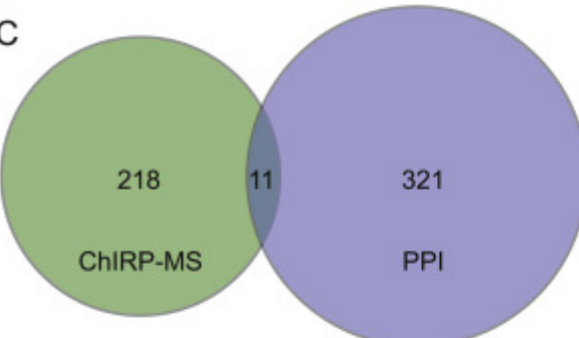
A



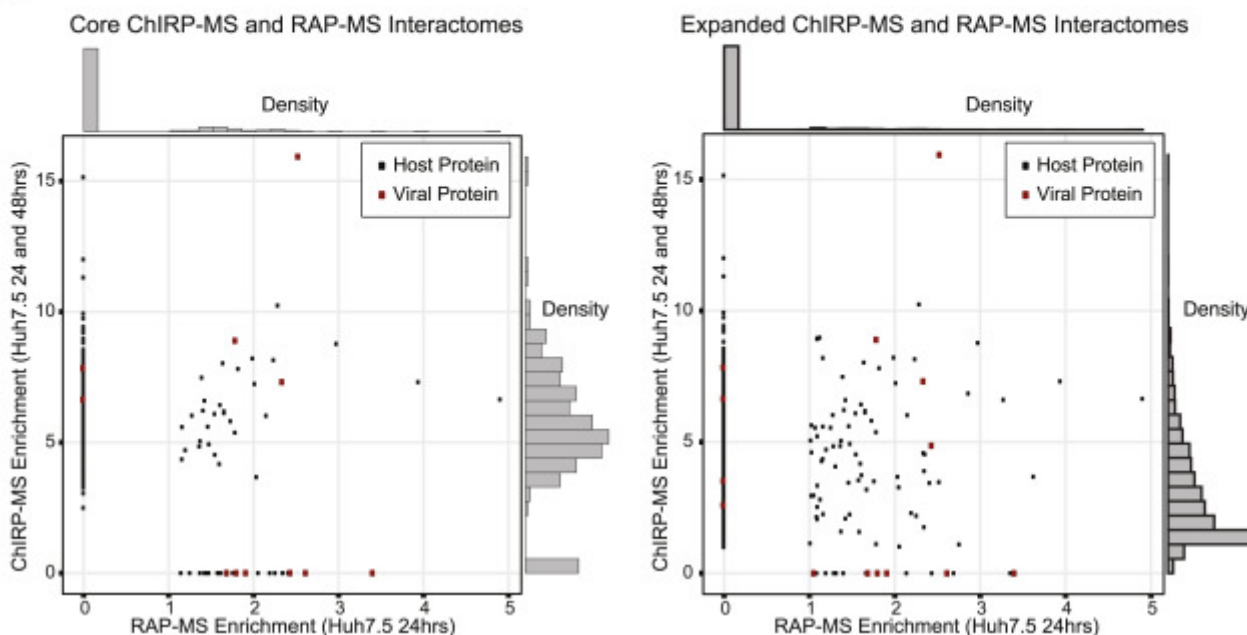
B



C



D



Download : Download high-res image (1MB) 下载 : 下载高分辨率图像 (1MB)

Download : Download full-size image 下载 : 下载全尺寸图片

Figure S3. Comparison of SARS-CoV-2 ChIRP-MS to other RNA- and protein-centric views of the viral interactome in human cells, related to [Figure 3](#)

图 S3。SARS-CoV-2 ChIRP-MS 与人类细胞中病毒相互作用组的其他以 RNA 和蛋白质为中心的观点的比较，与图 3 相关

(A) Comparison of the high-confidence SARS-CoV-2 RNA associated human proteome obtained by RAP-MS (UV crosslinking; ([Schmidt et al., 2021](#))) to that by formaldehyde crosslinking (ChIRP-MS; this study) and comparison of the SARS-CoV-2 RNA associated proteome to the SARS-CoV-2 protein associated proteome (PPI; ([Gordon et al., 2020](#))).

(A) RAP-MS (UV 交联 ; (Schmidt 等人 , 2021)) 与甲醛交联 (ChIRP-MS ; 本研究) 和 SARS-CoV-2 RNA 相关蛋白质组与 SARS-CoV-2 蛋白质相关蛋白质组的比较 (PPI ; (Gordon 等人 , 2020)) 。

(B) Overlap of human high-confidence interactomes obtained by RAP-MS or ChIRP-MS.

(B) 通过 RAP-MS 或 ChIRP-MS 获得的人类高置信度相互作用组的重叠。

(C) Overlap of PPI and ChIRP-MS interactomes.

(C) PPI 和 ChIRP-MS 相互作用组的重叠。

(D) Left: enrichment correlation of the human high-confidence interactomes obtained by RAP-MS or ChIRP-MS ($FDR \leq 0.05$). Right: enrichment correlation of the human expanded interactomes obtained by RAP-MS or ChIRP-MS (average enrichment $> = 1$).

(D) 左 : 通过 RAP-MS 或 ChIRP-MS 获得的人类高置信度相互作用组的富集相关性 ($FDR \leq 0.05$)。右图 : 通过 RAP-MS 或 ChIRP-MS 获得的人类扩增相互作用组的富集相关性 (平均富集 $> = 1$) 。

ChIRP-MS identifies factors expressed in human lung tissue ChIRP-MS 识别在人肺组织中表达的因子

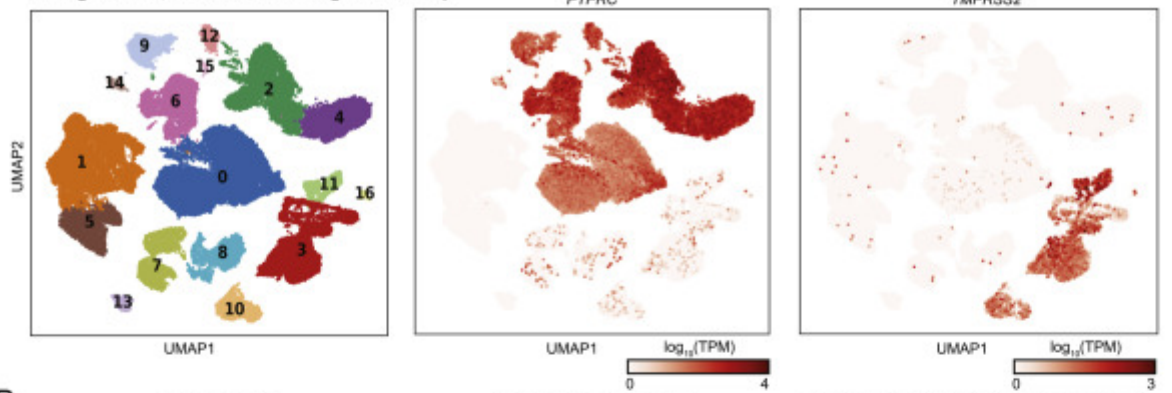
Although Huh7.5 and Vero E6 cells are common models for SARS-CoV-2 infection, neither is derived from the lung, which is the primary tissue targeted by SARS-CoV-2 infection. To understand whether host factors identified by ChIRP-MS in these cell lines may be relevant to human disease, we analyzed the expression of each host factor in single-cell RNA-seq (scRNA-seq) profiles from primary human lung cells ([Travaglini et al., 2020](#)). After excluding immune cells and putative doublets, we identified 30,700 cells that clustered into 17 distinct epithelial, endothelial, and stromal cell types ([Figures S4A–S4C](#)). Prior studies have demonstrated that multiple lung cell types express the SARS-CoV-2 entry receptor, ACE2, and the serine protease, TMPrSS2, including epithelial basal, club, and ciliated cells, and alveolar type 1 (AT-1) and 2 (AT-2) cells ([Hou et al., 2020](#); [Salahudeen et al., 2020](#); [Sungnak et al., 2020](#)). Human bronchial epithelial cell (HBEC) cultures have shown that ciliated cells may be the initial target of infection, which can later spread to other cell types ([Ravindra et al., 2020](#)). Therefore, we conservatively considered any cell type with moderate RNA expression levels of *ACE2* and *TMPrSS2* in the scRNA-seq data as relevant targets of SARS-CoV-2 ([Figure 3A](#)). The vast majority of core human ChIRP-MS factors (219/229; 95.6%) were

detectably expressed in SARS-CoV-2 target cell types, as well as other cell types, and 215/219 detected factors were expressed at a level equal to or greater than ACE2 (Figure 3B). These results suggest that the vast majority of SARS-CoV-2 RBPs identified in Huh7.5 cells are robustly expressed and relevant to infection in primary human target cells of SARS-CoV-2 infection, although confirmation studies in primary or model human lung cells are warranted (Figure 3C). More broadly, this analysis suggests that vRNA-binding factors may be broadly expressed across cell types and thus play a functional role across multiple viruses and target cells.

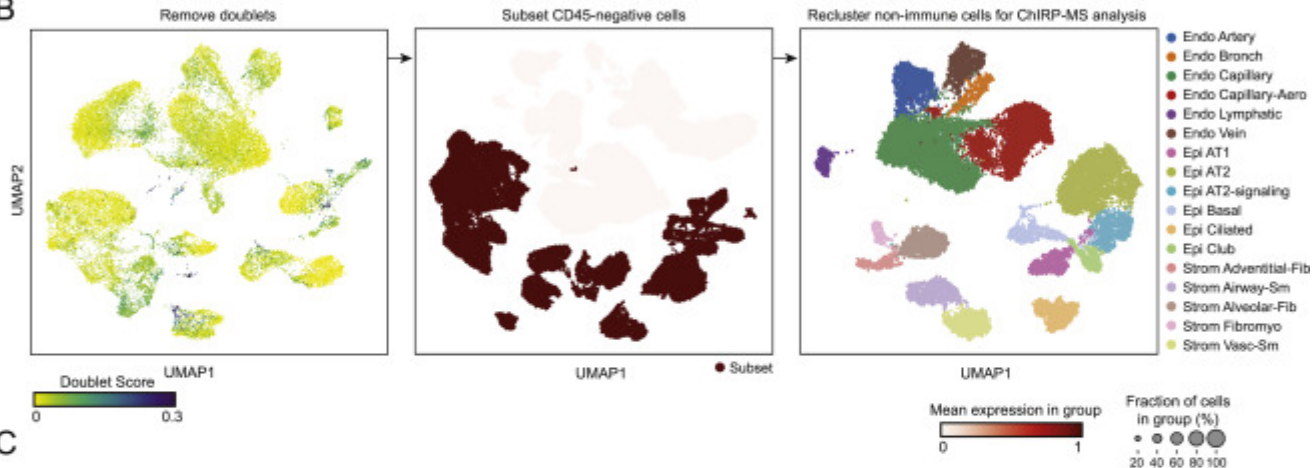
尽管 Huh7.5 和 Vero E6 细胞是 SARS-CoV-2 感染的常见模型，但两者都不是来自肺，而肺是 SARS-CoV-2 感染的主要目标组织。为了了解 ChIRP-MS 在这些细胞系中鉴定的宿主因子是否可能与人类疾病相关，我们分析了来自原代人肺细胞的单细胞 RNA-seq (scRNA-seq) 谱中每个宿主因子的表达 (Travaglini 等al., 2020)。在排除免疫细胞和假定的双联体后，我们确定了 30,700 个细胞，这些细胞聚集成 17 种不同的上皮细胞、内皮细胞和基质细胞类型 (图 S4A-S4C)。先前的研究表明，多种肺细胞类型表达 SARS-CoV-2 进入受体 ACE2 和丝氨酸蛋白酶 TMPRSS2，包括上皮基底细胞、棒状细胞和纤毛细胞，以及肺泡 1 型 (AT-1) 和 2 型 (AT-2) 细胞 (Hou 等人, 2020 年；Salahudeen 等人, 2020 年；Sungnak 等人, 2020 年)。人支气管上皮细胞 (HBEC) 培养物表明，纤毛细胞可能是感染的初始目标，随后可扩散到其他细胞类型 (Ravindra 等, 2020)。因此，我们保守地将 scRNA-seq 数据中具有中等 RNA 表达水平的 ACE2 和 TMPRSS2 的任何细胞类型视为 SARS-CoV-2 的相关靶标 (图 3A)。绝大多数核心人类 ChIRP-MS 因子 (219/229; 95.6%) 在 SARS-CoV-2 靶细胞类型以及其他细胞类型中可检测到表达，并且 215/219 检测到的因子表达水平相等达到或大于 ACE2 (图 3B)。这些结果表明，在 Huh7.5 细胞中鉴定的绝大多数 SARS-CoV-2 RBP 均表达强烈，并且与 SARS-CoV-2 感染的原代人类靶细胞的感染相关，尽管在原代或模型人肺细胞中进行了确认研究是有保证的 (图 3C)。更广泛地说，该分析表明 vRNA 结合因子可能在细胞类型中广泛表达，从而在多种病毒和靶细胞中发挥功能作用。

A

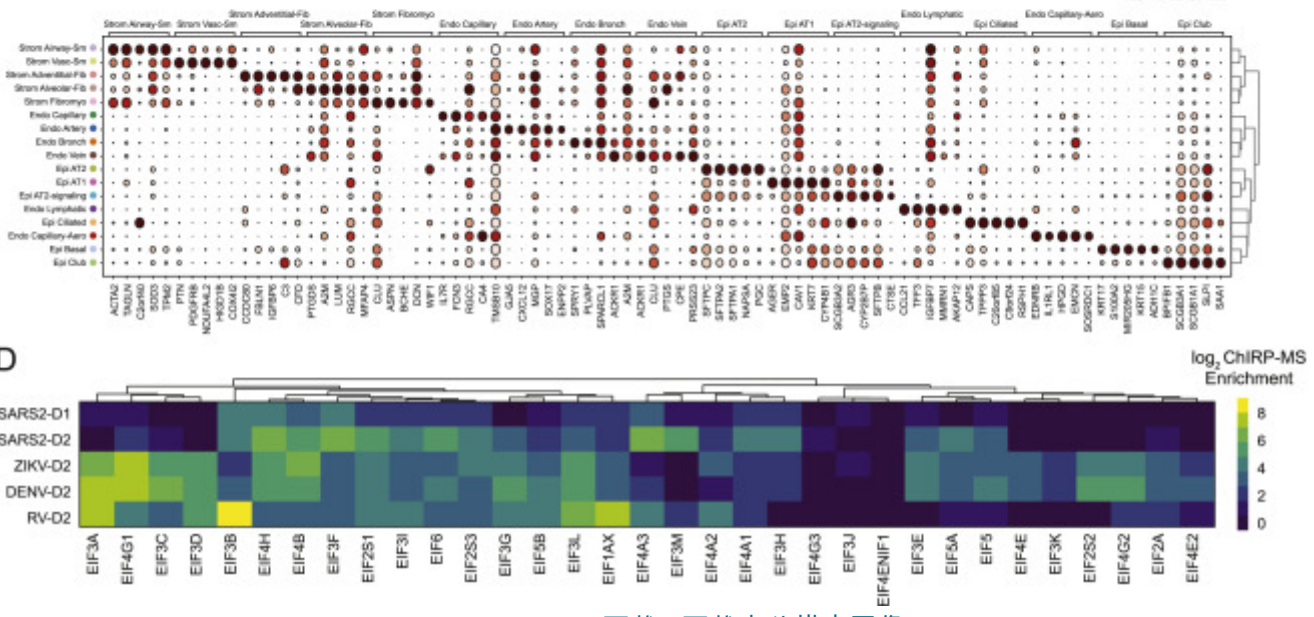
Travaglini et al., 2020: Human Lung scRNA-seq



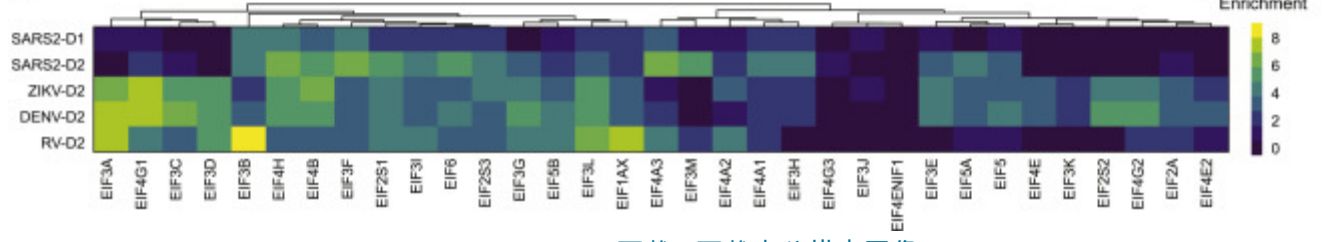
B



C



D



[Download](#) : [Download high-res image \(2MB\)](#) 下载 : [下载高分辨率图像 \(2MB\)](#)

[Download](#) : [Download full-size image](#) 下载 : [下载全尺寸图片](#)

Figure S4. Re-analysis of single-cell RNA-seq analysis of human lung tissue, related to [Figure 4](#)
图 S4。人肺组织单细胞 RNA-seq 分析的再分析，与图 4 相关

(A) Louvain clustering of all cells in the human lung scRNA-seq dataset are shown, alongside the expression of *PTPRC* (CD45) and *TMPRSS2*.

(A) 显示了人肺 scRNA-seq 数据集中所有细胞的 Louvain 聚类，以及 PTPRC (CD45) 和 TMPRSS2 的表达。

(B) For the final filtered dataset, putative doublets (doublet score > 0.15) were removed, and the subset of CD45-negative cells was identified. The resulting data was re-clustered and the cluster

labels are shown.

(B) 对于最终过滤的数据集，去除了假定的双峰（双峰得分 > 0.15 ），并确定了 CD45 阴性细胞的子集。结果数据被重新聚类并显示聚类标签。

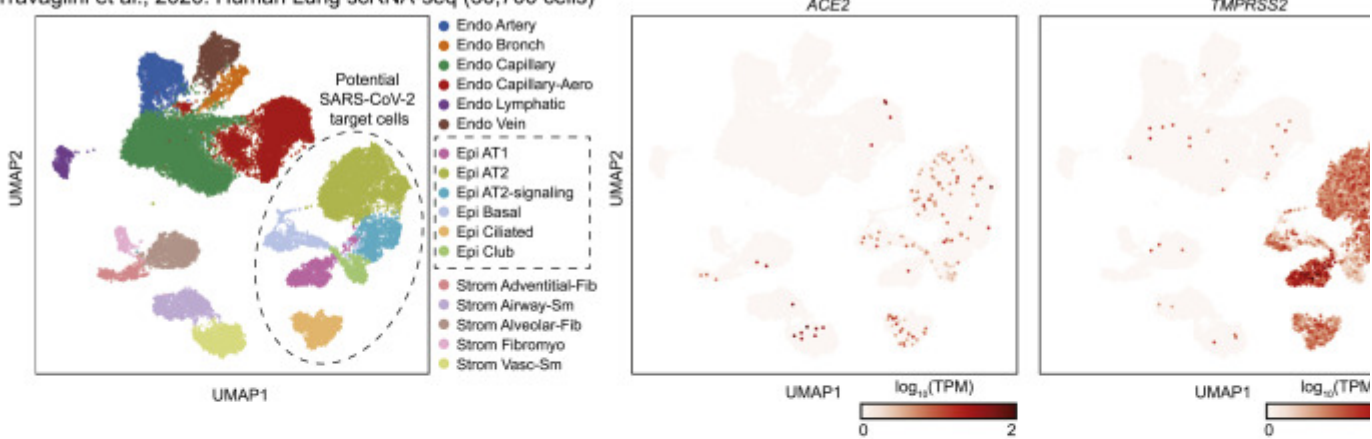
(C) Representative marker genes for each cluster.

(C) 每个簇的代表性标记基因。

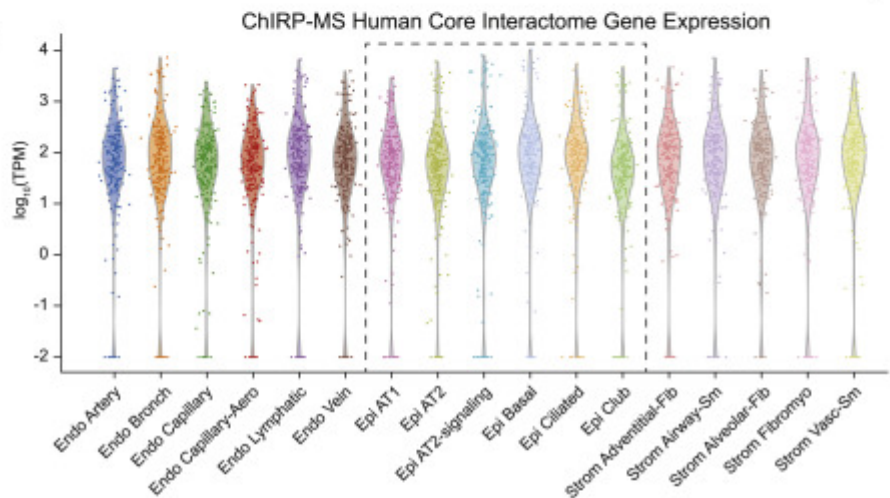
(D) Multi-viral comparison of associations with translation initiation (EIF) factors.

(D) 与翻译起始 (EIF) 因素关联的多病毒比较。

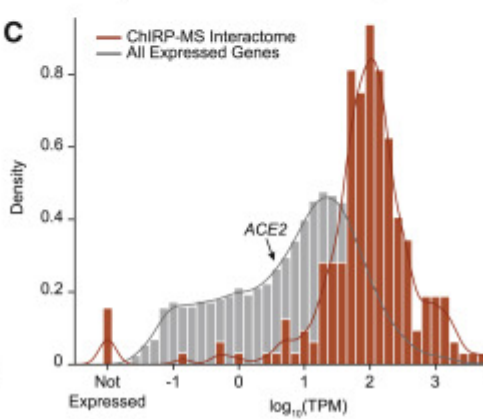
A Travaglini et al., 2020: Human Lung scRNA-seq (30,700 cells)



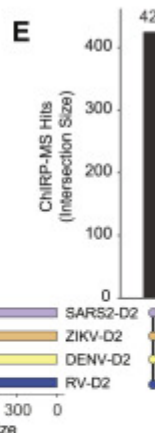
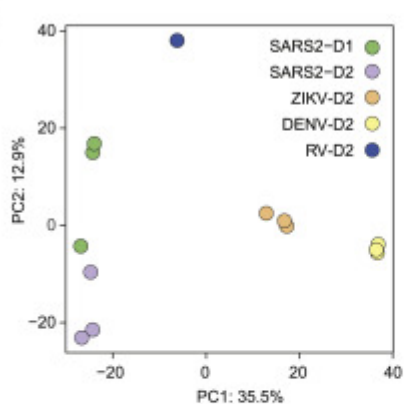
B



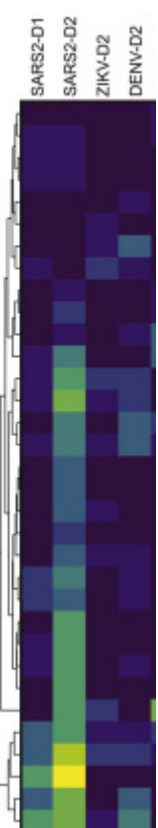
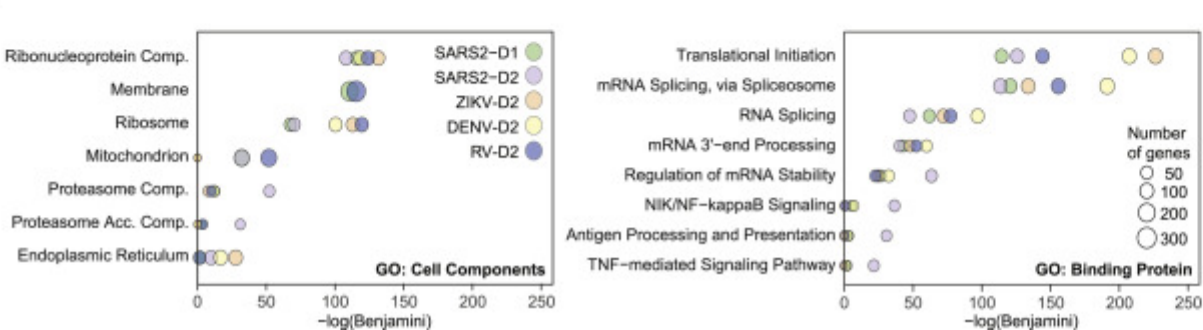
C



D



F



Download : Download high-res image (1MB) 下载 : 下载高分辨率图像 (1MB)

Download : Download full-size image 下载 : 下载全尺寸图片

Figure 3. Expression of the SARS-CoV-2 RNA-associated proteome across lung cell types and comparison to other RNA virus-associated proteomes

图 3. SARS-CoV-2 RNA 相关蛋白质组在肺细胞类型中的表达以及与其他 RNA 病毒相关蛋白质组的比较

(A) Clustering and dimensionality reduction and gene expression of non-immune single-cell RNA-seq profiles from primary human lung tissue.

(A) 来自原代人肺组织的非免疫单细胞 RNA-seq 谱的聚类和降维以及基因表达。

(B) Expression in single cells of the SARS-CoV-2 human core interactome. SARS-CoV-2 target clusters indicated with a box. Each dot represents the mean expression of a given gene in the core ChIRP-MS interactome across all cells in the indicated cluster.

(B) 在 SARS-CoV-2 人类核心相互作用组的单细胞中的表达。用方框表示的 SARS-CoV-2 目标簇。每个点代表核心 ChIRP-MS 相互作用组中指定基因在指定簇中的所有细胞中的平均表达。

(C) Histogram of expression of each gene in the core ChIRP-MS interactome (orange) compared with all other genes (gray) in the lung epithelial ciliated cell cluster.

(C) 与肺上皮纤毛细胞簇中的所有其他基因（灰色）相比，核心 ChIRP-MS 相互作用组（橙色）中每个基因的表达直方图。

(D) Principal component analysis of ChIRP enrichments in human cells across time points and viruses.

(D) 跨时间点和病毒的人类细胞中 ChIRP 富集的主成分分析。

(E) Upset plot comparing expanded interactomes of each virus.

(E) 比较每种病毒的扩展相互作用组的不安图。

(F) GO term analysis of the expanded interactome of each virus.

(F) 对每种病毒的扩展相互作用组进行 GO 术语分析。

(G) Comparison of proteasome subunits and proteasome accessory factor associations across viruses.

(G) 病毒间蛋白酶体亚基和蛋白酶体辅助因子关联的比较。

Inter-virus analysis of host factors reveals specificity of interacting cellular pathways 宿主因子的病毒间分析揭示了相互作用细胞途径的特异性

Interactions between vRNAs and host proteins play key roles in multiple aspects of viral infection (Fritzlar et al., 2019; Garcia-Blanco et al., 2016; Hosmillo et al., 2019). To understand how positive-stranded RNA viruses have evolved to interact with their host, we sought to compare the SARS-CoV-2 dataset to our previously generated ChIRP-MS data from the flaviviruses Zika (ZIKV, ZIKV-PRVABC59) and Dengue-2 (DENV, DENV-16681), as well as a human picornavirus and rhinovirus (RV, RV-B14; Ooi et al., 2019). We note that all datasets were collected from Huh7.5 cells except the rhinovirus data, which was collected from HeLa cells. Principal component analysis (PCA) of host factors enriched across viruses showed that PC1 separated all four viral types and PC2 further distinguished RV and demonstrated the time-dependent host factor changes for SARS-CoV-2 (Figure 3D). To facilitate a quantitative comparison across viruses, we defined an

“expanded interactome,” consisting of proteins reproducibly enriched for each ChIRP-MS dataset: SARS-CoV-2-D1 (Huh7.5 24 h.p.i.), SARS-CoV-2-D2 (Huh7.5 48 h.p.i.), ZIKV-D2, DENV-D2, and RV-D2 ([Table S3](#)), resulting in about 1,000 proteins ([Figure 3E](#)). We found that the largest group of 425 proteins was shared across all ChIRP-MS datasets, suggesting a common host strategy for interacting with positive polarity, ssRNA viruses ([Figure 3E](#)).

vRNA 和宿主蛋白之间的相互作用在病毒感染的多个方面起着关键作用 (Fritzlar 等人, 2019 年; Garcia-Blanco 等人, 2016 年; Hosmillo 等人, 2019 年)。为了了解正链 RNA 病毒如何进化以与其宿主相互作用, 我们试图将 SARS-CoV-2 数据集与我们之前生成的 ChIRP-MS 数据进行比较, 它们来自寨卡病毒 (ZIKV、ZIKV-PRVABC59) 和登革热 2 (DENV, DENV-16681), 以及人类小核糖核酸病毒和鼻病毒 (RV, RV-B14; Ooi 等, 2019)。我们注意到所有数据集都是从 Huh7.5 细胞中收集的。但鼻病毒数据是从 HeLa 细胞中收集的。跨病毒富集的宿主因子的主成分分析 (PCA) 显示 PC1 分离了所有四种病毒类型, PC2 进一步区分了 RV, 并证明了 SARS-CoV-2 的时间依赖性宿主因子变化 ([图 3D](#))。为了便于对病毒进行定量比较, 我们定义了一个“扩展的相互作用组”, 由每个 ChIRP-MS 数据集可重复富集的蛋白质组成: SARS-CoV-2-D1 (Huh7.5 24 hpi)、SARS-CoV-2-D2 (Huh7.5 48 hpi)、ZIKV-D2、DENV-D2 和 RV-D2 ([表 S3](#)), 产生大约 1,000 种蛋白质 ([图 3E](#))。我们发现最大的 425 种蛋白质在所有 ChIRP-MS 数据集中共享, 这表明与正极性 ssRNA 病毒相互作用的常见宿主策略 ([图 3E](#))。

We next performed gene ontology (GO) term analysis on the expanded interactomes of each virus. All viruses robustly enriched the intracellular RNP complex term; however, we found patterns of specificity when examining other terms ([Figure 3F](#)). For example, the SARS-CoV-2 interactome displayed a reduced enrichment of the ER and ribosome GO terms but an increased enrichment of mitochondria and proteasome GO terms ([Figure 3F](#)). Examining functional terms again corroborated a decreased enrichment of translation and splicing factor terms in the SARS-CoV-2 interactome, compared to that of the flaviviruses, but a specific increased enrichment of multiple immune pathways, such as antigen presentation, NF- κ b signaling, and TNF signaling ([Figure 3F](#)). To understand the specific proteins driving these enrichments, we visualized all the individual subunits of the proteasome present in the ChIRP-MS as an example ([Figure 3G](#)). Previous work has reported a functional connection between proper proteasome function and coronavirus life cycles ([Raaben et al., 2010](#)), which together with our ChIRP-MS data may suggest that the vRNA directly leverages the proteasome during infection, potentially to modulate antigen presentation and/or evade host adaptive immunity. The specificity of association between the proteasome and the SARS-CoV-2 RNA, and clear validation of this interaction in the literature, motivated us to explore the set of RNA-centric viral interactomes across a number of other important cellular pathways.

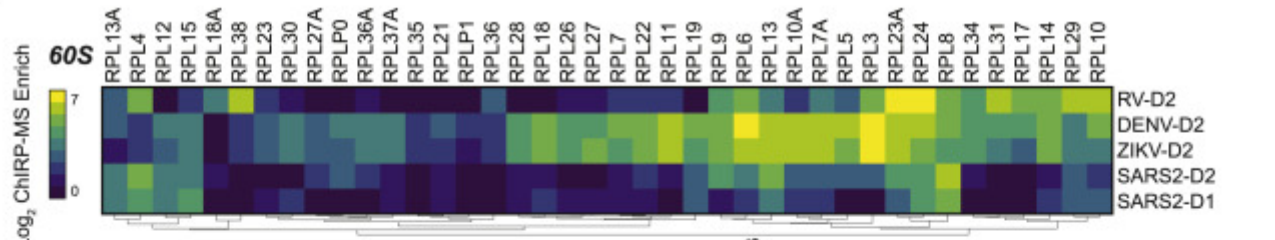
接下来，我们对每个病毒的扩展相互作用组进行了基因本体 (GO) 术语分析。所有病毒都极大地丰富了细胞内 RNP 复合体项；然而，我们在检查其他术语时发现了特异性模式（图 3F）。例如，SARS-CoV-2 相互作用组显示 ER 和核糖体 GO 术语的富集减少，但线粒体和蛋白酶体 GO 术语的富集增加（图 3F）。再次检查功能术语证实，与黄病毒相比，SARS-CoV-2 相互作用组中翻译和剪接因子术语的富集减少，但多种免疫途径的富集具体增加，例如抗原呈递、NF- κ b 信号传导、和 TNF 信号（图 3F）。为了了解驱动这些富集的特定蛋白质，我们以 ChIRP-MS 中存在的蛋白酶体的所有单个亚基为例（图 3G）。先前的工作报告了适当的蛋白酶体功能与冠状病毒生命周期之间的功能联系（Raaben 等，2010），这与我们的 ChIRP-MS 数据一起可能表明 vRNA 在感染期间直接利用蛋白酶体，可能会调节抗原呈递和/或逃避宿主适应性免疫。蛋白酶体和 SARS-CoV-2 RNA 之间关联的特异性，以及文献中对这种相互作用的明确验证，促使我们在许多其他重要的细胞途径中探索以 RNA 为中心的病毒相互作用组。

Translational apparatus 平移装置

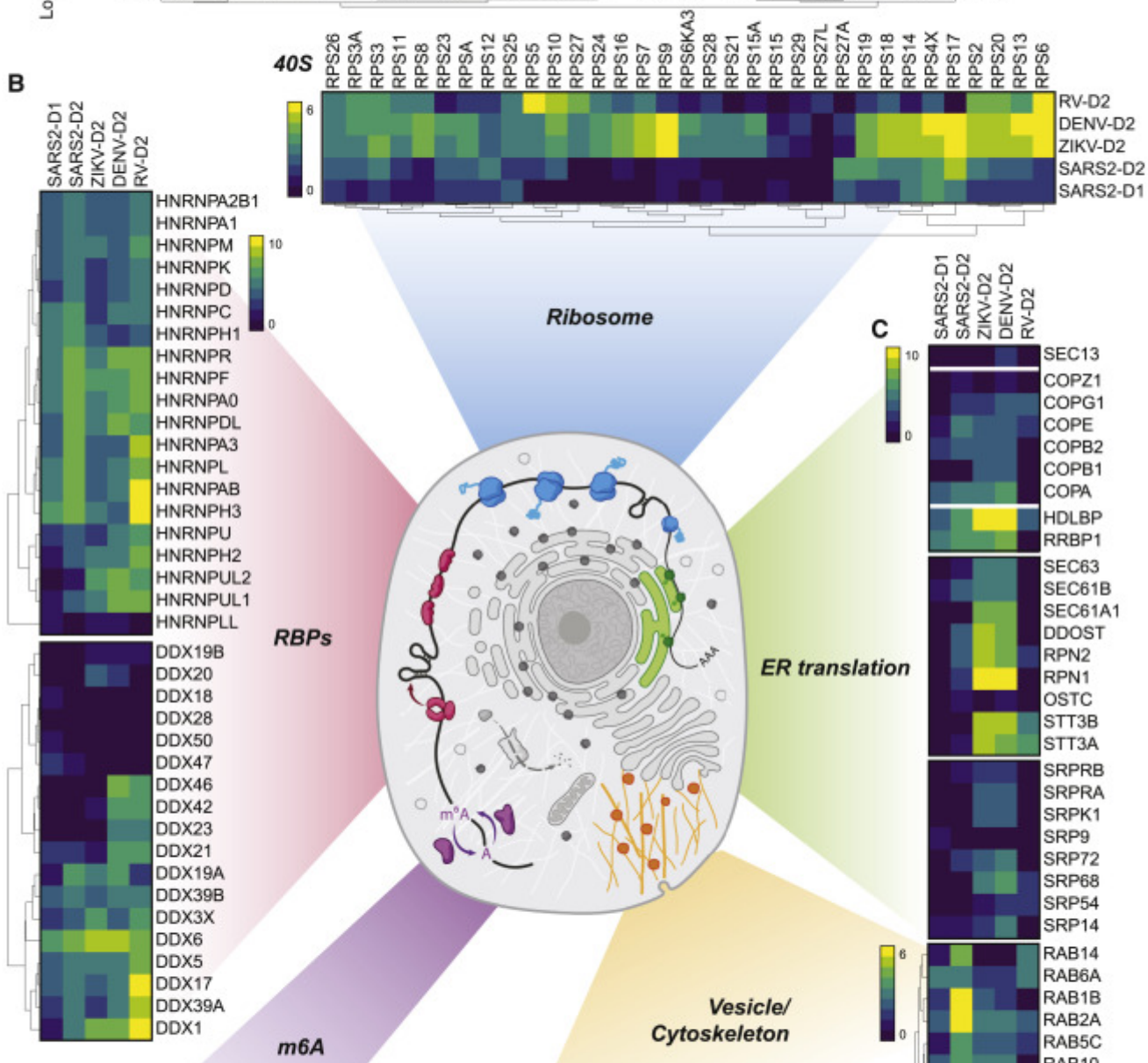
After entry into the cytosol, one of the first steps of the viral life cycle is to express the protein products encoded in its genome, which requires interactions with the host translational apparatus. Work examining the translational capacity of RNA viruses has shown that, in contrast to flaviviruses, coronaviruses do not translate their mRNAs at higher efficiency than cellular mRNAs during infection (Finkel et al., 2020). A comparison of enriched translation initiation factors (eIFs) demonstrated quantitative differences across the viruses: flaviviruses strongly enriched EIF3A, 4G1, 3C, and 3D, while SARS-CoV-2 was relatively depleted for these factors but preferred EIF3B, 4H, 4B, 3F, and A3 (Figure S4D). Beyond translational initiation, we visualized enrichment for the core components of the 80S ribosome (Figure 4A). Here, we note that while there was specificity in the enrichment of specific ribosomal proteins (RPs), more striking was the generalized lack of association of the vast majority of the RPs with the SARS-CoV-2 vRNA compared to either DENV or ZIKV (Figure 4A). This is consistent with recent reports demonstrating global translation inhibition by SARS-CoV-2 encoded nsp1 (Edgil et al., 2006; Roth et al., 2017; Schubert et al., 2020; Thoms et al., 2020).

进入细胞质后，病毒生命周期的第一步是表达其基因组中编码的蛋白质产物，这需要与宿主翻译装置相互作用。检查 RNA 病毒翻译能力的工作表明，与黄病毒相比，冠状病毒在感染期间不会以比细胞 mRNA 更高的效率翻译其 mRNA (Finkel 等，2020)。富集翻译起始因子 (eIF) 的比较表明病毒之间存在数量差异：黄病毒强烈富集 EIF3A、4G1、3C 和 3D，而 SARS-CoV-2 的这些因子相对耗尽，但首选 EIF3B、4H、4B、3F 和 A3 (图 S4D)。除了翻译起始，我们还可视化了 80S 核糖体核心成分的富集 (图 4A)。在这里，我们注意到，虽然特定核糖体蛋白 (RP) 的富集具有特异性，但与 DENV 或 ZIKV 相比，绝大多数 RP 与 SARS-CoV-2 vRNA 普遍缺乏关联。图 4A)。这与最近的报告一致，证明 SARS-CoV-2 编码的 nsp1 对全局翻译产生抑制 (Edgil 等人，2006 年；Roth 等人，2017 年；Schubert 等人，2020 年；Thoms 等人，2020 年)。

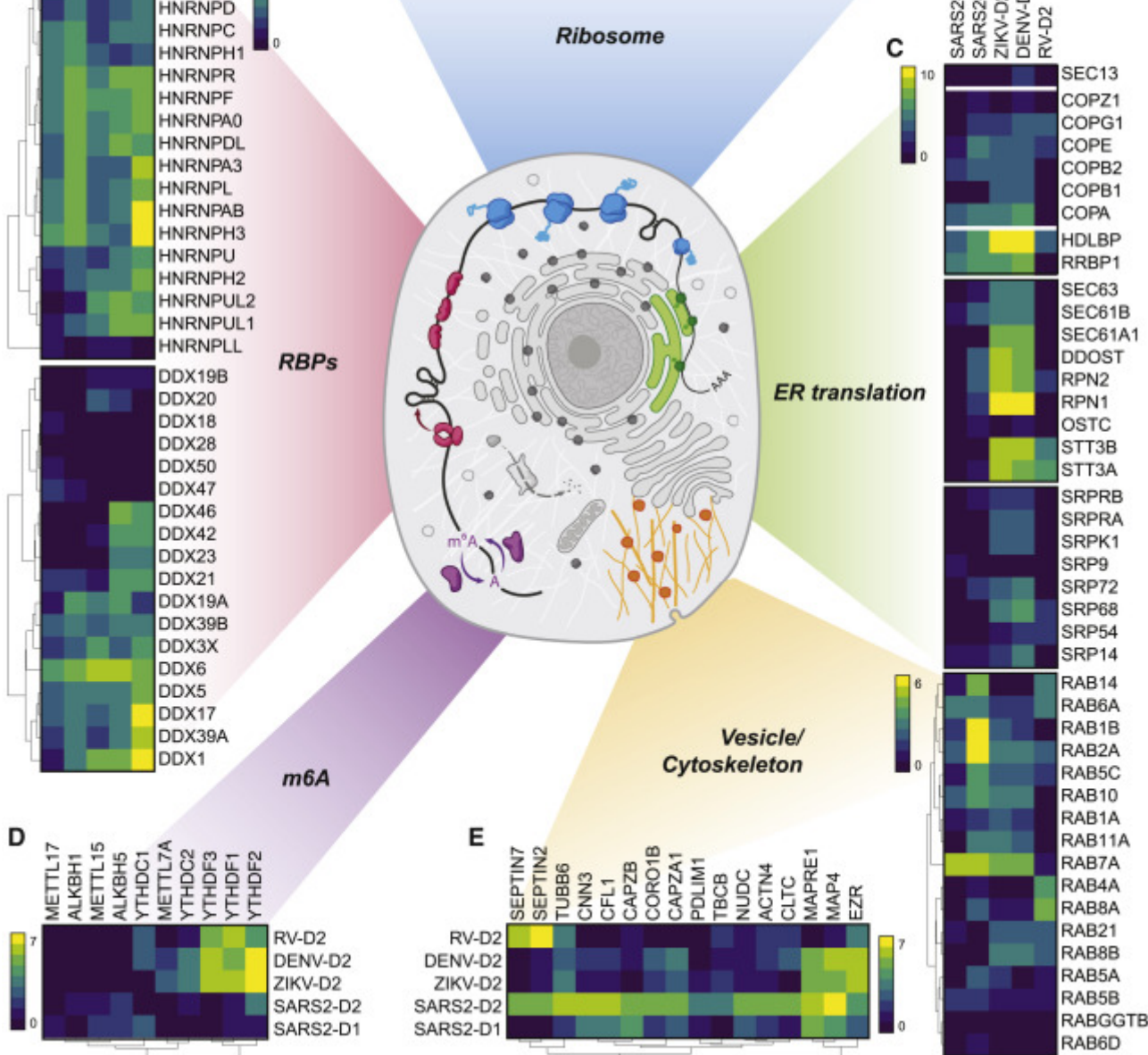
A



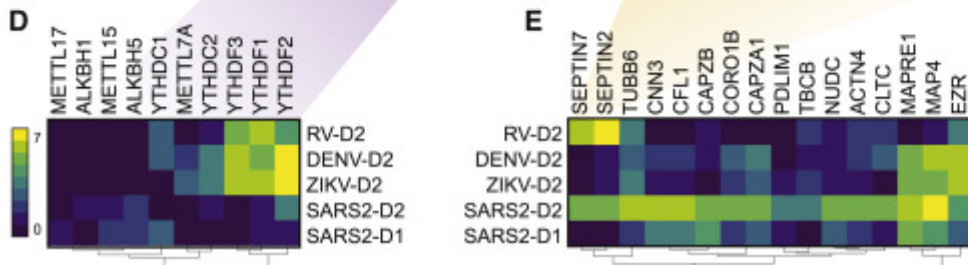
B



C



E



[Download : Download high-res image \(1MB\)](#) [下载 : 下载高分辨率图像 \(1MB\)](#)

[Download : Download full-size image](#) [下载 : 下载全尺寸图片](#)

Figure 4. Cellular context of expanded interactomes across viruses

图 4. 跨病毒扩展相互作用组的细胞环境

Selected groups of proteins; their enrichment in SARS-CoV-2, ZIKV, DENV, and RV ChIRP-MS; and their approximate subcellular localization or categorization in the ribosome (A), classical RBPs and RNA helicases (B), ER and ER-targeting factors (C), RNA post-transcriptional modification factors including m6A family proteins (D), and cytoskeleton and cellular vesicle factors (E). Heatmap colors indicate the log₂ of ChIRP-MS enrichment values. Each heatmap has a separate scale bar.

选定的蛋白质组；它们在 SARS-CoV-2、ZIKV、DENV 和 RV ChIRP-MS 中的富集；及其在核糖体 (A)、经典 RBP 和 RNA 解旋酶 (B)、ER 和 ER 靶向因子 (C)、RNA 转录后修饰因子包括 m6A 家族蛋白 (D) 和细胞骨架中的大致亚细胞定位或分类，以及细胞囊泡因子 (E)。热图颜色表示 ChIRP-MS 富集值的 log₂。每个热图都有一个单独的比例尺。

RNA-binding proteins RNA结合蛋白

RBPs have a wide array of cellular functions and are often recovered with host or pathogenic RNAs ([Geuens et al., 2016](#); [Meier-Stephenson et al., 2018](#); [Taschuk and Cherry, 2020](#)). Heterogeneous nuclear ribonucleoproteins (hnRNPs), a large set of adaptor proteins ([Geuens et al., 2016](#)), showed robust interaction with all four viruses and similar enrichments for the majority of the 20 proteins we identified ([Figure 4B](#)). Dead-box RNA helicases (DDX), which remodel RNA structural elements ([Jankowsky, 2011](#)), showed a more virus-specific binding profile wherein family members such as DDX3X, 5, 6, and 38B were similar across viruses, while DDX21, 23, 42, and 46 were more specifically associated with the DENV and RV RNAs ([Figure 4B](#)).

RBP 具有广泛的细胞功能，并且经常与宿主或致病性 RNA 一起回收（Geuens 等人，2016 年；Meier-Stephenson 等人，2018 年；Taschuk 和 Cherry，2020 年）。异质核核糖核蛋白 (hnRNP) 是一大组衔接蛋白 (Geuens 等人，2016 年)，显示出与所有四种病毒的强烈相互作用以及我们鉴定的 20 种蛋白质中的大多数的相似富集 (图 4B)。死盒 RNA 解旋酶 (DDX) 可重塑 RNA 结构元件 (Jankowsky, 2011)，显示出更具病毒特异性的结合特征，其中 DDX3X、5、6 和 38B 等家族成员在病毒间相似，而 DDX21、23、42 和 46 更具体地与 DENV 和 RV RNA 相关 (图 4B)。

Sec translocon, and ER-Golgi transport 秒转位子和内质网-高尔基体转运

We and others previously showed that RV weakly enriches factors related to membrane biology, in contrast to the functional use of membrane organelles like the ER by flaviviruses ([Fernandez-Garcia et al., 2009](#); [Mukhopadhyay et al., 2005](#); [Ooi et al., 2019](#)). Given the strong dependence of flaviviruses on the translocon, the channel for nascent peptide entry into the ER, we examined these factors ([Figure 4C](#)). We found that while SARS-CoV-2 does enrich ER-tethered (RRBP1) or associated (HDLBP/vigilin) RBPs, it is less strongly associated with the ER-targeting complex (SRP) or the Sec translocon itself. However, SARS-CoV-2's vRNA associates with the COPI vesicle complexes in a more similar manner to the flaviviruses. COPI proteins are canonically responsible for retrograde transport of vesicles from the Golgi to ER ([Szul and Sztul,](#)

2011). The association with COPI complex members is consistent with the reported cycling of SARS-CoV in the ER-Golgi network for eventual budding into the lumen ER-Golgi intermediate compartment (ERGIC; McBride et al., 2007).

我们和其他人之前表明，与黄病毒对 ER 等膜细胞器的功能性使用相比，RV 微弱地富集了与膜生物学相关的因子 (Fernandez-Garcia 等, 2009; Mukhopadhyay 等, 2005; Ooi 等, 2019)。鉴于黄病毒对易位子 (新生肽进入内质网的通道) 的强烈依赖性，我们检查了这些因素 (图 4C)。我们发现，虽然 SARS-CoV-2 确实丰富了 ER 系留 (RRBP1) 或相关 (HDLBP/vigilin) RBP，但它与 ER 靶向复合物 (SRP) 或 Sec 转位子本身的相关性较低。然而，SARS-CoV-2 的 vRNA 与 COPI 囊泡复合物的结合方式与黄病毒更相似。COPI 蛋白规范地负责囊泡从高尔基体到内质网的逆行运输 (Szul 和 Sztul, 2011)。与 COPI 复合体成员的关联与 ER-高尔基体网络中报道的 SARS-CoV 循环一致，最终萌芽到内腔 ER-高尔基体中间隔室 (ERGIC; McBride 等, 2007)。

N⁶-methyladenosine N6-甲基腺苷

Post-transcriptional modification of RNA is a broadly used regulatory mechanism, and among many, methylation of the N-6 position on adenine (m6A) has received renewed interest (Yue et al., 2015; Zaccara et al., 2019). Recently, it has been reported that m6A is deposited on the ZIKV vRNA contributing to an anti-viral response via binding of YTH family proteins (which recognize m6A) and degradation of the ZIKV vRNA (Lichinchi et al., 2016). We therefore examined the association of the writers (METTL family), readers (YTH family), and erasers (ALKBH family) of m6A with vRNA. We saw a robust association of the YTHDF family with ZIKV and DENV vRNAs (Figure 4D). RV also captured these proteins, while SARS-CoV-2 lacked robust enrichment of these factors. Conversely, we found relatively stronger enrichment of the m6A-demethylases associated with the SARS-CoV-2 vRNA, while ZIKV, DENV, and RV all poorly bound these proteins (Figure 4D).

RNA 的转录后修饰是一种广泛使用的调节机制，其中腺嘌呤 (m6A) 上 N-6 位的甲基化重新引起了人们的兴趣 (Yue 等人, 2015 年; Zaccara 等人, 2019 年)。最近，有报道称 m6A 沉积在 ZIKV vRNA 上，通过结合 YTH 家族蛋白 (识别 m6A) 和降解 ZIKV vRNA (Lichinchi 等, 2016)，有助于抗病毒反应。因此，我们检查了 m6A 的写入器 (METTL 家族)、读取器 (YTH 家族) 和擦除器 (ALKBH 家族) 与 vRNA 的关联。我们看到 YTHDF 家族与 ZIKV 和 DENV vRNA 之间存在很强的关联 (图 4D)。RV 也捕获了这些蛋白质，而 SARS-CoV-2 缺乏对这些因素的强大富集。相反，我们发现与 SARS-CoV-2 vRNA 相关的 m6A 去甲基化酶的富集相对较强，而 ZIKV、DENV 和 RV 都与这些蛋白质结合较差 (图 4D)。

Intracellular vesicles and trafficking 细胞内囊泡和运输

Lastly, we explored intracellular vesicle and trafficking complexes, given evidence of intracellular double-membrane vesicles produced during the SARS-CoV-2 life cycle

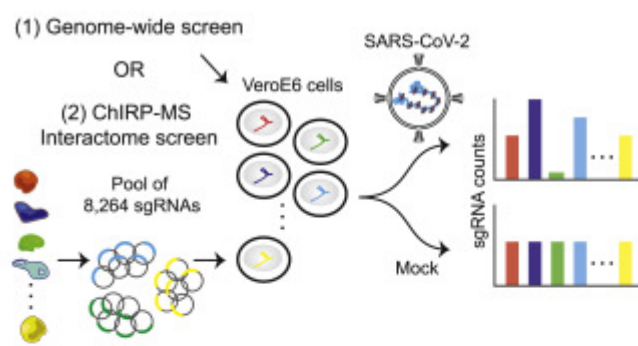
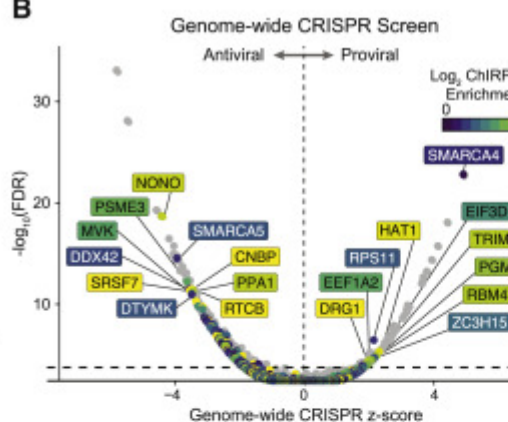
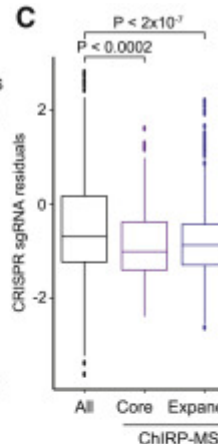
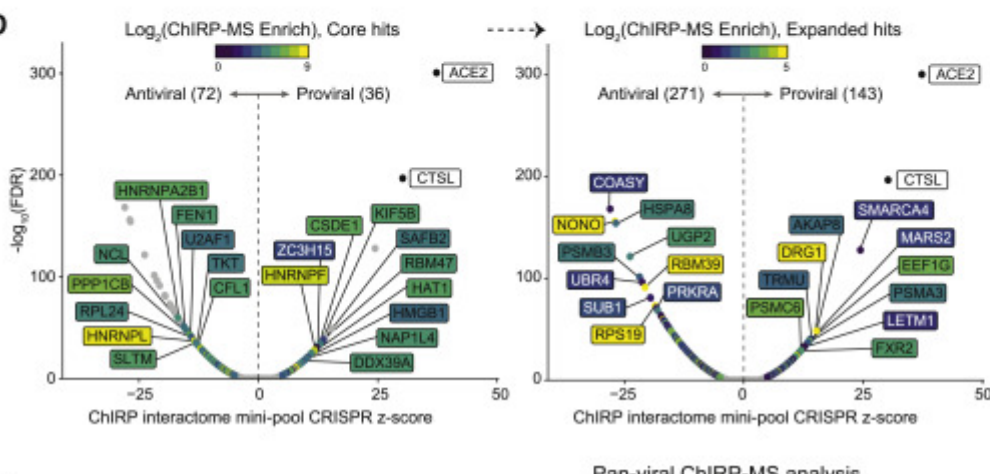
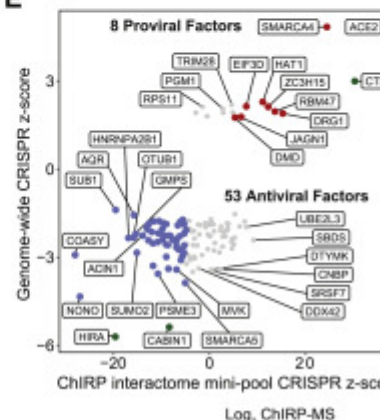
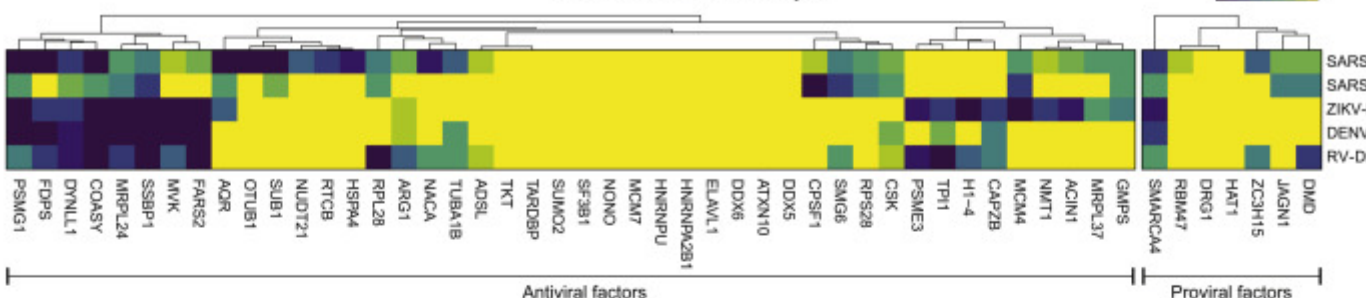
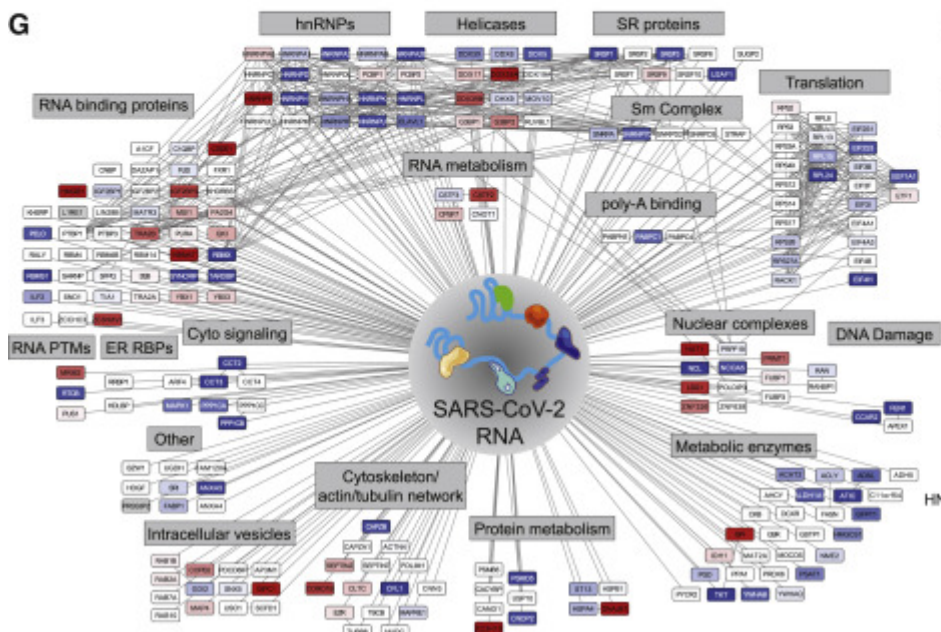
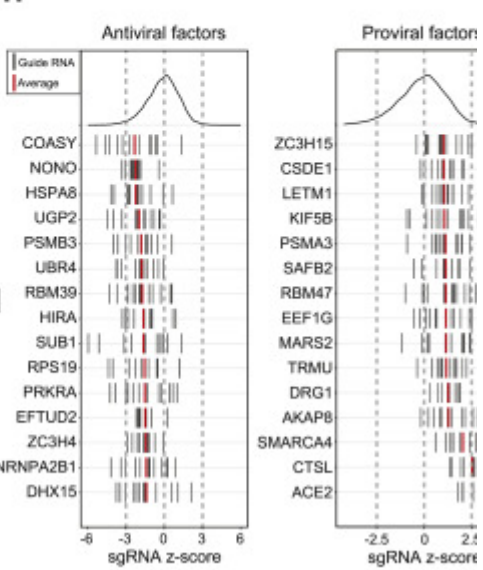
(Wolff et al., 2020). We found many host factors involved in cytokinesis, actin filaments, cytoskeleton, and microtubules were most strongly associated with the SARS-CoV-2 vRNA (Figure 4E). Recent reports highlighted the physical association of Rab GTPase family members with viral proteins and their functional importance in the temperature-dependent life cycle of coronaviruses (Gordon et al., 2020; Hoffmann et al., 2021). The ChIRP-MS data support these observations; four Rab proteins, RAB1B, RAB2A, RAB7A, and RAB10, were present in the SARS-CoV-2 high-confidence interactome (Figure 2D), with multiple others strongly associated with the SARS-CoV-2 vRNA (Figure 4E).

最后，我们探索了细胞内囊泡和运输复合物，有证据表明在 SARS-CoV-2 生命周期中产生了细胞内双膜囊泡（Wolff 等人，2020 年）。我们发现参与胞质分裂、肌动蛋白丝、细胞骨架和微管的许多宿主因子与 SARS-CoV-2 vRNA 的相关性最强（图 4E）。最近的报告强调了 Rab GTPase 家族成员与病毒蛋白的物理关联及其在冠状病毒温度依赖性生命周期中的功能重要性（Gordon 等人，2020 年；Hoffmann 等人，2021 年）。ChIRP-MS 数据支持这些观察结果；四种 Rab 蛋白 RAB1B、RAB2A、RAB7A 和 RAB10 存在于 SARS-CoV-2 高置信度相互作用组中（图 2D），其他多种蛋白与 SARS-CoV-2 vRNA 密切相关（图 4E）。

Genome-wide and targeted CRISPR screens of the SARS-CoV-2 interactome reveal functions of RNA-protein interactions SARS-CoV-2 相互作用组的全基因组和靶向 CRISPR 筛选揭示了 RNA-蛋白质相互作用的功能

To understand the functional role of SARS-CoV-2 RBPs in host infection, we used CRISPR-knockout (KO) perturbation screens. First, we intersected the ChIRP-MS interactome with genome-wide CRISPR perturbation data from our previous study (Wei et al., 2021). Second, we designed a custom pool of sgRNAs targeting the SARS-CoV-2 expanded interactome compatible with both human and monkey cells by intersecting the genome-wide sgRNA designs for *Homo sapiens* and *Chlorocebus sabaeus*. We included control sgRNAs targeting known proviral factors, *ACE2* and *CTSL*, and control sgRNAs targeting known antiviral factors, *HIRA* and *CABIN1*, as well as 100 non-targeting negative controls and 100 single-targeting negative controls. In total, our final custom sgRNA pool consisted of 8,264 sgRNAs targeting 1,331 of the 1,470 (90.5%) SARS-CoV-2 expanded interactome proteins, which we used to perform a screen for factors that impact virus-induced cell death (Table S4). The genome-wide screen and targeted interactome screens were both performed in Vero E6 cells using our previously developed screening protocol to identify putative pro- and antiviral host factors (Figure 5A). In this assay, KO of proviral factors causes resistance to virus-induced cell death and enrichment of their associated targeting sgRNAs, while KO of antiviral factors causes sensitization to virus-induced cell death and depletion of their associated targeting sgRNAs.

为了了解 SARS-CoV-2 RBP 在宿主感染中的功能作用，我们使用了 CRISPR 敲除 (KO) 扰动筛选。首先，我们将 ChIRP-MS 相互作用组与我们之前研究 (Wei 等人, 2021) 中的全基因组 CRISPR 扰动数据相交。其次，我们设计了一个定制的 sgRNA 池，该池针对 SARS-CoV-2 扩展的相互作用组，通过与智人和 *Chlorocebus sabaeus* 的全基因组 sgRNA 设计相交，与人和猴细胞兼容。我们包括靶向已知前病毒因子 ACE2 和 CTSL 的对照 sgRNA，以及靶向已知抗病毒因子 HIRA 和 CABIN1 的对照 sgRNA，以及 100 个非靶向阴性对照和 100 个单靶向阴性对照。总的来说，我们最终的定制 sgRNA 池由 8,264 个 sgRNA 组成，针对 1,470 (90.5%) 个 SARS-CoV-2 扩增的相互作用组蛋白中的 1,331 个，我们用来筛选影响病毒诱导细胞死亡的因素 (表 S4)。全基因组筛选和靶向相互作用组筛选均使用我们之前开发的筛选方案在 Vero E6 细胞中进行，以确定推定的促病毒和抗病毒宿主因子 (图 5A)。在该测定中，前病毒因子的 KO 导致对病毒诱导的细胞死亡的抗性及其相关靶向 sgRNA 的富集，而抗病毒因子的 KO 导致对病毒诱导的细胞死亡的敏感性及其相关靶向 sgRNA 的消耗。

A**B****C****D****E****F****G****H**

Download : Download high-res image (2MB) 下载 : 下载高分辨率图像 (2MB)

Download : Download full-size image 下载 : 下载全尺寸图片

Figure 5. Integration of ChIRP-MS and genome-wide and targeted interactome CRISPR screens identify pro- and antiviral host factors

图 5. ChIRP-MS 与全基因组和靶向相互作用组 CRISPR 筛选的整合识别前病毒和抗病毒宿主因子

(A) CRISPR screen schematic for genome-wide and targeted interactome screens.

(A) 全基因组和靶向相互作用组筛选的 CRISPR 筛选示意图。

(B) Expanded SARS-CoV-2 interactome overlaid on genome-wide CRISPR screen data.

(B) 覆盖在全基因组 CRISPR 屏幕数据上的扩展的 SARS-CoV-2 相互作用组。

(C) Comparison of sgRNA residuals for significant hits ($FDR \leq 0.05$) of all sgRNAs (left, black, $n = 3,189$), sgRNAs targeting genes present in the high-confidence SARS-CoV-2 RNA interactome (purple, middle, $n = 132$), or sgRNAs targeting genes present in the expanded SARS-CoV-2 RNA interactome (right, blue, $n = 400$). p values computed from Mann-Whitney test.

(C) 所有 sgRNA (左 , 黑色 , $n = 3,189$) 的显着命中 ($FDR \leq 0.05$) 的 sgRNA 残差比较 , sgRNA 靶向存在于高置信度 SARS-CoV-2 RNA 相互作用组中的基因 (紫色 , 中间 , $n = 132$) , 或 sgRNAs 靶向存在于扩大的 SARS-CoV-2 RNA 相互作用组中的基因 (右 , 蓝色 , $n = 400$) 。从 Mann-Whitney 检验计算的 p 值。

(D) Focused interactome screening results for the high-confidence interactome (left) and the rest of the expanded interactome (right).

(D) 高置信度交互组 (左) 和其余扩展交互组 (右) 的聚焦交互组筛选结果。

(E) Expanded interactome mini-pool results for hits identified in the genome-wide screen, showing proviral hits (red), antiviral hits (blue), or positive controls (green).

(E) 全基因组筛选中确定的点击的扩展交互组迷你池结果 , 显示前病毒点击 (红色) 、抗病毒点击 (蓝色) 或阳性对照 (绿色) 。

(F) Cytoscape network colored by enrichment or depletion in CRISPR screen.

(F) 通过 CRISPR 屏幕中的富集或消耗着色的 Cytoscape 网络。

(G) sgRNA Z scores for top mini-pool CRISPR hits. Individual CRISPR guides are represented by black lines. The average of these is shown in red.

(G) 顶级迷你池 CRISPR 命中的 sgRNA Z 分数。单个 CRISPR 指南由黑线表示。这些的平均值以红色显示。

(H) Inter-virus ChIRP-MS comparison of human ChIRP-MS/CRISPR hits identified in (E).

(H) (E) 中鉴定的人类 ChIRP-MS/CRISPR 命中的病毒间 ChIRP-MS 比较。

We first examined the genome-wide screening data and calculated CRISPR Z scores for the core (309) and expanded (1,430) host-protein interactomes identified by ChIRP-MS. We identified 131 factors (33 core factors and 98 expanded factors) that had a functional impact on host cell survival after SARS-CoV-2 infection ($FDR \leq 0.05$; [Figure 5B](#)). Strikingly, we observed a significant bias for overlapping factors to have antiviral function (29/33 core factors and 87/98 expanded factors), compared to the distribution of all hits in the genome-wide screen. These results suggest that a large fraction of intracellular vRNA-host protein interactions may represent the host cell's attempt to

prevent or combat viral pathogenicity, rather than proviral host pathways co-opted by the virus (Figure 5C).

我们首先检查了全基因组筛选数据并计算了由 ChIRP-MS 鉴定的核心 (309) 和扩展的 (1,430) 宿主-蛋白质相互作用组的 CRISPR Z 分数。我们确定了 131 个因素 (33 个核心因素和 98 个扩展因素) 对 SARS-CoV-2 感染后宿主细胞的存活有功能影响 (FDR ≤ 0.05; 图 5B)。引人注目的是，与全基因组筛选中所有命中的分布相比，我们观察到重叠因子具有抗病毒功能的显着偏差 (29/33 核心因子和 87/98 扩展因子)。这些结果表明，大部分细胞内 vRNA-宿主蛋白相互作用可能代表宿主细胞试图预防或对抗病毒致病性，而不是病毒选择的前病毒宿主途径 (图 5C)。

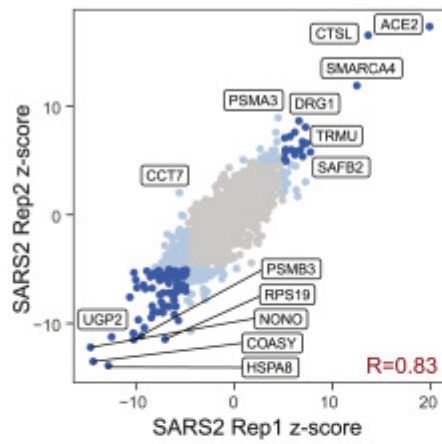
We previously demonstrated that a CRISPR mini-pool approach can provide further validation of genome-wide hits and increased sensitivity for the discovery of functional SARS-CoV-2 factors, due to a smaller sgRNA pool with more sgRNAs per gene (Wei et al., 2021). Therefore, we performed a SARS-CoV-2 survival screen using the expanded interactome CRISPR mini-pool (Figure 5A). We observed a high correlation of gene Z scores between biological replicates (Figure S5A, left), which were then merged. Using a conservative significance threshold (FDR ≤ 0.001), we identified 179 proviral factors (13.4% of the mini-pool) and 343 antiviral factors (25.8% of the mini-pool), and 108 of these functional factors were present in the core interactome (Figure 5D). We compared the mini-pool and genome-wide screens and identified 8 proviral factors and 53 antiviral factors that were hits in both screens (Figure 5E). We were particularly interested in the validated proviral hits since they may have direct relevance as therapeutic targets. We recently validated PFI-3, an inhibitor of SMARCA4 (the top proviral CRISPR hit in our interactome screen), as an inhibitor of viral replication *in vitro* (Wei et al., 2021), and drug targets nominated by PPI studies have also yielded promising candidates for SARS-CoV-2 (Gordon et al., 2020; White et al., 2021). To expand this analysis to additional compounds, particularly clinically approved compounds that may be amenable to drug repurposing, we compared the expanded ChIRP-MS interactome with known drug compound-target protein interactions and identified a list of 113 interactome proteins targeted by 275 compounds (Table S7). Focusing on CRISPR-validated proviral factors identified clofarabine as among the top drug candidates, and this compound has indeed been shown to have activity against SARS-CoV-2 in candidate drug screens (Table S7; Janes et al., 2018).

我们之前已经证明，由于每个基因具有更多 sgRNA 的较小 sgRNA 池，CRISPR 迷你池方法可以进一步验证全基因组命中并提高发现功能性 SARS-CoV-2 因子的敏感性 (Wei et al., 2021)。因此，我们使用扩展的交互组 CRISPR 迷你池进行了 SARS-CoV-2 生存筛选 (图 5A)。我们观察到生物复制之间基因 Z 分数的高度相关性 (图 S5A, 左)，然后将其合并。使用保守的显着性阈值 (FDR ≤ 0.001)，我们确定了 179 个前病毒因子 (微型库的 13.4%) 和 343 个抗病毒因子 (微型库的 25.8%)，其中 108 个功能因子存在于核心中交互组 (图 5D)。我们比较了小型池筛选和全基因组筛选，并确定了 8 个前病毒因

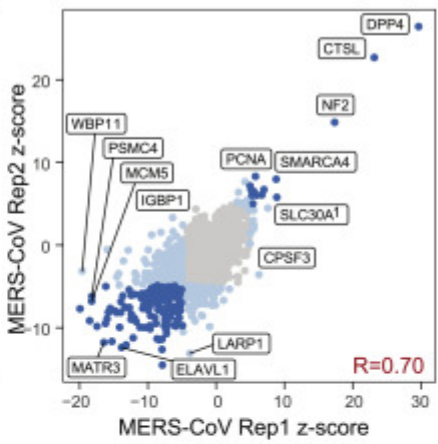
子和 53 个抗病毒因子，在这两个筛选中都被命中（图 5E）。我们对经过验证的前病毒命中特别感兴趣，因为它们可能与治疗靶点直接相关。我们最近验证了 PFI-3，一种 SMARCA4 抑制剂（在我们的交互组筛选中排名靠前的前病毒 CRISPR），作为体外病毒复制的抑制剂（Wei 等人，2021 年），并且 PPI 研究提名的药物靶点也产生了 SARS-CoV-2 的有希望的候选者（Gordon 等人，2020 年；White 等人，2021 年）。为了将此分析扩展到其他化合物，特别是可能适合药物再利用的临床批准化合物，我们将扩展的 ChIRP-MS 相互作用组与已知的药物化合物-靶蛋白相互作用进行了比较，并确定了 275 种化合物靶向的 113 种相互作用蛋白的列表（表 S7）。着眼于 CRISPR 验证的前病毒因子，将氯法拉滨确定为顶级候选药物之一，并且在候选药物筛选中确实显示该化合物具有抗 SARS-CoV-2 的活性（表 S7；Janes 等人，2018 年）。

A

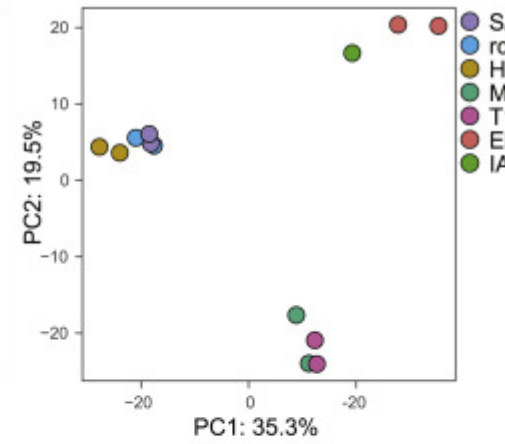
ChIRP-MS Interactome CRISPR Screen QC



- Discordant CRISPR hit
- Concordant CRISPR hit

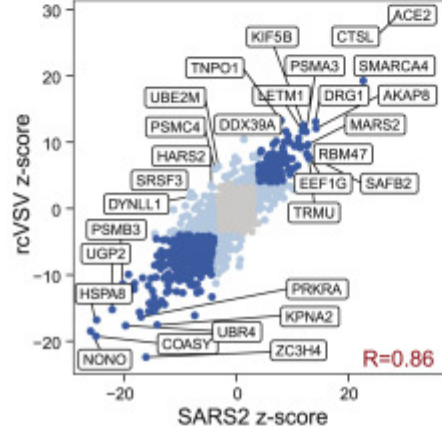


B

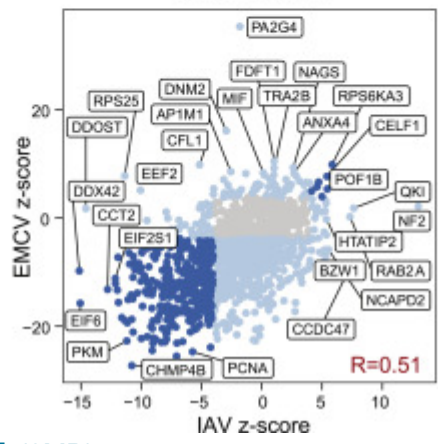
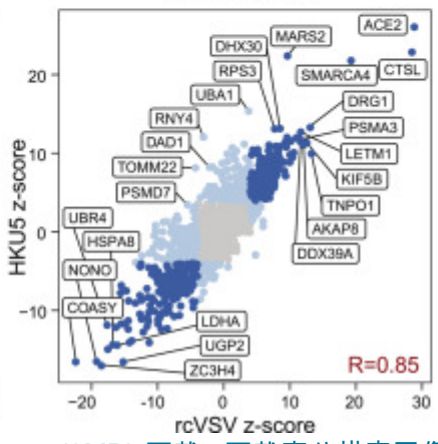
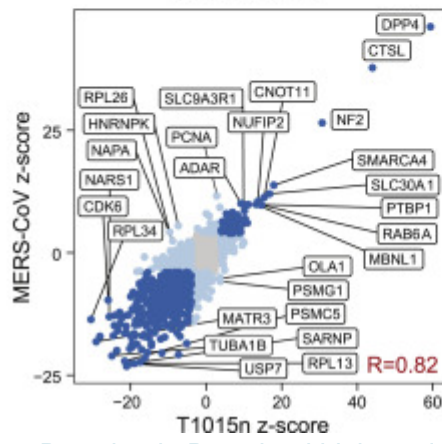
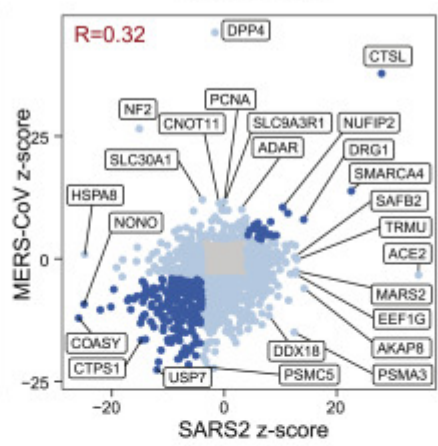
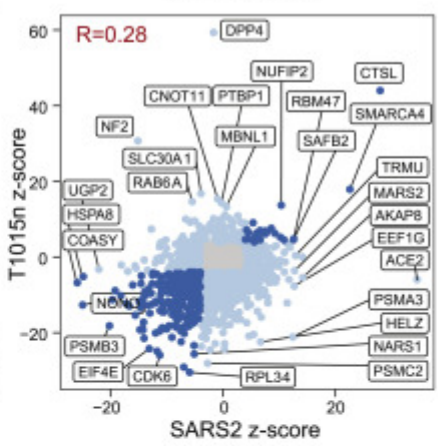
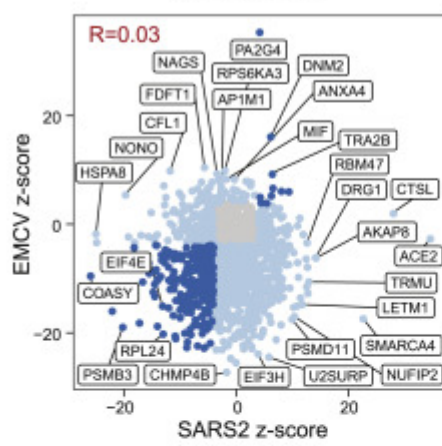
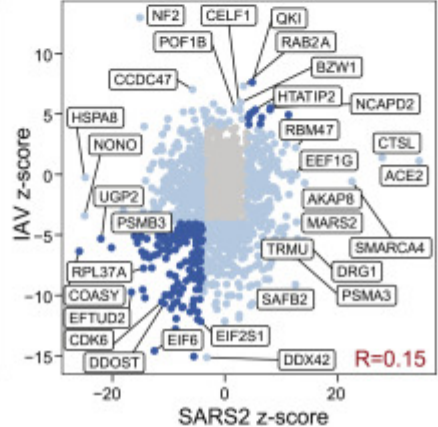
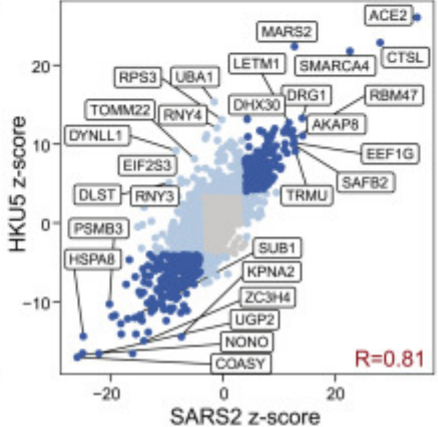


C

Expanded ChIRP-MS Mini-Pool Correlations



- Discordant CRISPR hit
- Concordant CRISPR hit



Download : Download high-res image (2MB) 下载 : 下载高分辨率图像 (2MB)

Download : Download full-size image 下载 : 下载全尺寸图片

Figure S5. Correlation analysis of expanded interactome CRISPR mini-pool screens, related to Figure 5

图 S5。扩展的交互组 CRISPR 迷你池屏幕的相关性分析，与图 5 相关

(A) Replicate correlations for SARS-CoV-2 (left) and MERS (right) expanded interactome CRISPR mini-pool screens.

(A) SARS-CoV-2 (左) 和 MERS (右) 扩展交互组 CRISPR 迷你池屏幕的复制相关性。

(B) Principal component analysis of gene-level z-scores for all expanded interactome CRISPR mini-pool screen conditions and replicates.

(B) 所有扩展的交互组 CRISPR 迷你池筛选条件和复制的基因级 z 分数的主成分分析。

(C) Pairwise correlations of selected pairs of conditions.

(C) 选定条件对的成对相关性。

Analysis of antiviral hits revealed known factors that regulate the innate immune response, including NONO, TARDBP, DDX5, DDX6, and HNRNPA2B1. NONO is a member of the *Drosophila behavior/human splicing* (DBHS) protein family, which contains conserved N-terminal RNA recognition motifs, and has been demonstrated to directly bind vRNA and alter viral pathogenicity by impacting vRNA processing or by impacting innate immune gene expression ([Knott et al., 2016](#); [Lahaye et al., 2018](#); [Lenarcic et al., 2013](#)). For example, in human immunodeficiency virus (HIV), NONO acts as an activator of the DNA sensor, cGAS, to trigger innate immunity and the interferon response ([Lahaye et al., 2018](#)). In SARS-CoV-2 infection, NONO may function in a similar manner, albeit with RNA-sensing proteins or pathways. TARDBP has also been shown to display antiviral activity in the context of HIV infection by directly binding to a particular regulatory motif within the HIV-1 RNA genome and thereby repressing viral gene expression ([Ou et al., 1995](#)). Interestingly, subsequent work has demonstrated that TARDBP preferentially binds UGUGUG RNA motifs, and a search of the SARS-CoV-2 genomic RNA found 11 UGUGUG motifs in the sense strand. Extending this concept, we found that the majority of validated hits were physically associated with multiple RNA viruses ([Figure 5F](#)), while a small subset showed SARS-CoV-2 specificity ([Figure 5F](#)). Finally, we analyzed the CRISPR hits in the context of the Cytoscape network and observed that many of the functional hits were RBPs, helicases, and hnRNPs, which bind the vRNA early during infection, suggesting that the host's initial response to viral infection is to mount a diverse vRNA recognition program to restrict the viral life cycle ([Figure 5G](#)). Examining all hits, we identified COASY, HSPA8, UGP2, PSMB3, and UBR4 as top antiviral factors ([Figure 5H](#), left) and SMARCA4, AKAP8, DRG1, and TRMU as top proviral factors ([Figure 5H](#), right). In summary, the genome-wide and mini-pool strategies provide independent functional validation of ChIRP-MS data and nominate pro- and antiviral factors in SARS-CoV-2 pathogenesis.

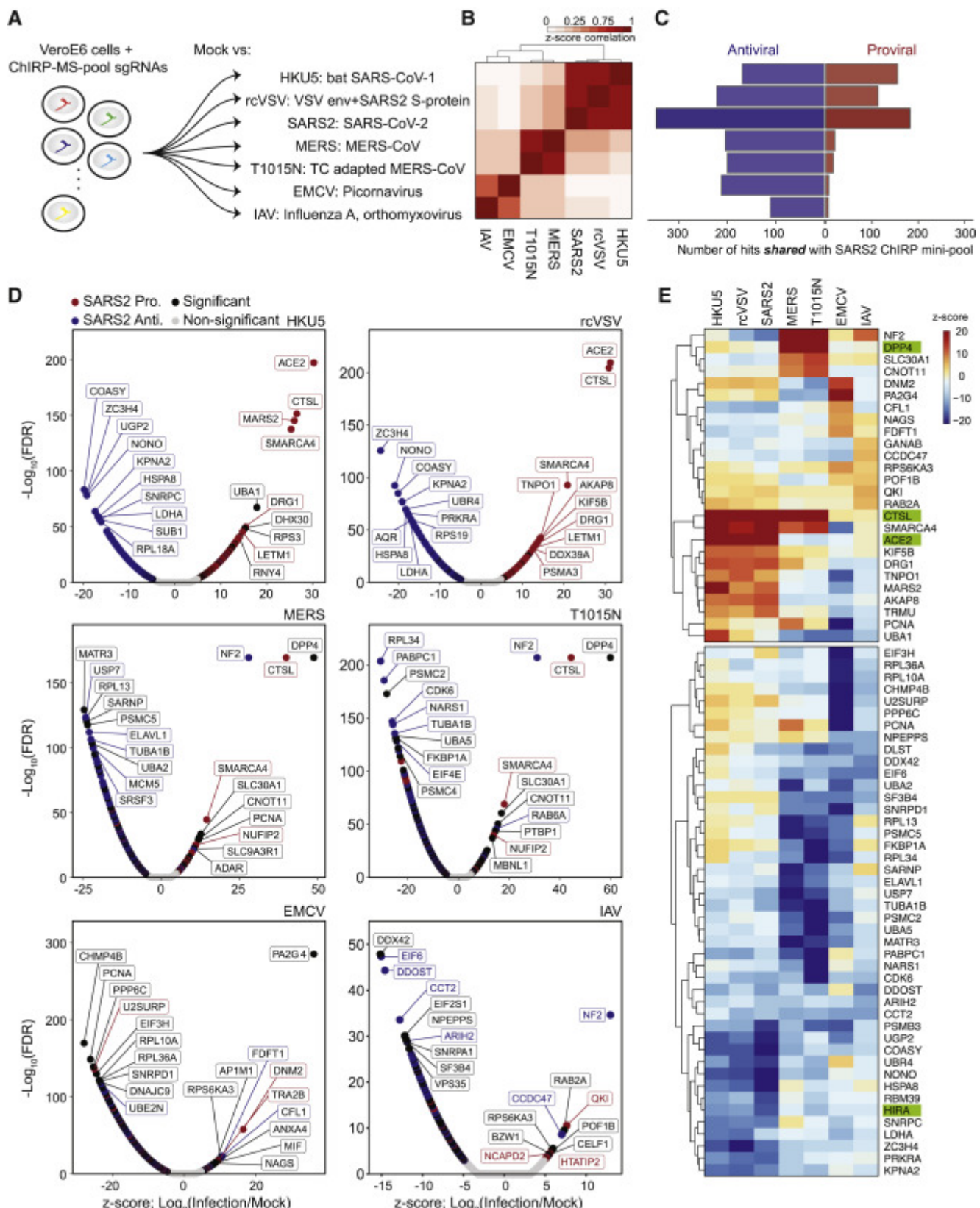
对抗病毒药物的分析揭示了调节先天免疫反应的已知因素，包括 NONO、TARDBP、DDX5、DDX6 和 HNRNPA2B1。NONO 是果蝇行为/人类剪接 (DBHS) 蛋白家族的成员，其中包含保守的 N 端 RNA 识别基序，并且已被证明可以通过影响 vRNA 加工或通过影响先天免疫基因表达直接结合 vRNA 并改变病毒的致病性 (Knott 等人, 2016 年；Lahaye 等人, 2018 年；Lenarcic 等人, 2013 年)。例如，在人类免疫缺陷病毒 (HIV) 中，NONO 充当 DNA 传感器 cGAS 的激活剂，以触发先天免疫和干扰素反应 (Lahaye 等, 2018)。在 SARS-CoV-2 感染中，NONO 可能以类似的方式发挥作用，尽管是通过 RNA 感应蛋白或通路。通过直接结合 HIV-1 RNA 基因组内的特定调控基序，TARDBP 也被证明在 HIV 感染的背景下显示出抗病毒活性，从而抑制病毒基因表达 (Ou 等, 1995)。有趣的是，随后的工作表明 TARDBP 优先结合 UGUGUG RNA 基序，对 SARS-CoV-2 基因组 RNA 的搜索在有义链中发现了 11 个 UGUGUG 基序。扩展这一概念，我们发现大多数经验证的命中与多种 RNA 病毒在物理上相关 (图 5F)，而一小部分显示出 SARS-CoV-2 特异性 (图 5F)。最后，我们在 Cytoscape 网络的背景下分析了 CRISPR 命中，并观察到许多功能性命中是 RBP、解旋酶和 hnRNP，它们在感染早期结合 vRNA，表明宿主对病毒感染的初始反应是用于限制病毒生命周期的多样化 vRNA 识别程序 (图 5G)。检查所有命中，我们将 COASY、HSPA8、UGP2、PSMB3 和 UBR4 确定为顶级抗病毒因子 (图 5H, 左)，将 SMARCA4、AKAP8、DRG1 和 TRMU 确定为顶级前病毒因子 (图 5H, 右)。总之，全基因组和迷你池策略提供了对 ChIRP-MS 数据的独立功能验证，并在 SARS-CoV-2 发病机制中指定了促病毒和抗病毒因素。

An expanded view of vRNA-associated factors across multiple RNA viruses 多种 RNA 病毒中 vRNA 相关因素的扩展视图

Since SARS-CoV-2 RBPs are broadly expressed in tissues and many are bound by other RNA viruses, we hypothesized that they may have functional roles in other viral infections. We performed the CRISPR mini-pool screen in six additional RNA viruses: (1) HKU5: a bat betacoronavirus using the SARS-CoV-1 spike protein for entry (a model of SARS-CoV-1), (2) rcVSV-SARS-CoV-2-S: a vesicular stomatitis virus (VSV) with an envelope engineered to use SARS-CoV-2 spike protein for entry, (3) Middle East respiratory syndrome coronavirus, MERS-CoV: another related betacoronavirus, (4) T1015N: a tissue culture-adapted form of MERS-CoV ([Agnihothram et al., 2014](#); [Scobey et al., 2013](#)), (5) encephalomyocarditis virus (EMCV): a non-enveloped picornavirus with a positive-polarity ssRNA genome, and (6) influenza A virus (IAV): an enveloped orthomyxovirus with a negative-polarity ssRNA genome ([Figure 6A; Wei et al., 2021](#))。These viruses contain diverse viral envelopes, genome polarities, and varying degrees of sequence similarity to the SARS-CoV-2 genome and enabled the analysis of shared and SARS-specific pro- and antiviral RNA-binding host factors.

由于 SARS-CoV-2 RBP 在组织中广泛表达，并且许多与其他 RNA 病毒结合，我们假设它们可能在其他病毒感染中具有功能作用。我们对另外六种 RNA 病毒进行了 CRISPR 迷你池筛选：(1) HKU5：一种使用 SARS-CoV-1 刺突蛋白进入的蝙蝠冠状病毒 (SARS-CoV-1)

的模型），(2) rcVSV-SARS-CoV-2-S：一种水泡性口炎病毒(VSV)，其包膜设计为使用SARS-CoV-2刺突蛋白进入，(3) 中东呼吸综合征冠状病毒，MERS-CoV：另一种相关的 β 冠状病毒，(4) T1015N：MERS-CoV的组织培养适应形式(Agnihothram等人，2014年；Scobey等人，2013年)，(5) 脑心肌炎病毒(EMCV)：一种具有正极性ssRNA基因组的无包膜小核糖核酸病毒，(6) 甲型流感病毒(IAV)：一种具有负极性ssRNA基因组的包膜正粘病毒(图6A；Wei等，2021)。这些病毒包含不同的病毒包膜、基因组极性以及与SARS-CoV-2基因组不同程度的序列相似性，并且能够分析共享的和SARS特异性的前病毒和抗病毒RNA结合宿主因子。



Download : Download high-res image (1MB) 下载 : 下载高分辨率图像 (1MB)

Download : Download full-size image 下载 : 下载全尺寸图片

Figure 6. SARS-CoV-2 ChIRP-MS interactome CRISPR screen in a panel of seven RNA viruses
图 6. 一组七种 RNA 病毒中的 SARS-CoV-2 ChIRP-MS 相互作用组 CRISPR 筛选

(A) CRISPR screen schematic.

(A) CRISPR 屏幕示意图。

(B) Correlation of gene Z scores for each condition.

(B) 每种条件下基因 Z 分数的相关性。

(C) Number of proviral and antiviral hits ($FDR \leq 0.001$) overlapping with the SARS-CoV-2 hits ($FDR \leq 0.001$) for all conditions.

(C) 在所有条件下，与 SARS-CoV-2 命中 ($FDR \leq 0.001$) 重叠的前病毒和抗病毒命中数 ($FDR \leq 0.001$)。

(D) Volcano plot for each condition.

(D) 每种条件的火山图。

(E) CRISPR Z scores for top hits for each virus. Top: proviral hits. Bottom: antiviral hits. Positive controls indicated in green.

(E) CRISPR Z 得分为每个病毒的最高命中。顶部：前病毒式命中。底部：抗病毒命中。阳性对照以绿色表示。

We first analyzed the technical quality of these screens and observed a high correlation of Z scores between biological replicates, which were then merged (Figures S5A and S5B). Next, we performed PCA analysis to understand the global similarity of gene Z scores across viruses, and we observed that the conditions clustered according to entry pathway (Figure 6B). Namely, SARS-CoV-2, HKU5, and rcVSV all require ACE2 for cell entry, while MERS and T1015N require DPP4 (Figures 6B, 6C, and S5B). In line with these observations, we compared functional conservation of SARS-CoV-2 pro- and antiviral genes in each additional RNA virus screen, which demonstrated that proviral hits were largely unique within virus families (and related to viral entry). In contrast, many SARS-CoV-2 antiviral factors were shared across viruses (25 antiviral factors shared across all viruses, 88 shared across SARS and MERS viruses; Figures 6C, 6D, and S5C; Table S6). We visualized the results of each screen in individual volcano plots, which highlighted top concordant and discordant hits between SARS-CoV-2 and other viruses (Figure 6D). Although each factor was present in the SARS-CoV-2 interactome, some showed specific function in other viruses, such as the RNA helicase DHX30 (HKU5), and PA2G4 (EMCV; Baggen et al., 2019; Bazzoni et al., 2019; Figure 6D). To more closely examine the conserved or divergent functions of highly scoring factors across viruses, we analyzed the top pro- and antiviral factors for each virus (Figure 6E). Among proviral factors, we first confirmed the expected specificity of the entry receptors, ACE2 and DPP4, for SARS and MERS viruses, respectively. Next, unbiased clustering revealed several proviral factors that were highly specific to SARS-related viruses (e.g., DRG1, TNPO1, MARS2, and AKAP8), MERS-related viruses (e.g., NF2 and SLC30A1), IAV (e.g., GANAB and CCDC47), and EMCV (DNM2 and PA2G4). In contrast to proviral factors, we observed a much greater degree of overlap of antiviral factors across viruses. We could still observe factors with antiviral specificity for viral families, for example KPNA2, ZC3H4, NONO, UGP2, and COASY in SARS-related viruses, and SARNP, USP7, RPL13, and MATR3 in MERS-related viruses. However, we also observed

a class of factors with antiviral activity conserved across virus families, and even in all viruses, including ARIH2, CCT2, and PSMB3. In summary, our focused mini-pool approach (1) validated selected functional hits identified from the genome-wide screen, (2) expanded the functional set of SARS-CoV-2 RNA-binding host proteins, particularly those with antiviral activity, and (3) established the virus-specific logic for each factor.

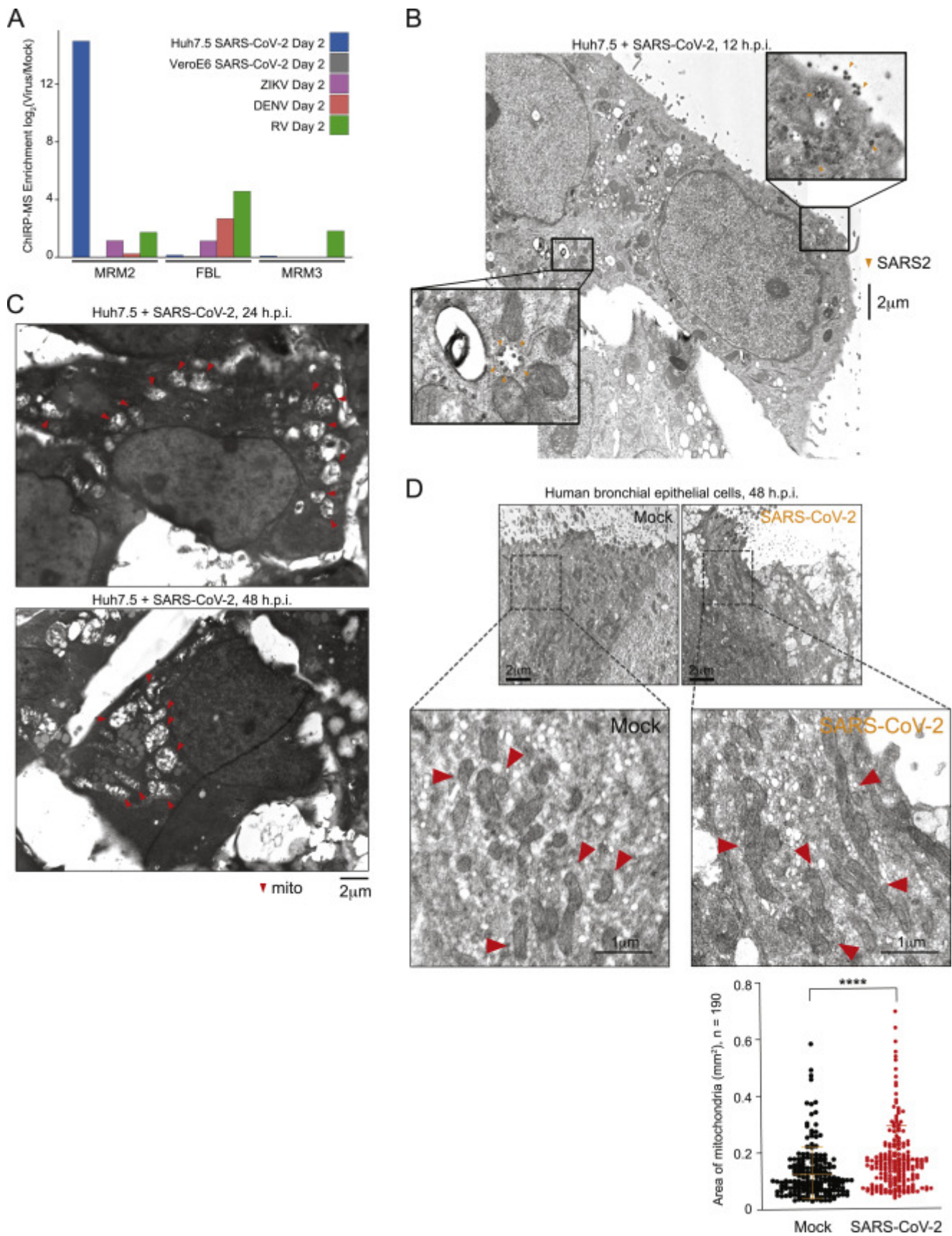
我们首先分析了这些屏幕的技术质量，并观察到生物重复之间 Z 分数的高度相关性，然后将其合并（图 S5A 和 S5B）。接下来，我们进行了 PCA 分析以了解病毒之间基因 Z 评分的全局相似性，我们观察到条件根据进入途径聚集（图 6B）。即，SARS-CoV-2、HKU5 和 rcVSV 都需要 ACE2 才能进入细胞，而 MERS 和 T1015N 需要 DPP4（图 6B、6C 和 S5B）。与这些观察结果一致，我们在每个额外的 RNA 病毒筛选中比较了 SARS-CoV-2 前病毒和抗病毒基因的功能保守性，这表明前病毒命中在病毒家族中在很大程度上是独一无二的（并且与病毒进入有关）。相比之下，许多 SARS-CoV-2 抗病毒因子在病毒之间共享（所有病毒共有 25 个抗病毒因子，SARS 和 MERS 病毒共有 88 个；图 6C、6D 和 S5C；表 S6）。我们在单个火山图中可视化了每个屏幕的结果，突出显示了 SARS-CoV-2 和其他病毒之间的最高一致性和不一致命中率（图 6D）。虽然每个因子都存在于 SARS-CoV-2 相互作用组中，但有些在其他病毒中显示出特定功能，例如 RNA 解旋酶 DHX30 (HKU5) 和 PA2G4 (EMCV；Baggen 等人，2019 年；Bazzzone 等人，2019 年；图 6D)。为了更仔细地检查跨病毒的高评分因子的保守或发散功能，我们分析了每种病毒的主要促病毒和抗病毒因子（图 6E）。在前病毒因素中，我们首先确认了进入受体 ACE2 和 DPP4 分别对 SARS 和 MERS 病毒的预期特异性。接下来，无偏聚类揭示了几个对 SARS 相关病毒（例如 DRG1、TNPO1、MARS2 和 AKAP8）、MERS 相关病毒（例如 NF2 和 SLC30A1）、IAV（例如 GANAB 和 CCDC47）高度特异性的前病毒因子和 EMCV（DNM2 和 PA2G4）。与前病毒因子相比，我们观察到病毒之间抗病毒因子的重叠程度要大得多。我们仍然可以观察到对病毒家族具有抗病毒特异性的因子，例如 SARS 相关病毒中的 KPNA2、ZC3H4、NONO、UGP2 和 COASY，以及 MERS 相关病毒中的 SARNP、USP7、RPL13 和 MATR3。然而，我们还观察到一类具有抗病毒活性的因子在病毒家族中保守，甚至在所有病毒中，包括 ARIH2、CCT2 和 PSMB3。总之，我们专注的迷你池方法 (1) 验证了从全基因组筛选中识别出的选定功能命中，(2) 扩展了 SARS-CoV-2 RNA 结合宿主蛋白的功能集，尤其是那些具有抗病毒活性的蛋白，以及(3) 为每个因素建立了病毒特定的逻辑。

An RNA-centric view of SARS-CoV-2 reveals a specific perturbation of mitochondria during infection SARS-CoV-2 的以 RNA 为中心的观点揭示了感染期间线粒体的特定扰动

Reexamining the list of vRNA-binding proteins, we noticed that MRM2 was the most strongly enriched host factor in Huh7.5 cells at 48 h.p.i. (Figure 2B). MRM2 is a mitochondrial-localized (nuclear-encoded) RNA 2'-O-methyltransferase (2'-O-MTase) and is of particular interest due to the previous characterization of FTSJ3/SPB1 (another 2'-O-MTase) as a factor that methylates the HIV RNA genome, which leads to proviral

shielding of the HIV RNA from MDA5 recognition (Ringeard et al., 2019). We asked whether this binding was specific to SARS-CoV-2 and if there were other 2'-O-MTases enriched in the ChIRP-MS data. MRM2 was highly selective for binding the SARS-CoV-2 RNA, while the nucleolar FBL was more enriched on DENV, ZIKV, and RV, and MRM3 was selective for RV (Figure S6A). To understand if the mitochondrial association of SARS-CoV-2 was supported by other aspects of the ChIRP data, we revisited the ChIRP-RNA-seq data that we initially used for quality control. We found a robust and consistent enrichment for the RNA components of the mitochondrial ribosome (mito-ribosome and 12S and 16S RNAs) in both Vero E6 and Huh7.5 cells (Figures S1B and S1C). This is consistent with a recent report that SARS-CoV-2 genomic RNAs, particularly the 5' untranslated region, contain sequence elements that strongly direct residency in mitochondria (Wu et al., 2020). The ChIRP RNA-seq also demonstrated recovery of a number of snoRNAs with the vRNAs in both Huh7.5 and Vero E6 cells (Figures S1B and S1C). SnoRNA-vRNA interactions and the importance of 2'-O-methylation has recently been independently validated by others (Yang et al., 2021). Together, our RNA-RNA and RNA-protein view of the SARS-CoV-2 vRNA highlight an association with the mitochondria and nominate specific RNA post-transcriptional modification enzymes within the organelle that may be important during infection.

重新检查 vRNA 结合蛋白的列表，我们注意到 MRM2 是 48 hpi 时 Huh7.5 细胞中最富集的宿主因子。（图 2B）。MRM2 是一种线粒体定位（核编码）RNA 2'-O-甲基转移酶（2'-O-MTase），并且由于先前对 FTSJ3/SPB1（另一种 2'-O-MTase）的表征而特别受关注一种使 HIV RNA 基因组甲基化的因素，这导致 HIV RNA 免受 MDA5 识别的前病毒保护（Ringeard 等，2019）。我们询问这种结合是否对 SARS-CoV-2 具有特异性，以及 ChIRP-MS 数据中是否富含其他 2'-O-MTase。MRM2 对结合 SARS-CoV-2 RNA 具有高度选择性，而核仁 FBL 在 DENV、ZIKV 和 RV 上更富集，而 MRM3 对 RV 具有选择性（图 S6A）。为了了解 SARS-CoV-2 的线粒体关联是否得到 ChIRP 数据其他方面的支持，我们重新审视了最初用于质量控制的 ChIRP-RNA-seq 数据。我们在 Vero E6 和 Huh7.5 细胞中发现了线粒体核糖体（线粒体核糖体和 12S 和 16S RNA）的 RNA 成分的稳健且一致的富集（图 S1B 和 S1C）。这与最近的一份报告一致，即 SARS-CoV-2 基因组 RNA，特别是 5' 非翻译区，包含强烈指导线粒体驻留的序列元件（Wu 等，2020）。ChIRP RNA-seq 还证明了在 Huh7.5 和 Vero E6 细胞中用 vRNA 回收了许多 snoRNA（图 S1B 和 S1C）。SnoRNA-vRNA 相互作用和 2'-O-甲基化的重要性最近已被其他人独立验证（Yang 等人，2021）。总之，我们对 SARS-CoV-2 vRNA 的 RNA-RNA 和 RNA-蛋白质视图突出了与线粒体的关联，并指定了细胞器内可能在感染过程中很重要的特定 RNA 转录后修饰酶。



Download : Download high-res image (2MB) 下载 : 下载高分辨率图像 (2MB)

Download : Download full-size image 下载 : 下载全尺寸图片

Figure S6. ChIRP-MS and electron microscopy analysis of mitochondria during SARS-CoV-2 infection, related to [Figure 6](#)

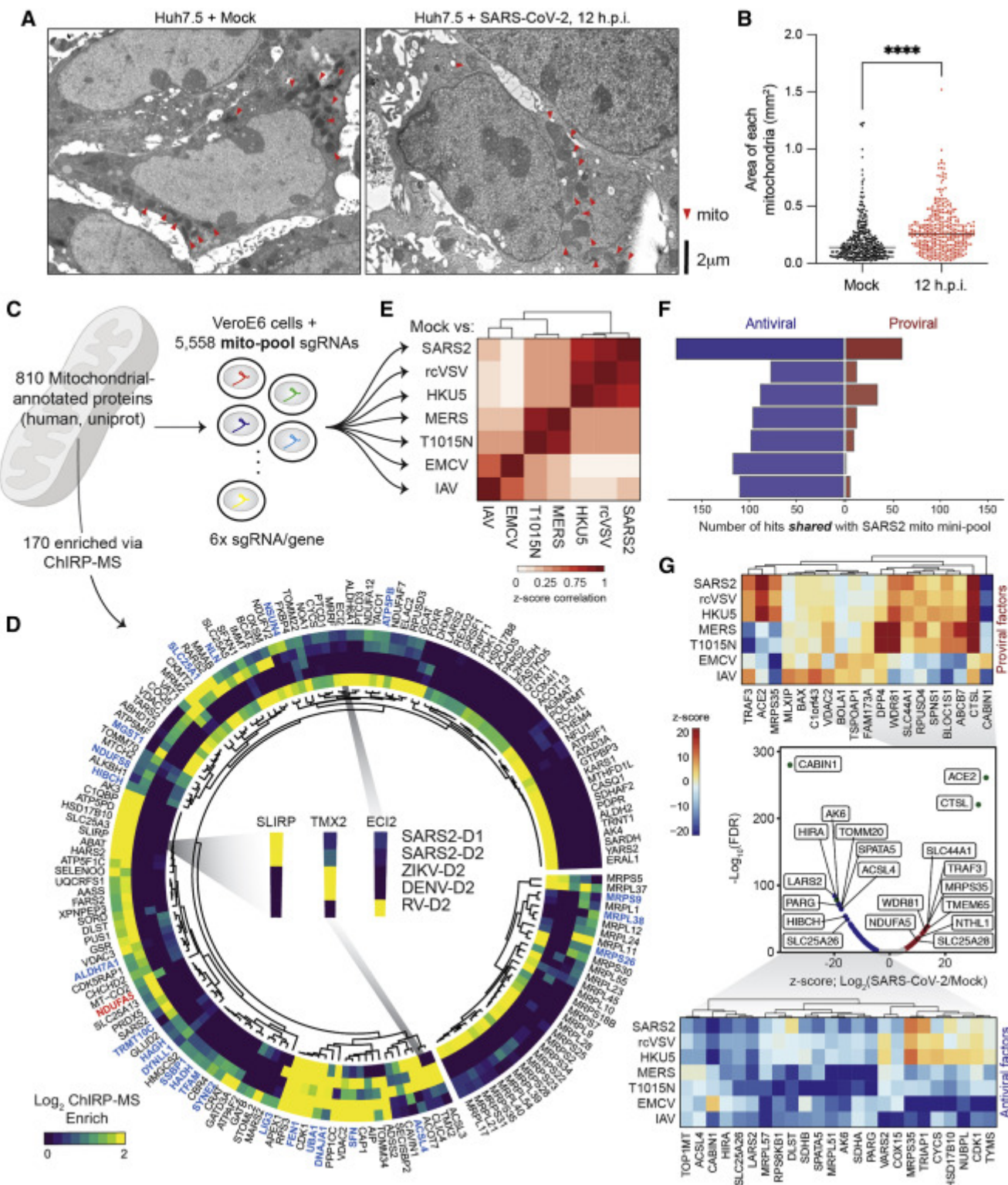
图 S6。SARS-CoV-2 感染期间线粒体的 ChIRP-MS 和电子显微镜分析，与图 6 相关

(A) ChIRP-MS enrichment of rRNA 2'-O-ribose methyltransferases across viruses.

- (A) ChIRP-MS 富集跨病毒的 rRNA 2'-O-核糖甲基转移酶。
- (B) Identification of SARS-CoV-2 virions (highlighted with orange arrow heads) in the 12 h.p.i. EM images, taken from the same samples as in [Figure 6](#) at different imaging depths.
(B) 在 12 hpi 中鉴定 SARS-CoV-2 病毒体（用橙色箭头突出显示）。EM 图像，取自与图 6 相同的样本，在不同的成像深度。
- (C) EM imaging of SARS-CoV-2 infected Huh7.5 cells at 24 and 48 h.p.i. Mitochondria are highlighted with red arrow heads.
(C) 感染 SARS-CoV-2 的 Huh7.5 细胞在 24 和 48 hpi 的 EM 成像。线粒体用红色箭头突出显示。
- (D) EM analysis of mitochondria in human bronchial epithelial cells (HBECs). Mitochondria are highlighted with red arrow heads. (D) Quantification of (C), n = 190 mitochondria in five infected or mock ciliated cells. P ≤ 0.001 by two-tailed Student's t test.
(D) 人支气管上皮细胞 (HBEC) 线粒体的 EM 分析。线粒体用红色箭头突出显示。 (D) 量化 (C) , n = 190 个受感染或模拟纤毛细胞中的线粒体。通过双尾学生 t 检验 , P ≤ 0.001。

We next assessed if there were morphological changes in the mitochondria over the course of SARS-CoV-2 infection. We performed electron microscopy of Huh7.5 cells infected with SARS-CoV-2 at different time points and quantified mitochondrial size. After 12 h.p.i., we found an increase in the average area of the mitochondria in infected cells ([Figures 7A](#) and [S7B](#)). At 24 h.p.i., mitochondria continued to increase in size, eventually leading to gross damage at 48 h.p.i. ([Figure S7C](#)). To confirm this observation in human lung cells, we examined previously published electron microscopy data ([Ravindra et al., 2020](#)) of SARS-CoV-2-infected HBECs (48 h.p.i.) and again found a significant increase in average mitochondrial size in cells infected with SARS-CoV-2 ([Figure S7D](#)). Altogether, these results suggest altered mitochondrial homeostasis during SARS-CoV-2 infection.

我们接下来评估了在 SARS-CoV-2 感染过程中线粒体是否存在形态学变化。我们在不同时间点对感染 SARS-CoV-2 的 Huh7.5 细胞进行了电子显微镜检查，并量化了线粒体大小。12 hpi 后，我们发现受感染细胞中线粒体的平均面积增加（图 7A 和 S7B）。在 24 h.p.i. 时，线粒体的大小继续增加，最终在 48 h.p.i. 时导致严重损伤。（图 S7C）。为了证实在人肺细胞中的这一观察结果，我们检查了先前发表的 SARS-CoV-2 感染 HBEC (48 hpi) 的电子显微镜数据 (Ravindra 等人, 2020 年)，并再次发现感染细胞的平均线粒体大小显著增加与 SARS-CoV-2 (图 S7D)。总而言之，这些结果表明 SARS-CoV-2 感染期间线粒体稳态发生了改变。



Download : Download high-res image (2MB) 下载 : 下载高分辨率图像 (2MB)

Download : Download full-size image 下载 : 下载全尺寸图片

Figure 7. SARS-CoV-2-associated proteins and a targeted mitochondrial CRISPR screen identify functional interactions between SARS-CoV-2 and host mitochondria.

图 7. SARS-CoV-2 相关蛋白和靶向线粒体 CRISPR 筛选确定了 SARS-CoV-2 和宿主线粒体之间的功能相互作用。

(A) Electron microscopy (EM) of Huh7.5 cells uninfected (left, mock) or infected by SARS-CoV-2 (right).

(A) 未感染 (左, 模拟) 或被 SARS-CoV-2 (右) 感染的 Huh7.5 细胞的电子显微镜 (EM)。

(B) Quantification of mitochondria size by EM in infected cells. n = 348 and n = 361 mitochondria from 15 (mock) and 12 (12 h.p.i.) Huh 7.5 cells were analyzed. p ≤ 0.0001 by two-tailed Student's t test.

(B) 通过 EM 在感染细胞中量化线粒体大小。分析了来自 15 (模拟) 和 12 (12 hpi) Huh 7.5 细胞的 n = 348 和 n = 361 个线粒体。p≤0.0001 通过双尾学生 t 检验。

(C) Mini-pool CRISPR screen design.

(C) 迷你池 CRISPR 屏幕设计。

(D) ChIRP-MS enrichments of mitochondrial proteins present in the expanded interactome of at least one virus. The larger segment of the circle corresponds to proteins encoded by the mitochondrial genome or proteins encoded by the nuclear genome which are localized or associated with the mitochondria. Components of the mitochondrial ribosome are shown on the smaller segment. Proteins that are significant hits in the CRISPR screen data in [Figure 5](#) are indicated with red labels (proviral hits) or blue labels (antiviral hits).

(D) ChIRP-MS 富集存在于至少一种病毒的扩展相互作用组中的线粒体蛋白。圆圈的较大部分对应于线粒体基因组编码的蛋白质或核基因组编码的位于线粒体或与线粒体相关的蛋白质。线粒体核糖体的成分显示在较小的片段上。在图 5 的 CRISPR 筛选数据中具有显着命中率的蛋白质用红色标签 (原病毒命中) 或蓝色标签 (抗病毒命中) 表示。

(E) Correlation of gene Z scores for each condition.

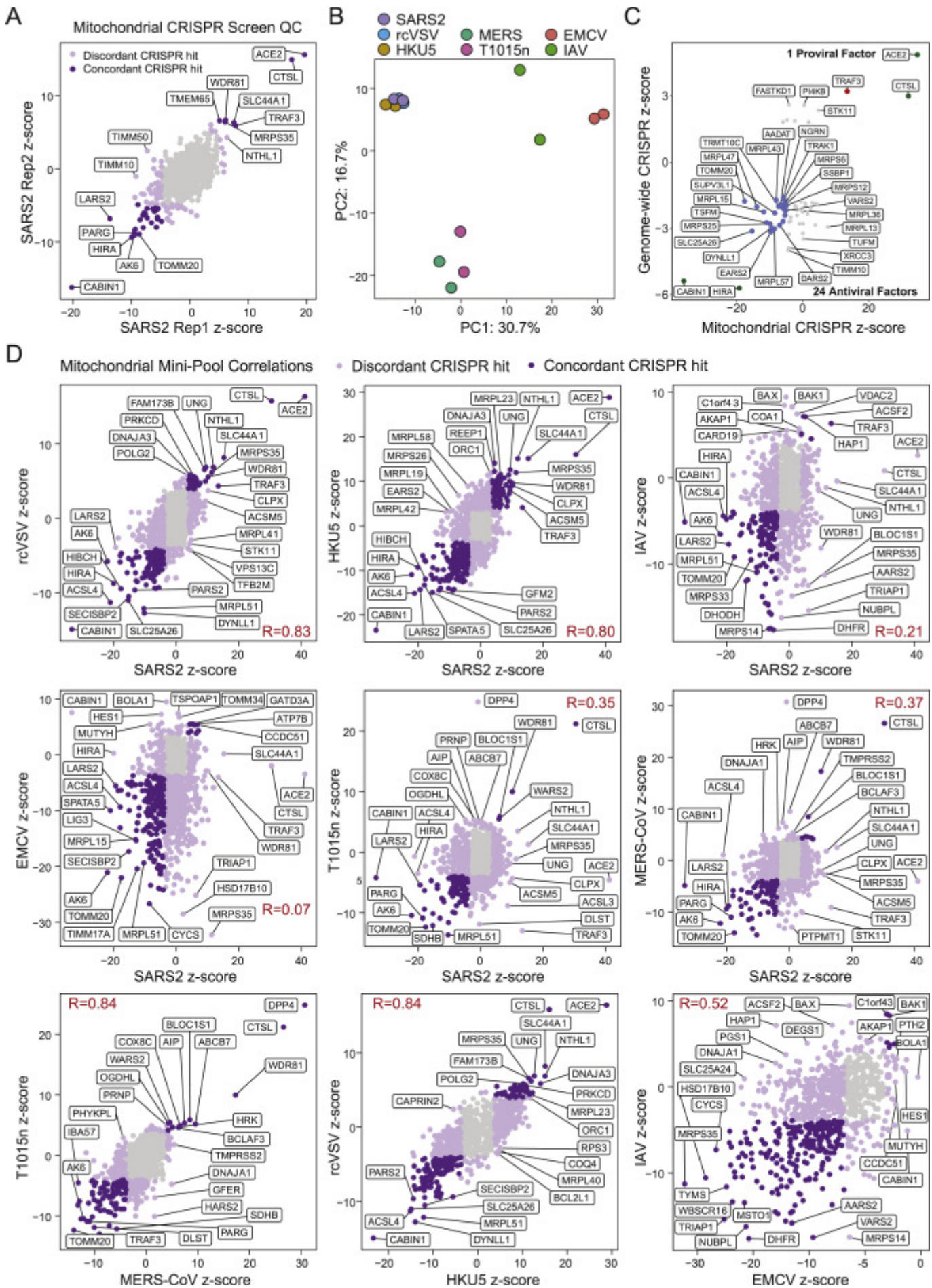
(E) 每种条件下基因 Z 分数的相关性。

(F) Number of proviral and antiviral hits (FDR ≤ 0.001) overlapping with the SARS-CoV-2 hits (FDR ≤ 0.001) for all conditions.

(F) 在所有条件下与 SARS-CoV-2 命中 (FDR ≤ 0.001) 重叠的前病毒和抗病毒命中数 (FDR ≤ 0.001)。

(G) Center: volcano plot for SARS-CoV-2 condition. Significant hits (FDR ≤ 0.001) indicated in black. Top: CRISPR Z scores for top proviral hits. Bottom: CRISPR Z scores for top antiviral hits.

(G) 中心 : SARS-CoV-2 条件的火山图。显着命中 (FDR ≤ 0.001) 以黑色表示。顶部 : CRISPR Z 得分最高的前病毒命中。底部 : 顶级抗病毒药物的 CRISPR Z 得分。



Download : Download high-res image (2MB) 下载 : 下载高分辨率图像 (2MB)

Download : Download full-size image 下载 : 下载全尺寸图片

Figure S7. Correlation analysis of mitochondria CRISPR mini-pool screens, related to Figure 7

图 S7。线粒体 CRISPR 迷你池筛选的相关性分析，与图 7 相关

- (A) Replicate correlations for SARS-CoV-2 mitochondria mini-pool CRISPR screens.
(A) SARS-CoV-2 线粒体迷你池 CRISPR 筛选的复制相关性。
- (B) Principal component analysis of gene-level z-scores for all mitochondria mini-pool screen conditions.
(B) 所有线粒体迷你池筛选条件的基因级 z 分数的主成分分析。
- (C) Mitochondria mini-pool CRISPR screen results for hits identified in the genome-wide screen. Red dots indicate proviral hits in both screens, blue dots indicate antiviral hits in both screens, and green dots indicate positive controls.
(C) 全基因组筛选中确定的命中的线粒体迷你池 CRISPR 筛选结果。红点表示两个屏幕中的原病毒命中，蓝点表示两个屏幕中的抗病毒命中，绿点表示阳性对照。
- (D) Pairwise correlations of selected pairs of conditions.
(D) 所选条件对的成对相关性。

Next, we assessed the interaction of SARS-CoV-2 vRNA with mitochondria-localized proteins by expanding our analysis of the ChIRP-MS data. We curated a set of 810 proteins that are annotated in Uniprot as physically localized to the mitochondria (UniProtKB subcellular location of SL-0173) and found that 170 of these proteins were present in the expanded interactome of at least one virus ([Figures 6C and 6D](#)). DENV and ZIKV had relatively poor recovery of these proteins, while RV and SARS-CoV-2 robustly bound to many mitochondrial factors, although specific protein associations were generally non-overlapping ([Figure 6D](#)). Given the specificity of vRNA binding to mitochondrially localized proteins, we systematically evaluated the functional impact of each of the 810 factors in the context of the seven RNA virus infections (described above) by designing a second custom CRISPR mini-pool of 5,558 CRISPR sgRNAs targeting these 810 genes, as well as positive and negative controls ([Figure 6C; Table S5](#)). We performed survival screens with the mitochondrial mini-pool with each virus. To confirm the technical quality of each screen, we compared data from biological replicates ([Figure S7A](#)) and performed PCA to visualize every replicate and condition ([Figure S7B](#)). We then merged the replicates and compared the gene-level *Z* scores ([Figure 7E](#)). Next, we analyzed the distribution of pro- and antiviral function among mitochondrial factors, and their conservation across viruses. In the SARS-CoV-2 screen, we identified 57 proviral factors and 175 antiviral factors (FDR ≤ 0.001 ; [Figure 7G](#), middle), which validated 1 proviral factor (TRAF3) and 24 antiviral factors identified in the genome-wide screen ([Figure S7C](#)). Expanding our analysis to other viruses, we first computed the number of hits overlapping with SARS-CoV-2 in each condition and observed that each virus had a substantial overlap of antiviral hits with SARS-CoV-2 ([Figure 7F](#)). However, unlike the interactome screening, the proviral hits were less well conserved, consistent with the concept that proviral hits are driven by the viral entry

pathway and mitochondria are minimally (if at all) involved in viral entry ([Figure 7F](#)). Comparing the top pro- and antiviral factors for each condition across all viruses, we found proviral factors that were highly specific to SARS-related viruses (e.g., [TRAF3](#) and [MRPS35](#)), SARS- and MERS-related viruses (e.g., [SLC44A1](#) and [SPNS1](#)), or IAV or EMCV (e.g., [BOLA1](#)), while many antiviral factors displayed multi-viral activity (22 antiviral hits shared across all viruses, 46 shared across SARS and MERS viruses; [Figures 7G](#) and [S7D](#)). Altogether these data provide insights into the specific mitochondrial factors that associate with SARS-CoV-2 RNA, likely contributing to a central role of mitochondria as intracellular hubs for antiviral activity.

接下来，我们通过扩展对 ChIP-MS 数据的分析来评估 SARS-CoV-2 vRNA 与线粒体定位蛋白的相互作用。我们整理了一组 810 种蛋白质，这些蛋白质在 Uniprot 中注释为物理定位于线粒体（SL-0173 的 UniProtKB 亚细胞定位），并发现其中 170 种蛋白质存在于至少一种病毒的扩展相互作用组中（图 6C 和 6D）。DENV 和 ZIKV 对这些蛋白质的恢复相对较差，而 RV 和 SARS-CoV-2 与许多线粒体因子牢固结合，尽管特定的蛋白质关联通常不重叠（图 6D）。鉴于 vRNA 与线粒体定位蛋白结合的特异性，我们通过设计第二个定制的 5,558 个 CRISPR sgRNA 的定制 CRISPR 迷你池，系统地评估了 810 个因素在七种 RNA 病毒感染（如上所述）的背景下的功能影响这 810 个基因，以及阳性和阴性对照（图 6C；表 S5）。我们用每种病毒的线粒体迷你池进行了生存筛选。为了确认每个屏幕的技术质量，我们比较了生物重复的数据（图 S7A）并执行 PCA 以可视化每个重复和条件（图 S7B）。然后我们合并重复并比较基因水平的 Z 分数（图 7E）。接下来，我们分析了线粒体因子中促病毒和抗病毒功能的分布，以及它们在病毒之间的保守性。在 SARS-CoV-2 筛选中，我们确定了 57 个前病毒因子和 175 个抗病毒因子（FDR ≤ 0.001 ；图 7G，中间），验证了全基因组筛选中确定的 1 个前病毒因子（[TRAF3](#)）和 24 个抗病毒因子（图 S7C）。将我们的分析扩展到其他病毒，我们首先计算了每种条件下与 SARS-CoV-2 重叠的命中数，并观察到每种病毒与 SARS-CoV-2 的抗病毒命中有大量重叠（图 7F）。然而，与相互作用组筛选不同，前病毒命中的保守性较差，这与前病毒命由病毒进入途径驱动并且线粒体最少（如果有的话）参与病毒进入的概念一致（图 7F）。比较所有病毒中每种情况的前病毒和抗病毒因子，我们发现了对 SARS 相关病毒（例如 [TRAF3](#) 和 [MRPS35](#)）、SARS 和 MERS 相关病毒（例如 [SLC44A1](#) 和 [SPNS1](#)）高度特异性的前病毒因子或 IAV 或 EMCV（例如 [BOLA1](#)），而许多抗病毒因子显示出多病毒活性（所有病毒共有 22 个抗病毒命中，SARS 和 MERS 病毒共有 46 个；图 7G 和 S7D）。总之，这些数据提供了对与 SARS-CoV-2 RNA 相关的特定线粒体因素的见解，这可能有助于线粒体作为抗病毒活性的细胞内中心的核心作用。

Discussion 讨论

In summary, our results provide an RNA-centric view of the landscape of the host proteins interacting with SARS-CoV-2 RNA during infection. By integrating our analysis across time points, cell lines, and other viruses, we identify shared and SARS-CoV-2-specific patterns of RNA-host protein interactions. In the context of the rapidly evolving

literature on subcellular mechanisms of SARS-CoV-2 pathogenicity, the ChIRP-MS data provide an orthogonal but complementary resource to existing PPI, RNA-protein interaction, and phenotypic CRISPR screening studies (Banerjee et al., 2020; Gordon et al., 2020; Hoffmann et al., 2021; Schmidt et al., 2021; Wang et al., 2020; Wei et al., 2021). In particular, we find that the vRNA:host protein interface is largely distinct from that of viral proteins and nominates roles for previously unappreciated biological processes and host proteins in SARS-CoV-2 infection.

总而言之，我们的结果提供了以 RNA 为中心的视角，了解感染期间宿主蛋白与 SARS-CoV-2 RNA 相互作用的情况。通过整合我们对时间点、细胞系和其他病毒的分析，我们确定了 RNA-宿主蛋白相互作用的共享和 SARS-CoV-2 特异性模式。在关于 SARS-CoV-2 致病性亚细胞机制的文献迅速发展的背景下，ChIRP-MS 数据为现有的 PPI、RNA-蛋白质相互作用和表型 CRISPR 筛选研究提供了正交但互补的资源 (Banerjee 等人，2020；Gordon 等，2020；Hoffmann 等，2021；Schmidt 等，2021；Wang 等，2020；Wei 等，2021)。特别是，我们发现 vRNA：宿主蛋白的界面与病毒蛋白的界面大不相同，并且在 SARS-CoV-2 感染中指定了以前未被重视的生物过程和宿主蛋白的作用。

Integration of the SARS-CoV-2 ChIRP-MS data with ChIRP-MS of three other positive-sense RNA viruses provided several new insights into the “molecular arms race” that takes place between the virus and host. First, this analysis identified shared and unique strategies employed by viruses to hijack the host for trafficking and replication. For example, SARS-CoV-2 and flavivirus RNAs both associate with the Rab GTPase proteins RAB10 and RAB2A, which are involved in subcellular trafficking, and CRISPR perturbation revealed that these proteins are required for viral replication and virus-induced cell death (Gordon et al., 2020; Hoffmann et al., 2021). In contrast, despite the fact that both viral families depend on glycoproteins to produce infectious virions, there was a limited association of SARS-CoV-2 RNA with the Sec/Translocon/OST complexes, compared to flaviviruses (Ooi et al., 2019). There are known differences between flavivirus and coronavirus replication strategies: flavivirus may physically leverage the translocon complex, which eventually forms invaginated vesicles or spherules (Fernandez-Garcia et al., 2009; Mukhopadhyay et al., 2005), whereas coronaviruses leverage the ERGIC and eventually form double-membrane vesicles (McBride et al., 2007). Therefore, the differences in the ChIRP-MS data likely reflect established differences in these viral life cycles, but our data provide specific host factors within each pathway that are closely associated with the vRNA genomes and thus may play physical roles in these processes.

将 SARS-CoV-2 ChIRP-MS 数据与其他三种正义 RNA 病毒的 ChIRP-MS 整合，为病毒与宿主之间发生的“分子军备竞赛”提供了一些新见解。首先，该分析确定了病毒用于劫持宿主进行贩运和复制的共享和独特策略。例如，SARS-CoV-2 和黄病毒 RNA 都与参与亚细胞运输的 Rab GTPase 蛋白 RAB10 和 RAB2A 相关联，CRISPR 扰动表明这些蛋白是病毒复制和病毒诱导的细胞死亡所必需的 (Gordon 等 al.，2020 年；Hoffmann 等人，2021

年）。相比之下，尽管两个病毒家族都依赖糖蛋白来产生感染性病毒粒子，但与黄病毒相比，SARS-CoV-2 RNA 与 Sec/Translocon/OST 复合物的关联有限（Ooi 等，2019）。黄病毒和冠状病毒复制策略之间存在已知差异：黄病毒可能在物理上利用易位复合体，最终形成内陷囊泡或小球（Fernandez-Garcia 等人，2009 年；Mukhopadhyay 等人，2005 年），而冠状病毒则利用 ERGIC 和最终形成双膜囊泡（McBride 等，2007）。因此，ChIRP-MS 数据的差异可能反映了这些病毒生命周期的既定差异，但我们的数据提供了每个途径中与 vRNA 基因组密切相关的特定宿主因素，因此可能在这些过程中发挥物理作用。

Integration of the ChIRP-MS data with genome-wide CRISPR screen data, as well as targeted screening of a custom pool of sgRNAs against the SARS-CoV-2 interactome, provides extensive functional characterization of the RNA interactome proteins. In the context of SARS-CoV-2 infection, an unexpected finding from the intersection of ChIRP-MS and CRISPR screen datasets was that many vRNA-binding proteins were antiviral factors. Additional targeted screens in the context of six other viruses enabled us to decode their specificity and revealed SARS-specific and multi-viral host factors. A striking difference between pro- and antiviral factors was their conservation across viruses, which perhaps suggests distinct RNA sequence specificity and logic for each class of factors. Many of these factors were broadly expressed in human lung tissue, bound the vRNA early during infection, were commonly bound to multiple RNA virus families, and demonstrated antiviral function across RNA viruses, including related betacoronaviruses, and also more distant viral families. These results suggest that host cells deploy a diverse array of proteins to physically recognize and counteract viral infection and that these proteins are not limited to those with well-characterized viral recognition function, such as Toll-like receptors (TLRs) and retinoic acid inducible gene-I-like receptors (RLRs), but also extend to many other protein families with RNA-binding capacity.

ChIRP-MS 数据与全基因组 CRISPR 筛选数据的整合，以及针对 SARS-CoV-2 相互作用组的定制 sgRNA 池的靶向筛选，提供了 RNA 相互作用组蛋白的广泛功能表征。在 SARS-CoV-2 感染的背景下，从 ChIRP-MS 和 CRISPR 筛选数据集的交叉中得出的一个意外发现是，许多 vRNA 结合蛋白都是抗病毒因子。在其他六种病毒的背景下进行的额外目标筛选使我们能够解码它们的特异性并揭示 SARS 特异性和多病毒宿主因子。促病毒和抗病毒因子之间的一个显着差异是它们在病毒之间的保守性，这可能表明每一类因子都有不同的 RNA 序列特异性和逻辑。其中许多因子在人肺组织中广泛表达，在感染早期结合 vRNA，通常与多个 RNA 病毒家族结合，并在 RNA 病毒（包括相关的 β 冠状病毒）以及更远距离的病毒家族中表现出抗病毒功能。这些结果表明宿主细胞部署了多种蛋白质来物理识别和抵抗病毒感染，并且这些蛋白质不仅限于那些具有充分表征的病毒识别功能的蛋白质，例如 Toll 样受体 (TLR) 和视黄酸诱导基因-I 样受体 (RLR)，但也扩展到许多其他具有 RNA 结合能力的蛋白质家族。

Finally, we identified a functional connection between SARS-CoV-2 RNA and the mitochondria. Both RNA and protein components of the mitochondria were robustly captured with the SARS-CoV-2 RNA in Vero E6 and Huh7.5 cells, suggesting a close physical interaction, and electron microscopy demonstrated changes in mitochondrial shape and size after infection. Interestingly, other viruses, including HIV, have been reported to physically enter the mitochondria, providing evidence that vRNA can gain access to the mitochondria during infection (Somasundaran et al., 1994). Mitochondria are central to the underlying health of a cell, play an active role in sensing and signaling during cellular stress, and act as a hub for innate immune signaling. Based on the ChIRP-MS results, we propose that RNA viruses may follow a distinct logic when causing mitochondrial stress; that is, many viruses may interact with and perturb this organelle, but the precise manner in which stress is caused, and thus signaling occurs, is virus specific. Indeed, our custom mitochondria-focused CRISPR mini-pool screens revealed many pro- and antiviral factors associated with the mitochondria. These results further support the concept that mitochondria may serve as an organelle platform in the antiviral innate immune response to RNA viruses, perhaps exemplified best by the RLR family of RNA helicases (which signal on the outer mitochondrial membrane; Loo and Gale, 2011), and possibly also extending to a broader set of proteins identified here. Altogether, this study provides an unbiased and comprehensive catalog of functional SARS-CoV-2 RNA-host protein interactions, revealed a functional link between SARS-CoV-2 and the mitochondria, and may inform future studies to understand the mechanisms of viral pathogenesis and nominate strategies to combat the virus for therapeutic benefit.

最后，我们确定了 SARS-CoV-2 RNA 和线粒体之间的功能联系。Vero E6 和 Huh7.5 细胞中的 SARS-CoV-2 RNA 强有力地捕获了线粒体的 RNA 和蛋白质成分，表明存在密切的物理相互作用，电子显微镜显示感染后线粒体形状和大小发生了变化。有趣的是，据报道，包括 HIV 在内的其他病毒会以物理方式进入线粒体，从而证明 vRNA 可以在感染期间进入线粒体（Somasundaran 等，1994）。线粒体是细胞潜在健康的核心，在细胞应激期间在传感和信号传导中发挥积极作用，并充当先天免疫信号传导的枢纽。基于 ChIRP-MS 结果，我们提出 RNA 病毒在引起线粒体应激时可能遵循不同的逻辑；也就是说，许多病毒可能会与该细胞器相互作用并干扰该细胞器，但引起压力并因此产生信号的确切方式是病毒特异性的。事实上，我们定制的专注于线粒体的 CRISPR 迷你池筛选揭示了许多与线粒体相关的促病毒和抗病毒因子。这些结果进一步支持了线粒体可以作为对 RNA 病毒的抗病毒先天免疫反应的细胞器平台的概念，也许最好的例子是 RNA 解旋酶的 RLR 家族（在线粒体外膜上发出信号；Loo 和 Gale，2011），并且可能还扩展到这里确定的更广泛的蛋白质组。总而言之，这项研究提供了功能性 SARS-CoV-2 RNA-宿主蛋白相互作用的公正和全面的目录，揭示了 SARS-CoV-2 与线粒体之间的功能联系，并可能为未来的研究提供信息，以了解病毒发病机制和提名对抗病毒的策略以获得治疗益处。

Limitations of the study 研究的局限性

There are several limitations to our study. First, ChIRP-MS experiments were performed in cell lines that were not derived from the lung. Therefore, investigation of these vRNA-binding factors in additional models is warranted. Second, our functional studies utilized survival CRISPR screens in Vero E6 cells. Future screens focused on other aspects of the viral life cycle, as well as screening primary human cells and other cell types, particularly type I interferon-sufficient cells, may identify additional functional aspects of these factors. In this regard, the pro- and antiviral terminology is used here for clarity and does not signify specific functional archetypes; these factors may function at any stage of the viral life cycle, including but not limited to, vRNA processing or replication pathways, viral trafficking within the cell, innate immune pathways, and stress responses to maintain cellular metabolism or fitness during infection.

我们的研究有几个局限性。首先，在不衍生自肺的细胞系中进行Chirp-MS实验。因此，有必要对额外模型中这些VRNA结合因素进行调查。其次，我们的功能研究利用VERO E6细胞中的存活克隆屏幕。未来屏幕专注于病毒生命周期的其他方面，以及筛查初级人体细胞和其他细胞类型，特别是I型干扰素 - 足细胞，可以识别这些因素的额外功能方面。在这方面，在此用于清楚起见，并且不表示特定的功能原型;这些因素可以在病毒生命周期的任何阶段起作用，包括但不限于VRNA加工或复制途径，细胞内的病毒贩运，先天免疫途径和应激反应，以在感染期间维持细胞代谢或适应性。

STAR★Methods 星★方法

Key resources table 关键资源表

REAGENT or RESOURCE	SOURCE	IDENTIFIER
Bacterial and Virus Strains		
SARS-CoV-2 isolate USA-WA1/2020	BEI Resources	Cat#NR-48814
Chemicals, Peptides, and Recombinant Proteins		
1M Tris-HCl, pH 7	Thermo Fisher Scientific	Cat#AM9850G
UltraPure 0.5M EDTA	Thermo Fisher Scientific	Cat#15575020
UltraPure 10% SDS	Thermo Fisher Scientific	Cat#15553027
UltraPure Formamide	Thermo Fisher Scientific	Cat#15515026
UltraPure 5M NaCl	Thermo Fisher Scientific	Cat#24740011
20x SSC	Thermo Fisher Scientific	Cat#15557044
50mM D-Biotin	Thermo Fisher Scientific	Cat#B20656

REAGENT or RESOURCE	SOURCE	IDENTIFIER
20% N-Lauroylsarcosine sodium salt solution	Sigma	Cat#L7414
Sodium deoxycholate	Sigma	Cat#30970
1M HEPES	Thermo Fisher Scientific	Cat#15630106
Trichloroacetic acid	Sigma	Cat#T6399
Acetone	Sigma	Cat#179124
4x NuPAGE LDS Sample Buffer	Thermo Fisher Scientific	Cat#NP0007
UltraPure™ Dithiothreitol	Thermo Fisher Scientific	Cat#15508013
Pierce Acetonitrile (ACN), LC-MS Grade	Thermo Fisher Scientific	Cat#51101
Ammonium bicarbonate	Sigma	Cat#A6141
Formic Acid, 99.0%, Optima LC/MS Grade	Fisher Scientific	Cat#A117
Iodoacetamide	Sigma	Cat#I1149
Proteinase K	Thermo Fisher Scientific	Cat#AM2546
Sequencing Grade Modified Trypsin	Promega	Cat# V5111
DNase I (RNase-free)	New England Biolabs	Cat#M0303S
Critical Commercial Assays		
TAKARA Bio SMART-Seq Stranded Kit	Takara Bio	Cat#634442
Colloidal Blue Staining Kit	Thermo Fisher Scientific	Cat#LC6025
Deposited Data		
CRISPR-KO Screen in VeroE6 after SARS-CoV-2 Infection	Wei et al., 2021	N/A
ChIRP-RNA-seq in VeroE6 and Huh7.5 cell after SARS-CoV-2 Infection	This Study	GSE167341
CRISPR-KO mini-pool screen sequencing data from VeroE6 cells; ChIRP-MS and mitochondrial pools	This Study	GSE167341
Experimental Models: Cell Lines		
Huh7.5	ATCC	CVCL-7927
VeroE6	ATCC	CRL-1586
Oligonucleotides		

REAGENT or RESOURCE	SOURCE	IDENTIFIER
See Table S1 for ChIRP-MS Oligos	N/A	N/A
Software and Algorithms		
R	https://www.r-project.org/	R 3.6
Cytoscape	https://cytoscape.org/	Cytoscape 3.8.1
Differential Enrichment analysis of Proteomics Data (DEP)	https://rdrr.io/bioc/DEP/man/DEP.html	DEP 1.10.0
DESeq2	https://bioconductor.org/packages/release/bioc/html/DESeq2.html	DESeq2 1.28.1
DAVID Bioinformatics Resources	https://david.ncifcrf.gov/	DAVID 6.8

试剂或资源源标识符 细菌和病毒菌株 SARS-COV-2隔离USA-WA1 / 2020 Bei Resources
Cat # NR-48814 化学品 , 肽和重组蛋白 1M Tris-HCl , PH 7 Thermo Fisher Scientific Cat # AM9850G 超纯0.5米EDTA Thermo Fisher Scientific猫 # 15575020 超纯10% sds thermo fisher科学猫 # 15553027 超纯甲酰胺热渔民科学猫 # 15515026 超纯5m NaCl Thermo Fisher Scientific猫 # 24740011 20x ssc thermo fisher科学猫 # 15557044 50mm d-biotin thermo fisher scientific猫 # b20656 20% N-Lauroylsarcosine钠盐溶液Sigma Cat # L7414 脱氧核酸钠西格玛猫 # 30970 1M HEPES Thermo Fisher Scientific猫 # 15630106 三氯乙酸Sigma猫 # T6399 丙酮Sigma猫 # 179124 4x NUPAGE LDS样本缓冲器 Thermo Fisher Scientific猫 # NP0007 Ultrapure™Dithiothreitol Thermo Fisher Scientific猫 # 15508013 皮尔斯乙腈 (ACN) , LC-MS等级Thermo Fisher Scientific猫 # 51101 铵碳酸氢铵锡格玛猫 # a6141 甲酸 , 99.0% , Optima LC / MS等级Fisher Scientific Cat # A117 碘乙酰胺Sigma Cat # i1149 蛋白酶K Thermo Fisher Scientific Cat # AM2546 测序等级修饰胰蛋白酶promega cat # v5111 Dnase I (无RNASE) 新英格兰Biolabs猫 #mo303s 关键的商业测定 Takara Bio Smart-SEQ Stranded Kit Takara Bio Cat # 634442 胶体蓝色染色套件Thermo Fisher Scientific猫#LC6025 存放数据 SARS-COV-2感染后 Veroe6中的Crispr-Ko屏幕威等人 , 2021 N / A 在SARS-COV-2感染后 , VEROE6和 HUH7.5细胞中的Chirp-RNA-SEQ CERCONICHING167341 CRISPR-KO迷你池筛网测序来自Veroe6细胞的数据; Chirp-MS和线粒体游泳池本研究GSE167341 实验模型 : 细胞系 HUH7.5 ATCC CVCL-7927 Veroe6 ATCC CRL-1586 嘌核苷酸 有关Chirp-MS Oligos N / A N / A的表S1 软件和算法 r <https://www.r-project.org/> r 3.6 cytoscape <https://cytoscape.org/> cytoscape 3.8.1 蛋白质组学数据的差异浓缩分析 (DEP) <https://rdrr.io/bioc/dep/man/dep.html> dep 1.10.0 deseq2 <https://biocumon.org/packages/release/bioc/html/deseq2.html> deseq2 1.28.1 David生物信息学资源<https://david.ncifcrf.gov/> David 6.8

Resource availability 资源可用性

Lead contact 铅接触

Further information and requests for resources and reagents should be directed to and will be fulfilled by the Lead Contact, Ryan Flynn (ryan.flynn@childrens.harvard.edu).
进一步的信息和资源和试剂请求应予以指导，并将通过Ryan Flynn
(Ryan.flynn@Childrens.Harvard.edu) 的铅接触来实现。

Materials availability 材料可用性

All reagents generated in this study are available from the Lead Contact upon request.
本研究中产生的所有试剂可根据要求可从铅接触中获得。

Data and code availability 数据和代码可用性

Source code is available on GitHub (https://github.com/juliabelk/sarscov2_chirp_ms) along with original spreadsheets for the MS and CRISPR analyses. Sequencing data has been deposited on NCBI GEO as series GSE167341 which includes the ChIRP RNA-seq and CRISPR screening experiments.

源代码可在GitHub (https://github.com/juliabelk/sarscov2_chirp_ms) 上找到原始电子表格，用于MS和CRISPR分析。测序数据已寄存在NCBI Geo上，作为GSE167341系列，其中包括Chirp RNA-SEQ和CRISPR筛选实验。

Experimental model and subject details 实验模型和主题细节

Cell lines 细胞系

Huh7.5 (male), Vero-E6 (female), and Vero-E6-Cas9v2 cell lines were grown in Dulbecco's Modified Eagle Medium (DMEM) supplemented with 10% heat-inactivated fetal bovine serum (FBS), and 1% Penicillin/Streptomycin. All cell lines tested negative for mycoplasma contamination prior to use in experiments and were authenticated by morphological evaluation by microscopy. None of the cell lines used in this study are listed in the commonly misidentified cell lines database (ICLAC). All procedures with infectious virus were done at a Biosafety Level 3 (BSL3) laboratory and approved by the Yale University Biosafety Committee.

Huh7.5 (男性)，Vero-E6 (女性) 和Vero-E6-Cas9v2细胞系在Dulbecco的改性鹰培养基 (DMEM) 中生长，补充有10%的热灭活胎牛血清 (FBS) 和1%青霉素/链霉素。在实验中使用之前，所有细胞系测试了支原体污染的阴性，并通过显微镜的形态学评估进行了认证。本研究中使用的细胞系均未列在常识的细胞系数据库 (ICLAC) 中列出。所有含有传染病病毒的程序都是在生物安全3级 (BSL3) 实验室完成的，并由耶鲁大学生物安全委员会批准。

Human samples 人类样品

Human scRNA-seq data was previously published. No other human samples were used.
人类ScRNA-SEQ数据之前已发布。没有使用其他人类样品。

Animal models 动物模型

No animal experiments were performed in this study.

本研究中没有进行动物实验。

Method details 方法详情

Cell lines, SARS-CoV-2 infection, and cell processing 细胞系，SARS-CoV-2感染和细胞加工

Vero-E6 (female) and Huh7.5 (male) cells were seeded at 1×10^6 cells per T150 flask and were grown in Dulbecco's Modified Eagle Medium (DMEM) supplemented with 10% heat-inactivated fetal bovine serum (FBS), and 1% Penicillin/Streptomycin. Three T150 flasks were assigned per condition: 0, 1, and 2 days post-infection (dpi). The next day, the media was removed, and cells were inoculated with SARS-CoV-2 isolate USA-WA1/2020 (BEI Resources #NR-48814) at MOI of 0.01. Flasks were incubated at 37°C for 1 h with gentle rocking every 15 min. At 0, 1, and 2 dpi, supernatant from the flasks were discarded, and cells were washed with 1X PBS twice. 4 mL of 4% of paraformaldehyde was added on each of the flasks and incubated for 30 min at room temperature. Afterward, cells were quenched with 250 μ L of 2 M glycine (final concentration of 125 mM) for each flask. Cells were scraped, harvested in pre-weighed microcentrifuge tubes, and spun at 1000 \times g for 5 min at 4°C. All supernatants aspirated, and the final pellet were weighed. Cells were frozen at -80°C until used.

在每T150烧瓶 1×10^6 个细胞上接种Vero-E6（雌性）和Huh7.5（男性）细胞，并在补充10%热灭活胎牛血清（FBS）的Dulbecco改良 Eagle 培养基（DMEM）中生长，1%青霉素/链霉素。每种条件分配三个T150烧瓶：感染后2天和2天（DPI）。第二天，除去培养基，用SARS-CoV-2分离USA-WA1 / 2020（BEI资源 # NR-48814）接种细胞在0.01的情况下接种。每15分钟，在37°C下在37°C下孵育1小时。在0,1和2 dpi下，丢弃来自烧瓶的上清液，用1X PBS洗涤细胞两次。在每个烧瓶中加入4ml 4%的多聚甲醛，并在室温下孵育30分钟。之后，将细胞用250 μ l 2M甘氨酸（终浓度为125mm）淬灭，每个烧瓶。将细胞刮擦，在预先称量的微量离心管中收获，并在4°C下以1000 \times g跨越5分钟。所有吸气的上清液都称重和最终沉淀。将细胞在-80°C冷冻直至使用。

Comprehensive identification of RNA binding proteins by mass spectrometry
(ChIRP-MS) 质谱法综合RNA结合蛋白 (Chirp-MS)

SARS-CoV-2 targeting probes were designed online (<https://www.biostech.com/stellaris>), with repeat masking setting of 3 and even coverage of the whole transcript. Full probe sequences available in **Table S1**. Oligos were synthesized with a 3' biotin-TEG modification at Stanford Protein and Nucleic Acid Facility (panoligo@stanford.edu).

SARS-CoV-2靶向探针在线设计 (HTTPS://www.BiosearchTech.com/Stellaris) , 重复屏蔽设置为3甚至整个成绩单覆盖。表S1中可用的全探针序列。在斯坦福蛋白和核酸设施 (Panoligo@stanford.edu) , 用3'生物素-TEG改性合成寡核苷酸。

ChIRP-MS was performed largely as described in (Chu et al., 2015). Cells were cultured, infected, and crosslinked as described above in the BSL3 facility. Lysate was generated by resuspending cell pellets in 1 mL lysis buffer (50 mM Tris-HCl pH 7.0, 10 mM EDTA, 1% SDS) per 100 mg of cell pellet weight (~100 μ L pellet volume). Lysates were sonicated using a focused-ultrasonicator (Covaris, E220) until the average RNA length was ~500 nucleotides as determined by agarose gel analysis and stored at -80°C. Stored lysates were thawed on ice and prepared for pre-clearing. Precleared was achieved by adding 30 μ L washed MyOne C1 beads per mL of lysate at 37°C for 30 min on rotation.

Preclearing beads were removed twice from lysate using a magnetic stand; for this and all subsequent magnetic stand steps allow for > 1 min of separation before removing any supernatant. Next, for every 1 mL of sonicated lysate 2 mL of ChIRP hybridization buffer (750 mM NaCl, 1% SDS, 50 mM Tris-HCl pH 7.0, 1 mM EDTA, 15% formamide; made fresh) and 2.5 μ L of 100 μ M ChIRP Probe Pools were added per mL of lysate. ChIRP Probe Pools (**Table S1**) were composed of an equimolar mix of 108 antisense oligos. For each biological triplicate, a total of 7 mL of sonicated cell lysate was used. Hybridization took place on rotation for 16 h at 37°C. Subsequently, 250 μ L of washed MyOne C1 beads per mL of lysate were added to each sample and incubated on rotation for 45 min at 37°C. Enriched material was collected on the beads with a magnetic stand, and beads were washed 5x 2 min in 1 mL of ChIRP Wash Buffer (2x NaCl-Sodium Citrate (SSC, ThermoFisher Scientific), 0.5% SDS) at 37°C. After washing, 1% of each sample was saved for RNA extraction and RNA-seq library preparation (below). To elute enriched proteins, beads were collected on magnetic stand, resuspended in ChIRP biotin elution buffer (12.5 mM biotin, 7.5 mM HEPES, pH 7.9, 75 mM NaCl, 1.5 mM EDTA, 0.15% SDS, 0.075% sarkosyl, and 0.02% Na-Deoxycholate), mixed at 25°C for 20 min on rotation and at 65°C for 15 min shaking. Eluent was transferred to a fresh tube, and beads were eluted again. The two eluents were pooled (~1200 μ L), and residual beads were removed again using the magnetic stand. 25% total volume (300 μ L) trichloroacetic acid was added to the clean eluent, vortexed, and then samples were placed at 4°C overnight for precipitation. The next day, proteins were pelleted at 21,000 rcf at 4°C for 60 min. Supernatant was carefully removed, and protein pellets were washed once with ice-cold acetone. Samples were spun at 21,000 rcf at 4°C for 5 min.

Acetone supernatant was removed, tubes briefly centrifuged again and, after removal of residual acetone, were left to air-dry on the bench-top. Proteins were then solubilized in 1x LDS Buffer in NT2 with 20 mM DTT and boiled at 95°C for 30 min with occasional mixing for reverse-crosslinking.

Chirp-MS在很大程度上如上所述进行 (Chu 等 , 2015)。如上所述在BSL3设施中培养 , 感染和交联细胞。通过每100mg细胞颗粒重量 (~100μl颗粒体积) 将细胞粒料重新悬浮在1ml裂解缓冲液中 (50mM Tris-HCH 7.0, 1% , 1% SDS) 产生裂解物。使用聚焦超声波 (Covaris , E220) 超声处理裂解物 , 直到通过琼脂糖凝胶分析测定的平均RNA长度为约500个核苷酸 , 并储存在-80°C下。将储存的裂解物在冰上解冻并准备预清除。通过在37°C下在37°C下加入30μl洗涤的氰化物C1珠 , 旋转30分钟 , 通过加入30μl洗涤的氰化物珠粒来实现。使用磁铁支架从裂解物中除去光珠两次;对于此 , 在除去任何上清液之前 , 所有后续的磁静物步骤允许> 1分钟的分离。接下来 , 对于每1mL的ChIRP杂交缓冲液 (750mM NaCl , 1% SDS , 50mM Tris-HCl pH 7.0, 1mM EDTA , 15% 甲酰胺; 制成新鲜) 和2.5μL100μmChIRP每毫升裂解液加入探针池。Chirp探针池 (表S1) 由108个反义寡核苷酸的等摩尔混合物组成。对于每个生物三份 , 使用总共7ml的超声裂解细胞裂解物。杂交在37°C时旋转16小时。随后 , 将250μl洗涤的氰化物C1珠粒加入每个样品中 , 并在37°C下旋转45分钟。将富集的物质收集在具有磁性支架的珠粒上 , 在37°C时将珠子在1mlChIRP洗涤缓冲液中 (2x NaCl-柠檬酸钠 (SSC , ThermoFisher Scientific) , 0.5% SDS) 中洗涤5倍2分钟。洗涤后 , 将每个样品的1%用于RNA提取和RNA-SEQ文库制备 (下面)。为了洗脱富集的蛋白质 , 在磁场上收集珠子 , 重悬于ChIRP生物素洗脱缓冲液 (12.5mM 生物素 , 7.5mM Hepes , pH 7.9, 75mM NaCl , 1.5mM EDTA , 0.15% SDS , 0.075% 甲糖基和0.02% Na - 氧胆酸盐) , 在25°C下旋转混合20分钟 , 在65°C下摇动15分钟。洗脱液转移到新鲜管中 , 再次洗脱珠子。合并两种洗脱液 (~1200μL) , 再次使用磁台再次除去残留的珠子。将25% 总体积 (300μL) 三氯乙酸加入到清洁洗脱液中 , 涡旋 , 然后将样品置于4°C过夜进行沉淀。第二天 , 在4°C下以21,000 rcf沉淀蛋白质60分钟。小心地除去上清液 , 用冰冷的丙酮洗涤蛋白质粒料。将样品在21,000 rcf下在4°C下旋转5分钟。除去丙酮上清液 , 再次短暂离心管 , 并在除去残留的丙酮后 , 留在台面上空干燥。然后用20mMDTT在NT2中的1×LDS缓冲液中溶解蛋白质 , 并在95°C下偶尔煮沸30分钟 , 偶尔混合用于反向交联。

Protein samples were size-separated on bis-tris SDS-PAGE gels (Bio-Rad), and the gel was fixed and stained with the Colloidal Blue Staining Kit (ThermoFisher Scientific) as per the manufacturer's instructions. Each ChIRP-MS experiment (1 lane in the gel) was cut into 2 slices from the SDS-PAGE and prepared independently. Gel slices were prepared for mass spectrometry by rinsing sequentially in 200 μL HPLC-grade water, 100% Acetonitrile (ACN, ThermoFisher Scientific), 50 mM Ammonium Bicarbonate (AmBic). Samples were reduced by adding 200 μL of 5 mM DTT in 50 mM AmBic and incubating at 65°C for 35 min. The reduction buffer was discarded, and samples were cooled to room temperature. Alkylation was achieved by adding 200 μL of 25 mM iodoacetamide in 50 mM AmBic for 20 min at 25°C in the dark. The alkylation buffer

was discarded, samples were rinsed once in 200 μ L 50 mM AmBic, and then they were washed twice for 10 min each in 200 μ L of freshly prepared 50% ACN in 50 mM AmBic. After each wash, the supernatant was discarded, and after all washes, samples were dried for 3 h using a SpeedVac. Once dry, proteins were digested by adding 100 ng of trypsin in 200 μ L of 50 mM AmBic for 16 h at 37°C. Samples were subsequently acidified by adding formic acid to a final concentration of 1% and incubating at 37°C for 45 min. Finally, samples were desalted using HyperSep Filter Plates with a 5-7 μ L bed volume (ThermoFisher Scientific) following the manufacturer's instructions. Samples were eluted twice in 100 μ L 80% ACN in 0.2% formic acid, dried on a SpeedVac, and resuspended in 10 μ L 0.1% formic acid for mass spectrometry analysis.

在BIS-TRIS SDS-PAGE凝胶 (Bio-rad) 上尺寸分离蛋白质样品，并且根据制造商的说明，用胶体蓝染色试剂盒 (Thermo Fisher Scientific) 固定并染色凝胶。将每个Chirp-MS实验 (凝胶中的1个车道) 从SDS-PAGE切成2片并独立制备。通过在200 μ lHPLC级水中依次冲洗，100%乙腈 (ACN , ThermoFisher Scientific) , 50mM碳酸氢铵 (Ambic) , 通过依次冲洗来制备凝胶切片。通过在50mM的范围内加入200 μ l5mMDTT并在65°C下孵育35分钟来降低样品。将还原缓冲液丢弃，并将样品冷却至室温。通过在25°C下在25°C下在50mm Ambic中加入200 μ l25mM碘乙酰胺来实现烷基化。弃去烷基化缓冲液，将样品在200 μ l50mm的范围内冲洗一次，然后将它们洗涤两次，每次在50mm Ambic中以200 μ l新鲜制备的50%ACN洗涤10分钟。在每次洗涤后，弃去上清液，并在洗涤后，使用SpeedVac将样品干燥3小时。一旦干燥，通过在37°C下在200 μ l50mmAmic的200 μ l50mmbic中加入100ng胰蛋白酶，消化蛋白质。随后通过将甲酸加入终浓度为1%并在37°C下孵育45分钟，酸化样品。最后，使用具有5-7 μ L床体积 (ThermoFisher Scientific) 之后的Hypersep滤板，脱盐样品。将样品在100 μ l80%AcN中在0.2%甲酸中洗脱两次，在SpeedVac上干燥，并重新悬浮在10 μ l0.1%甲酸中进行质谱分析。

All samples were resuspended in 10 μ L 0.2% formic acid in water and 4 μ L were injected on column for each sample. Peptides were separated over a 50 cm EasySpray reversed phase LC column (75 μ m inner diameter packed with 2 μ m, 100 Å, PepMap C18 particles, Thermo Fisher Scientific). The mobile phases (A: water with 0.2% formic acid and B: acetonitrile with 0.2% formic acid) were driven and controlled by a Dionex Ultimate 3000 RPLC nano system (Thermo Fisher Scientific). An integrated loading pump was used to load peptides onto a trap column (Acclaim PepMap 100 C18, 5 μ m particles, 20 mm length, ThermoFisher) at 5 μ L/min, which was put in line with the analytical column 6 min into the gradient for the total protein samples. Gradient elution was performed at 300 nL/min. The gradient increased from 0% to 5% B over the first 6 min of the analysis, followed by an increase from 5% to 25% B from 6 to 86 min, an increase from 25% to 90% B from 86 to 94 min, isocratic flow at 90% B from 94 to 102 min, and a re-equilibration at 0% for 18 min for a total analysis time of 120 min. Precursors were ionized using an EASY-Spray ionization source (Thermo Fisher Scientific) source held at +2.2 kV compared to ground, and the column was held at 45°C.

The inlet capillary temperature was held at 275 °C, and the RF lens was held at 60%. Survey scans of peptide precursors were collected in the Orbitrap from 350-1350 Th with an AGC target of 1,000,000, a maximum injection time of 50 ms, and a resolution of 120,000 at 200 m/z. Monoisotopic precursor selection was enabled for peptide isotopic distributions, precursors of z = 2-5 were selected for data-dependent MS/MS scans for 2 s of cycle time, and dynamic exclusion was set to 45 s with a ± 10 ppm window set around the precursor monoisotope. An isolation window of 1 Th was used to select precursor ions with the quadrupole. MS/MS scans were collected using HCD at 30 normalized collision energy (nce) with an AGC target of 50,000 and a maximum injection time of 54 ms. Mass analysis was performed in the Orbitrap with a resolution of 30,000 at 200 m/z and an automatically determined mass range.

将所有样品重悬于10 μ L 0.2%的甲酸中，在水中注入4 μ L，每个样品注入柱上。肽在50cm EasySpray反相LC柱上分离（75 μ m内直径，用2 μ m，100埃，Pepmap C18颗粒，Thermo Fisher Scientific）。通过Dionex Ultimate 3000 RPLCNANO系统（Thermo Fisher Scientific）驱动和控制移动相（A：用0.2%甲酸和B：乙腈，乙腈，含有0.2%的甲酸）。将一个集成的装载泵用于将肽加载到捕集柱上（适应薄膜100C18,5 μ m颗粒，20mm长度，热调味汁），其在5 μ l/min中，将其与分析柱纳入梯度的6分钟总蛋白质样品。梯度洗脱在300nl/min下进行。梯度在分析的前6分钟内增加到0%至5% B，然后从6%到86分钟增加到5%至25% B，从86到94分钟增加到25%至90% B.，在94至102分钟的90% B以90% B的等植物流动，并且在0%以0%的重新平衡18分钟，总分析时间为120分钟。与地面相比，使用易于喷雾电离源（Thermo Fisher Scientific）源（Thermo Fisher Scientific）来源电离前体，柱子在45°C下保持。入口毛细管温度在275°C下保持，RF透镜保持在60%。肽前体的测量扫描从350-1350°C收集在1,000,000的AGC靶标中，最大喷射时间为50 ms，分辨率为120,000°C/米。为肽同位素分布使单位异位前体选择能够选择Z = 2-5的前体，用于循环时间的数据依赖性MS / MS扫描，并且动态排除设定为45秒，设置为±10 ppm窗口前体单异位镜。第1次的分离窗口用于选择具有四极的前体离子。使用HCD在30个标准化碰撞能量（NCE）中收集MS / MS扫描，AGC目标为50,000，最大喷射时间为54毫秒。在壁图中进行质量分析，分辨率为30,000，在200m/z和自动测定的质量范围内。

FASTA sequences of the human proteome (Uniprot: UPooooo5640) were used and FASTA sequences of the viral proteins from SARS-CoV-2 (Uniprot: PoDTC1, PoDTD1, PoDTC2, PoDTC3, PoDTC4, PoDTC5, PoDTC6, PoDTC7, PoDTD8, PoDTC8, PoDTC9, PoDTD2, PoDTD3, AoA663DJA2), DENV (Uniprot: AoA173DS53), ZIKV (Uniprot: AoA140D2T1), RV (Uniprot: Po3303) were appended to the end of the human proteome reference file. For the VeroE6 reference: GreenMonkey (*Chlorocebus sabaeus*, Uniprot: UPooooo29965). This concatenated file was used to search the ChIRP-MS data with MaxQuant with the following parameters: semi-specific cleavage specificity at the C-terminal site of R and K allowing for 2 missed cleavages. Mass tolerance was set at 12 ppm for MS1s, 0.4 for MS2s. Methionine oxidation, asparagine deamidation, and N-

term acetylation were set as variable modifications. Cysteine carbamidomethylation was set as a fixed modification.

使用人蛋白质组 (UNIPROT : UPooooo5640) 的 Fasta 序列和来自 SARS-CoV-2 的病毒蛋白的 Fasta 序列 (UNIPROT : PoDTC1 , PoDTD1 , PoDTC2 , PoDTC3 , PoDTC4 , PoDTC5 , PoDTC6 , PoDTC7 , PoDTD8 , PoDTC8 , PoDTC9 , PoDTD2 , PoDTD3 , AoA663DJA2) , DENV (UNIPROT : AoA173DS53) , ZIKV (UNIPROT : AoA140D2T1) , RV (UNIPROT : Po3303) 被附加到人类蛋白质组参考文件的末尾。对于 VeroE6 参考 : Greenmonkey (Chartocebus Sabaeus , Uniprot : UPoooo029965) 。该连接文件用于搜索 Chirp-MS 数据 , 以最大的参数使用 MaxQuant : R 和 K 的 C 端部位的半特异性切割特异性 , 允许 2 个错过的裂解。 MS1S 为 MS1S 的 12ppm 设定大众耐受性 , 对于 MS2S 为 0.4 。甲硫氨酸氧化 , 天冬酰胺脱酰胺和 N- 术乙酰化被设定为可变修饰。将半胱氨酸氨基甲酰化被设定为固定改性。

The above procedure yielded two spreadsheets: one containing the data obtained from human cells (SARS-CoV-2-D1, SARS-CoV-2-D2, ZIKV-D2, DENV-D2, RV-D2) and one containing the data obtained from monkey cells (SARS-VeroE6-D1, SARS-VeroE6-D2). Label-free quantitation (LFQ) values from each MaxQuant output spreadsheet were imported into R for downstream analysis. First, log2-normalized ChIRP-MS enrichment values were obtained for each condition by subtracting the appropriate log-normalized Mock condition. Before computing enrichments, high correlations of the Mock conditions within each group (e.g., Mock SARS 1,2,3, Mock Flavivirus 1,2,3, etc) were confirmed and then the Mock replicates were averaged to ensure any observed variability would be attributable to variation in the infected conditions rather than variability in the mock samples. At this step, we also computed average enrichments across replicates to create a succinct representation of the data for each virus. Next, we matched protein IDs to gene names by querying the uniprot server using
`'https://www.uniprot.org/uniprot/?query='`. When multiple gene names matched a given protein, we used the first one as the `name` of the hit which was used for most downstream gene lookups. However, we also retained alternate names in the `gene.x` and `gene.y` columns of **Table S3**. Throughout the manuscript we have visualized enrichments for specific genes using heatmaps—rectangular heatmaps (e.g., in **Figure 4**) were visualized using R package `pheatmap` while circular heatmaps (e.g., in **Figure 7**) were visualized using R package `RCircos` . Examples of code for this analysis as well as analysis below can be found: https://github.com/juliabelk/sarscov2_chirp_ms

上述过程产生了两种电子表格 : 一种包含从人细胞获得的数据 (SARS-CoV-2-D1 , SARS-CoV-2-D2 , ZIKV-D2 , DENV-D2 , RV-D2) 以及包含所获得的数据的数据来自猴细胞 (SARS-VeroE6-D1 , SARS-VEROE6-D2) 。从每个 MaxQuant 输出电子表格的无标签定量 (LFQ) 值被导入到下游分析的 R 中。首先 , 通过减去适当的日志归一化模拟条件 , 为每个条件获得 LOG2 归一化 Chirp-MS 浓缩值。在计算富集之前 , 确认了每组内的模拟条件的高相关 (例如 Mock SARS 1,2,3, Mock Flavivirus 1,2,3, 等) , 然后平均模拟重复

以确保任何观察到的可变性可归因于受感染条件的变化而不是模拟样本中的变异性。在此步骤中，我们还计算了跨复制的平均浓缩，以创建每个病毒的数据的简洁表示。接下来，我们通过使用`<https://www.uniprot.org/uniprot/>查询UniProt Server匹配蛋白ID到基因名称？查询= `。当多个基因名称匹配给定的蛋白质时，我们将第一个作为“名称”的命名为最多用于大多数下游基因查找。但是，我们还保留了表S3的“Gene.x”和“基因”列中的替代名称。在整个稿件中，我们使用R包裹`Pheatmap`可视化了使用热手套 - 矩形热插拔的特定基因的可视化浓缩（例如，在图4中），同时使用R包裹`rcircos`可视化圆形热插拔（例如，图7中的图7）。可以找到此分析的代码的示例以及下面的分析：

https://github.com/juliabelk/sarscov2_chirp_ms

We defined the “high-confidence” interactome of each SARS-CoV-2 infection condition (D1 / D2 and VeroE6 / Huh7.5 using R package `Differential Enrichment analysis of Proteomics data` (DEP). DEP has its own procedure for data preprocessing, so for this analysis, filtering, normalization, and imputation were performed directly on MaxQuant outputs using the DEP default workflow (i.e., instead of the enrichment computation procedure described above). Enriched protein sets were defined using cutoffs log2 fold change > 0 and adjusted p value ≤ 0.05, comparing infected cells after SARS RNA pulldown to identically treated uninfected (mock) cells. After defining these high-confidence protein sets, the processed enrichments described in the preceding paragraph were used for all downstream analyses.

我们定义了每个SARS-COV-2感染条件的“高置信”互联蛋白（D1 / D2和Veroe6 / Huh7.5）使用R包裹的蛋白质组学数据（DEP）的差分富集分析。DEP有自己的数据程序预处理，因此，使用DEP默认工作流程直接在MaxQuant输出上直接执行过滤，过滤，归一化和估算，而不是上述富集计算程序）。使用截止值Log2折叠变化> 0和富集蛋白集。0和调整的P值≤0.05，比较SARS RNA下拉后感染的细胞相同地处理未感染的（模拟）细胞。在定义这些高置信蛋白套后，前段中描述的加工富集用于所有下游分析。

Principal component analysis was performed to visualize the differences between replicates and viruses (Figure 3D). To compute principal components, we used the standard R package `stats` and function `prcomp(t(x),scale = T)` where x represents the matrix of proteins by ChIRP-MS enrichments in each condition. We additionally defined an “expanded interactome” for each condition as the set of all proteins with mean enrichment $> = 1$, to aid comparisons across viruses. For GO term analysis, expanded interactomes of each virus were annotated with the DAVID Bioinformatics Resource (Huang et al., 2009a, 2009b). Annotations for Cellular Components, Binding Proteins, and Protein Domains were used to compute enrichments for each expanded interactome. Finally, to perform integrative analysis with the genome-wide CRISPR screen and CRISPR mini-pools we merged the above, initially separate human and monkey tables based on gene name to create one large table encompassing all attributes of the dataset. This table is provided as Table S3.

进行主成分分析以可视化复制和病毒之间的差异（图3D）。为了计算主成分，我们使用标准R包裹`和功能`和功能`prcomp (t (x) , scale = t) `，其中x表示每个条件下的chirp-ms富集的蛋白质矩阵。我们另外将每个条件定义为每种条件的“扩展互联蛋白酶”，作为具有均匀富集 $>= 1$ 的所有蛋白质的组，以帮助跨病毒的比较。对于转入术语分析，每种病毒的扩展副间在David生物信息学资源（Huang等，2009a，2009b）中注释了副杂志。用于细胞成分，结合蛋白和蛋白质结构域的注释用于计算每个膨胀蛋白酶的富集。最后，通过基因组 - 范围的CRISPR屏幕和CRISPR迷你池进行综合分析，我们将基于基因名称合并上述，最初单独的人员和猴表，以创建一个包含数据集的所有属性的大表。此表作为表S3提供。

ChIRP-RNA-seq and analysis Chirp-RNA-SEQ和分析

Input lysate samples and enriched RNA samples (1% of the ChIRP sample) were first digested of their cellular proteins which also acts to effectively reverse the formaldehyde crosslinking. RNA samples were brought to 50 μ L with 1x PBS and 5 μ L Proteinase K (Thermo Fisher Scientific) and incubated at 55°C for 30 min. RNA was cleaned using the Zymo Clean and Concentrate 5 column (Zymo Research) and eluted in 2x 20 μ L (final 40 μ L). DNA was removed by adding 2 μ L DNaseI and 5 μ L 10x DNase buffer (NEB) to the purified RNA and incubated at 37°C for 30 min. The RNA was cleaned up as above with the Zymo Clean and Concentrate 5 column but eluted 2x 10 μ L (final 20 μ L). To construct RNA seq libraries, TAKARA Bio SMART-Seq Stranded Kit User Manual (TAKARA Bio) was used with the following modifications. Up to 5 ng RNA was reverse-transcribed and amplified by PCR following the SMART-seq protocol. To increase cDNA yield and detection efficiency, we started from first-strand cDNA synthesis without fragmentation. The number of PCR1 cycles was 5. We purified the cDNA product with 50 μ L AMPure beads (1:1 ratio) and eluted into 20 μ L water. Then the 20 μ L purified cDNA was used as input for the final RNA-Seq library amplification. To reduce the amount of primer dimer artifacts, we purified the RNA-Seq library with 90 μ L AMPure beads (x0.9 selection) and eluted into 20 μ L water. Sequencing was performed using the Nextseq 500/550 Sequencing system (Illumina) with 2 \times 75 bp paired-end reads and 2 \times 8 bp index reads.

输入裂解物样品和富集的RNA样品（1%的ChIRP样品）首先消化其细胞蛋白质，其也作用于有效地逆转甲醛交联。用1×PBS和5 μ L蛋白酶K（Thermo Fisher Scientific）达到50 μ L的RNA样品，并在55°C下孵育30分钟。使用Zymo清洁和浓缩5柱（Zymo Research）进行清洁RNA，并在2×20 μ L（最终40 μ L）中洗脱。通过将2 μ LDNASEI和5 μ L10XDNA酶缓冲液（NEB）加入纯化的RNA并在37°C下孵育30分钟，除去DNA。如上用上述清除RNA清洁并浓缩5柱但洗脱2×10 μ L（最终20 μ L）。为了构建RNA SEQ库，Takara Bio Smart-SEQ Scranced Kit用户手册（Takara Bio）配合使用以下修改。在Smart-SEQ协议之后，通过PCR逆转录和扩增高达5ng的RNA。为了增加cDNA产量和检测效率，我们从第一链cDNA合成开始而不进行碎片。PCR1循环的数量为5.我们用50 μ LAmpure珠粒（1：1的比例）纯化CDNA产物并洗脱成20 μ L水中。然后使用20 μ L纯化的cDNA作为最终RNA-SEQ

文库扩增的输入。为了减少引物二聚体伪像的量，我们用90 μ L Ampure珠粒（X0.9选择）纯化了RNA-SEQ文库，并洗脱成20 μ L水。使用NextSeq 500/550测序系统（Illumina）进行测序，其中2 \times 75bp配对端读取和2 \times 8bp索引读取。

Adapters were automatically detected and trimmed using fastp (Chen et al., 2018). Host genomes (for *Homo sapiens* and *chlorocebus sabaeus*) were obtained from Ensembl along with annotation (gtf) files for use with feature counts. The SARS-CoV-2 genome was obtained from NCBI. Hisat2 was used to index all genomes and align reads (Kim et al., 2019). Fastq files were initially aligned to a file of known “repeat” sequences—specific sequences which are present in multiple locations in the genome and which can cause a high percentage of multi-mapped reads. Remaining reads were then aligned to the SARS-CoV-2 genome. SARS-CoV-2 genome coverage was visualized in the Integrative Genomics Viewer to assess pulldown efficiency. Remaining reads were then aligned to the host genome and reads overlapping genomic features (genes) were quantified using the featureCounts command line utility (Liao et al., 2014). Aggregated counts matrices were loaded into DESeq2 for normalization and differential gene expression analysis (Love et al., 2014). Mirroring our ChIRP-MS protein analysis, differential gene expression analysis was performed by comparing SARS-CoV-2 infected samples to mock samples.

使用FastP自动检测和修剪适配器（Chen等，2018）。主机基因组（对于HOMO SAPIENS和CHARONCEBUS SABAEUS）是从ENSEMBL获得的，以及用于特征计数的注释（GTF）文件。SARS-COV-2基因组是从NCBI获得的。Hisat2用于指定所有基因组并对齐读数（Kim等，2019）。FASTQ文件最初对准到已知的“重复”序列特定序列的文件，其存在于基因组中的多个位置，并且可以导致高百分比的多映射读取。然后将剩余的读数与SARS-COV-2基因组对齐。SARS-COV-2基因组覆盖范围在综合基因组观察者中可视化，以评估下拉效率。然后将剩余的读数与宿主基因组对齐，并使用FeatureCounts命令行实用程序（Liao等人，2014）定量读取重叠的基因组特征（基因）。将聚集计数矩阵加载到DESEQ2中以进行归一化和差分基因表达分析（Love等，2014）。通过将SARS-COV-2受感染的样品与模拟样品进行比较来进行镜像ChIRP-MS蛋白质分析，进行差异基因表达分析。

Electron Microscopy 电子显微镜

Huh 7.5 cells infected with SARS-CoV-2 were analyzed at different time points (12, 24 and 48 h.p.i.), and HBECs samples were from Wei et al., 2021. The samples were prepared in the following way: HBECs were fixed using 2.5% glutaraldehyde in 100 mM phosphate buffer, osmicated in 1% osmium tetroxide, and dehydrated in ethanol. During dehydration, 1% uranyl acetate was added to the 70% ethanol to enhance ultrastructural membrane contrast. After dehydration the cells were embedded in Durcupan and ultrathin sections were cut on a Leica Ultra-Microtome, collected on Formvar-coated

single-slot grids, and analyzed with a Tecnai 12 Biotwin electron microscope (FEI). ImageJ software was used to measure mitochondrial area.

在不同的时间点（12,24和48 HPI）分析HUH 7.5细胞（12,24和48 HPI），HBECS样品来自Wei等，2021.以下列方式制备样品：使用HBEC使用2.5%戊二醛在100mM磷酸盐缓冲液中，在十六氧化物1%锇溶液中溶解，并在乙醇中脱水。在脱水期间，将1%乙酸铀加入到70%乙醇中以增强超微结构膜对比。在脱水后，将细胞嵌入Durcupan中，在Leica超微电池上切割超薄部分，收集在FormVar涂覆的单槽电网上，并用Tecnai 12 Biotwin电子显微镜（Fei）分析。imagej软件用于测量线粒体区域。

sgRNA design and cloning SGRNA设计和克隆

Two sgRNA pools were designed: one targeting the SARS-CoV-2 expanded interactome, and one targeting the set of mitochondrially annotated proteins. Six sgRNAs per gene were used, and sgRNA sequences were selected from the previously described genome-wide African Green Monkey and Human sgRNA libraries ([Wei et al., 2021](#)). To create a pool compatible with both human and monkey cell lines, we first intersected the genome-wide guide designs for the two species to obtain cross-species compatible guides. The majority of guides were selected based on the highest ranked cross-species guides. Genes not present in both libraries were selected based on the highest ranked single-species guides. Positive control genes ACE2, CTS1, DPP4, CABIN1, and HIRA were included in both pools, as well as 100 non-targeting controls and 100 single-targeting controls.

设计了两个SARNA池：靶向SARS-COV-2扩增的互蛋白酶，以及靶向线粒体注释蛋白的一组。使用每种基因的六个SGRNA，并选自先前描述的基因组的非洲绿猴和人类SGRNA文库（Wei等，2021）。要创建与人类和猴细胞系兼容的池，我们首先与两种物种相交的基因组导向器设计，以获得跨物种兼容导游。基于排名最高的跨物种指南选择了大部分指南。基于排名最高的单种图指南选择不存在于两个库中的基因。阳性对照基因ACE2，CTS1，DPP4，CABAG1和HIRA包括在两个池中，以及100个非靶向控制和100个单一目标控制。

Oligos were designed as (fw_primer)(Esp3I site)G(sgRNA)(Esp3I site)(rev_primer) for golden gate cloning into a lentiGuidePuro vector modified to express a 2A-EGFP fusion in frame with the puromycin resistance gene. Vector was pre-digested overnight with restriction enzyme Esp3I and purified on an agarose gel. Oligos were PCR amplified for 20 cycles and purified with a commercial PCR cleanup kit. One step digestion / ligation was performed by combining 1 μL T4 DNA ligase, 1 μL Esp3I, 2 μL T4 DNA ligase buffer, 200 ng digested vector, and 40 ng purified PCR product in a 20 uL reaction. Reaction was incubated at 37°C for 1 h and then heat inactivated at 65°C for 15 min. 1 μL of the reaction was electroporated into 25 μL electrocompetent cells, grown overnight in liquid culture, and purified by maxiprep. Guide representation was confirmed by sequencing.

将寡核苷酸设计为（ESP3I）（ESP3I位点）G（SGRNA）（ESP3I站点）（REV_PRIMER），用于金栅极克隆到修饰的LENTIGUIDEPURO载体中，以用嘌呤霉素抗性基因表达框架中的2A-EGFP融合。向量用限制酶ESP3i预先消化过夜，并在琼脂糖凝胶上纯化。将寡核苷酸扩增20个循环并用商业PCR清理试剂盒纯化。通过组合1μLT4DNA连接酶，1μLESP3I，2μLT4DNA连接酶缓冲液，200ng消化载体和40μg反应中的40ng纯化的PCR产物来进行一步消化/连接。将反应在37°C下孵育1小时，然后在65°C下灭活15分钟。将1μl反应电穿过25μL电加工细胞，在液体培养中生长过夜，并通过MaxiPrep纯化。通过测序确认指南表示。

CRISPR screens CRISPR屏幕

Lentivirus for each pool was transduced into our previously described VeroE6-Cas9 cell line at an MOI of 0.1 (Wei et al., 2021). Three days later, puromycin was added to the media to select transduced cells. Puromycin selection was performed for ten days prior to commencing screens. Seven viruses were used for the CRISPR screen, including HKU5-SARS-CoV-1-S, SARS-CoV-2, rcVSV-SARS-CoV-2-S, MERS-CoV, MERS-CoV T1015N, IAV and EMCV. All the viruses were screened in duplicate. 3×10^6 transduced VeroE6 cells were plated in 5% FBS in T150 flasks. Mock infected cells were harvested 48 h after seeding and served as a reference for sgRNA enrichment analysis. At 4 d.p.i., 80% of the media was exchanged for fresh media. At 7 d.p.i., cell lysates were harvested in DNA/RNA shield buffer and gDNA of surviving cells was isolated for sequencing. Briefly, we used a standard three round amplification procedure. In the first round, all gDNA was split into 125 μL reactions of up to 5 μg gDNA each and amplified for 23 cycles. In the second round, adapters compatible with Illumina indexing were added, and 0-8 nucleotide offsets were appended to the beginning of the PCR product to increase library complexity for sequencing. Finally, sample indices were added. The resulting libraries were sequenced in dual indexed 1x75 format on an Illumina NextSeq. 每个池的慢病毒被转换为0.1的MOI的先前描述的Veroe6-Cas9细胞系（Wei等人，2021）。三天后，将嘌呤霉素加入介质中以选择转导细胞。在开始屏幕之前进行嘌呤霉素选择10天。七种病毒用于CRISPR筛选，包括HKU5-SARS-COV-1-S，SARS-COV-2，RCVSV-SARS-COV-2-S，MERS-COV，MERS-COV T1015N，IAV和EMCV。所有病毒都是重复筛选的。 3×10^6 转导的VeroE6细胞在T150烧瓶中以5% FBS镀。在播种后收获48小时的模拟感染的细胞，作为SGRNA富集分析的参考。在4 D.P.I，为新媒体交换了80%的媒体。在7d.p.i处，在DNA / RNA屏蔽缓冲液中收获细胞裂解物，并分离存活细胞的GDNA进行测序。简而言之，我们使用标准的三个圆形放大程序。在第一轮中，将所有GDNA分成125μL最高可达5μgGDNA的反应，并扩增23个循环。在第二轮中，加入与Illumina指数相容的适配器，并将0-8个核苷酸偏移追加到PCR产物的开始，以增加库复杂性进行测序。最后，添加了样本指标。在Illumina NextSeq上以双重索引1x75格式进行测序。

CRISPR screen analysis CRISPR屏幕分析

Reads were trimmed by fastp to remove flanking sequences with `fastp -f 10 -t 15` . Trimmed reads were aligned to the library designs using hisat2. Resulting bam files were converted to counts tables for each sample using package `Rsamtools` . Counts tables were processed using our previously described procedure (Wei et al., 2021). Briefly, counts for each guide were depth normalized to counts per million and then log transformed. Log fold changes for each condition were computed by subtracting the mock condition. Negative control guides were used to obtain z-scores for each guide's log fold change, from which gene-level z-scores and p values were computed. FDR values were obtained using `p.adjust` in R. PCA analysis was performed as described above for the ChIRP-MS data except on the table of gene-level z-scores for each condition. For genome-wide data, a cutoff of FDR ≤ 0.05 was used to define “hits.” For mini-pool results, we used a conservative threshold of FDR ≤ 0.001 to define hits.

用Fastp修剪读取以除去侧翼序列，用`FastP-F 10 -T 15`。修剪读取与使用Hisat2对齐图书馆设计。使用Package `rasamtools` 转换为每个样本的表格转换为计算表格。使用先前描述的程序处理计数表 (Wei等人，2021)。简而言之，每个指南的计数是深度归一化以计算每百万，然后对数转换。通过减去模拟条件来计算每个条件的日志折叠更改。对于每个导向的日志折叠变化，使用负控制引导件用于获得Z分数，从而计算基因级Z分数和P值。使用“p.Adjust”在R.CA分析中获得FDR值，如上所述进行CHIRP-MS数据，除了每个条件的基因级Z分数表。对于基因组数据，FDR ≤ 0.05 的截止值用于定义“命中”。对于迷你池结果，我们使用FDR ≤ 0.001 的保守阈值来定义命中。

Drug target analysis 药物目标分析

Drug-target interaction data was downloaded from DrugCentral (<https://drugcentral.org/download>). The full database was filtered to include only compounds targeting proteins which were present in the SARS-CoV-2 expanded interactome and compounds with data on human proteins. We added the SARS-CoV-2 ChIRP-MS enrichment (maximum average value across the VeroE6 and Huh7.5 datasets) and the SARS-CoV-2 expanded interactome screening data and have provided the data as Table S8.

药物 - 目标交互数据从药物 (HTTPS://drugCentral.org/Download) 下载。过滤完整的数据库，仅包括靶向蛋白质的化合物，该化合物存在于SARS-COV-2扩增的蛋白酶和具有人体蛋白质数据的化合物中的蛋白质。我们添加了SARS-COV-2 Chirp-MS浓缩 (veroe6 和Huh7.5数据集的最大平均值)，SARS-COV-2扩展互乱互动筛选数据，并为数据提供了表S8。

Analysis of lung single-cell RNA-sequencing data 肺单细胞RNA测序数据分析

Human lung single-cell RNA-sequencing data from Travaglini et al., 2020 was downloaded from Synapse (accession #syn21041850) as a processed cell-by-gene counts table. The data processed using Scanpy version 1.6.0 and Scrublet version 0.2.1. First,

low-quality cells were removed (cells with fewer than 250 detected genes, fewer than 500 total UMI counts, or greater than 0.25% mitochondrial reads). Then, the data was depth-normalized to a total of 10,000 reads per cell, and log-transformed. The top 2000 variable genes were identified, any batch effects due to the number of counts detected per cell were regressed out, and the data was scaled with a maximum value of 10. PCA, nearest neighbors, and UMAP calculations were performed using default settings. Leiden clustering was performed with resolution 0.2 to allow identification of non-immune clusters, i.e., CD45 (PTPRC) negative clusters. These non-immune cells were then re-processed, and a low-quality cluster containing a high number of doublets, as well as any other cells with a doublet score greater than 0.15, were filtered out, resulting in the final filtered set of high-quality non-immune cells.

来自Travaglini等人的肺单细胞RNA测序数据从Synapse下载2020个，作为处理的细胞逐个计数表下载了2020年。使用scipy 1.6.0和擦擦版本0.2.1处理的数据。首先，除去低质量的细胞（具有少于250个检测到的基因的细胞，少于500个总UMI计数，或大于0.25%线粒体读数）。然后，将数据深度归一化为每个单元格的总数为10,000读，并记录转换。鉴定了Top 2000变量基因，由于每个单元检测到的计数数量而导致的任何批量效应都被退出，并且数据以最大值为10. PCA，最近邻居和UMAP计算使用默认设置进行缩放。使用分辨率0.2进行leiden聚类，以允许鉴定不免疫簇，即CD45 (PTPRC) 负簇。然后将这些非免疫细胞重新加工，滤出含有大量双峰的低质量簇，以及具有大于0.15的双峰分数的任何其他电池，导致最终过滤的高 - 质量不免疫细胞。

These cells were then selected from the original, un-processed data; and re-processed with the same workflow as described above, with the exception of removing patient-patient batch effects by integrating the data with BBKNN with the patient information as the batch key. Clusters were labeled using the cluster IDs reported in Travaglini et al. as a guide. Cluster-identifying genes, as identified using the rank_genes_groups function with method = 'logreg' in Scanpy, are shown in [Figure S4C](#).

然后选自原始未处理数据的这些细胞；并通过如上所述的相同工作流程重新处理，除了通过将数据与BBKnn与患者信息作为批处理密钥集成数据来除去患者患者批量效果。使用Travaglini等人的群集ID标记群集。作为指导。使用Rank_genes_Groups在Scanpy中使用Rank_genes_Groups函数标识的群集识别基因如图S4C所示。

Quantification and statistical analysis 量化和统计分析

Proteomics statistics (e.g., [Figures 2A and 2B](#)) were determined by R package `Differential Enrichment analysis of Proteomics data` (DEP). RNA-seq statistics were determined by R package `DESeq2.` CRISPR screen statistics were determined with the R code available at https://github.com/juliabelk/sarscov2_chirp_ms. Statistics for mitochondria size quantification were determined using GraphPad Prism. Quantification details are available in the figure legends.

蛋白质组学统计（例如，图2A和2B）由蛋白质组学数据（DEP）的R包装`差异富集分析确定。RNA-SEQ统计数据由R包裹`DESEQ2确定。CRICPR屏幕统计数据是使用`HTTPS://github.com/juliabelk/sarscov2_chirp_ms`获得的R代码确定的。使用GraphPad Prism确定线粒体尺寸定量的统计数据。量化细节可在图中提供。

Acknowledgments 致谢

We thank Nicholas Riley for designing the mass spec methods and operating the instrument, Chris Richards and Chris Lapointe for helpful discussions, John Doench and Ruth Hanna for assistance analyzing CRISPR data, and Sigrid Knemeyer and Christine Shan at SciStories LLC for illustrations. This work was supported by the National Institutes of Health grants [Ko8CA230188](#) (A.T.S.), [U54CA260517](#) (A.T.S. and H.Y.C.), [Ko8AI128043](#) (C.B.W.), [Ro1AI140186S](#) (J.E.C), [Ro1AI141970](#) (J.E.C.), and [RM1HG007735](#) (H.Y.C.); the Burroughs Wellcome Fund Career Award for Medical Scientists (R.A.F., A.T.S., and C.B.W.); the Bill and Melinda Gates Foundation (A.T.S.), the Stanford Innovative Medicine Accelerator and Stanford ChEM-H (A.T.S.); the Ludwig Family Foundation (C.B.W.); Patterson Trust (C.B.W.); Mathers Foundation (C.B.W.), and Fast Grants from Emergent Ventures (A.T.S. and C.B.W.). R.A.F. was supported by the Damon Runyon Cancer Research Foundation [DRG-2286-17](#). J.A.B and K.R.P. were supported by Stanford Graduate Fellowships. J.A.B. was supported by the National Science Foundation Graduate Research Fellowship under grant no. [DGE-1656518](#). A.T.S. was supported by a Parker Bridge Scholar Award from the Parker Institute for [Cancer Immunotherapy](#) and a Cancer Research Institute Technology Impact Award. J.E.C. was supported by the Burroughs Wellcome Investigators in the Pathogenesis of Infectious Disease Award. H.Y.C was supported by the Pershing Square Foundation. C.R.B. and H.Y.C. are Investigators of the Howard Hughes Medical Institute. The sequencing data were generated at the Stanford [Functional Genomics](#) Facility with instrumentation purchased with NIH grants [S10OD018220](#) and [1S10OD021763](#).

我们感谢Nicholas Riley设计大规模规范和操作仪器，克里斯理查兹和克里斯拉波特为有用的讨论，John Doionds和Ruth Hanna寻求援助，分析Crispr数据和Sigrid Knemeyer和Christine Shan在Scistories LLC进行插图。该工作得到了国家健康机构授予Ko8CA230188 (A.T.)，U54CA260517 (A.T.S.)，Ko8ai128043 (C.B.W.)，Ro1ai140186S (J.E.c)，Ro1ai141970 (J.E.C.) 和RM1HG007735 (H.Y.C.)；Burroughs Wellcome基金医学家 (R.A.F.，A.T.S.和C.B.W.) 的职业奖;比尔和梅林达盖茨基金会 (A.T.S.)，斯坦福创新医学加速器和斯坦福·科学H (A.T.S.)；Ludwig家族基金会 (C.B.W.)；帕特森信托 (C.B.W.)；Mathers Foundation (C.B.W.)，以及来自紧急企业 (A.T.S.和C.B.W) 的快速补助金。r.a.f.被达蒙漫死癌癌研究基金会DRG-2286-17支持。J.A.B和K.R.P.斯坦福毕业生奖学金得到了支持。戳。由国家科学基金会研究生研究奖学金授予的支持。DGE-1656518。A.T.S.由Parker癌症免疫疗法和癌症研究所技术

影响奖项的帕克桥学者奖得到支持。J.E.C.受到破产病的支持者在传染病奖发病机制中得到了支持。H.Y.c得到歌舞广场基金会的支持。C.R.B.和h.y.c.是霍华德休斯医学院的调查员。在斯坦福函数基因组学设施中产生测序数据，其中用NIH授权S1018220和1S10OD021763购买的仪器。

Author contributions 作者捐款

R.A.F., M.R.M., C.B.W., and A.T.S. conceived the study. R.A.F., Y.Q., C.O.S., and C.B.W. performed SARS-CoV-2 and ChIRP experiments. R.A.F., J.A.B., A.L., and K.R.P. performed analysis of ChIRP data. J.A.B., J.W., M.M.A., Q.S., P.C.D., and C.B.W. performed and analyzed CRISPR screens. Y.Y., E.W., and T.L.H. performed mitochondrial imaging experiments. R.A.F., J.A.B., H.Y.C., T.H., J.E.C., C.R.B., C.B.W., and A.T.S. oversaw and guided experiments and analysis. R.A.F., J.A.B., C.B.W., and A.T.S. drafted the manuscript, and all authors reviewed and provided comments on the manuscript.

R.A.F. , M.R.M. , C.B.W.和A.S.。构思了这项研究。R.A.F. , Y.Q. , C.O.S.和C.B.W.进行SARS-COV-2和Chirp实验。r.a.f. , J.A.B. , A.L.和K.R.P.对ChIRP数据进行分析。J.A.B. , J.W. , M.M.A. , Q..S. , P.C.D和C.B.W.进行并分析了CRISPR屏幕。Y.Y. , E.W.和T.L.H.进行线粒体成像实验。R.A.F. , J.A.B. , H.Y.C. , T.H. , J.E.c. , C.R.B. , C.B.W.和A. ..监督和指导实验和分析。r.a.f. , J.A.B. , C.B.W.和A.T.S.起草了稿件，所有作者审查并向稿件进行了评论。

Declaration of interests 兴趣宣言

A.T.S. is a scientific co-founder of Immunai and receives research funding from Arsenal Biosciences and 10x Genomics. K.R.P., H.Y.C., and A.T.S. are co-founders of Cartography Biosciences. H.Y.C. is a co-founder of Accent Therapeutics, Boundless Bio, and an advisor for 10x Genomics, Arsenal Biosciences, and Spring Discovery. Yale University (C.B.W.) has a patent pending related to this work entitled: “Compounds and Compositions for Treating, Ameliorating, and/or Preventing SARS-CoV-2 Infection and/or Complications Thereof.” Yale University has committed to rapidly executable non-exclusive royalty-free licenses to intellectual property rights for the purpose of making and distributing products to prevent, diagnose, and treat COVID-19 infection during the pandemic and for a short period thereafter.

A.T.S.是一个Immunai的科学联合创始人，并从阿森纳生物科学和10X基因组学获得研究资金。K.R.P. , H.Y.C.和A.T.S.S.是制图生物科学的联合创始人。H.Y.C.是重点治疗，无限生物的联合创始人，以及10X基因组学，阿森纳生物科学和春季发现的顾问。耶鲁大学(C.B.W.)与题为：“用于治疗，改善和/或预防SARS-COV-2感染和/或其并发症的化合物和组合物有关的专利。”Yale University致力于迅速可执行的非独家免版税许可证，以便在大流行期间制定和分配产品以防止，诊断和治疗Covid-19感染的目的。

Supplemental information 补充信息

Help 帮助

 Download : [Download spreadsheet \(37KB\)](#)

Table S1. Sequences of 108 biotinylated ChIRP probes, related to Figure 1.

 Download : [Download spreadsheet \(527KB\)](#)

Table S2. Mass spectrometry data for viral proteins and host proteins with mean enrichment ≥ 1 in SARS-CoV-2 ChIRP-MS datasets, related to Figure 2.

 Download : [Download spreadsheet \(3MB\)](#)

Table S3. Complete matrix of data for all proteins in all datasets, related to Figure 3. Full data for all proteins in all datasets including multi-virus data, high-confidence interactomes, expanded interactomes, genome-wide CRISPR screen results, and presence in other datasets (such as UV-crosslinking data, PPI data).

 Download : [Download Comma Separated Value file \(819KB\)](#)

Table S4. CRISPR mini-pool designs, related to Figures 5, 6, and 7. SARS-CoV-2 interactome CRISPR mini-pool design and mitochondrial CRISPR mini-pool design. Includes target genes, controls, and cross-species compatibility of each sgRNA.

 Download : [Download Comma Separated Value file \(290KB\)](#)

Table S5. Expanded ChIRP-MS interactome CRISPR mini-pool screen, related to Figures 5 and 6. Results for SARS-CoV-2 and six other viruses. Z-scores and FDRs are included for each gene and condition.

 Download : [Download Comma Separated Value file \(186KB\)](#)

Table S6. Mitochondria CRISPR mini-pool screen, related to Figure 7. Results for SARS-CoV-2 and six other viruses. Z-scores and FDRs are included for each gene and condition.

 [Download : Download Comma Separated Value file \(126KB\)](#)

Table S7. ChIRP-MS overlap with DrugCentral database, related to Figure 5. Intersection of SARS-CoV-2 expanded interactome and a database of drug targets from DrugCentral (<https://drugcentral.org/>).

下载：下载电子表格（37KB）表S1。108个生物素化的ChIRP探针的序列，与图1相关。
下载：下载电子表格（527KB）表S2。在SARS-CoV-2 Chirp-MS Datasets中具有平均富集 ≥ 1 的病毒蛋白和宿主蛋白的质谱数据，与图2相关。下载：下载电子表格（3MB）表S3。完整的所有数据集中所有蛋白质的数据矩阵，相关图3.所有数据集中的所有蛋白质的完整数据，包括多病毒数据，高置信副间，扩增的副间，基因组CRISPR屏幕结果以及其他数据集中的存在（例如UV交联数据，PPI数据）。下载：下载逗号分隔值文件（819KB）表S4。与图5,6和7.SARS-CoV-2互乱迷你游泳池设计和线粒体CRISPR迷你池设计有关的CRISPL迷你池设计。包括每个SGRNA的靶基因，对照和跨物种兼容性。下载：下载逗号分隔值文件（290KB）表S5。扩展的Chirp-MS互联池CrispRP迷你池屏幕，与图5和6. SARS-CoV-2和其他六种病毒的结果。每个基因和条件包括Z分数和FDRS。下载：下载逗号分隔值文件（186KB）表S6。线粒体Crisprp迷你池屏幕，相关图7. SARS-CoV-2和其他六种病毒的结果。每个基因和条件包括Z分数和FDRS。下载：下载逗号分隔值文件（126KB）表S7。Chirp-MS与药物数据库重叠，与图5.SARS-CoV-2扩增互联蛋白组和药物组织靶标数据库（[HTTPS://drugcentral.org/](https://drugcentral.org/)）。

References 参考

[Agnihothram et al., 2014 Agnihothram等人。, 2014年 S. Agnihothram, B.L. Yount Jr., E.F.](#)

Donaldson, J. Huynh, V.D. Menachery, L.E. Gralinski, R.L. Graham, M.M. Becker, S. Tomar, T.D. Scobey, *et al.*

A Mouse Model for Betacoronavirus Subgroup 2c Using a Bat Coronavirus Strain HKU5 Variant

mBio, 5 (2014)

e00047-14

[Google Scholar 谷歌学术](#)

[Ahlquist, 2006 Ahlquist , 2006年 P. Ahlquist](#)

Parallels among positive-strand RNA viruses, reverse-transcribing viruses and double-stranded RNA viruses

Nat. Rev. Microbiol., 4 (2006), pp. 371-382

[CrossRef 十字架](#) [View Record in Scopus 在Scopus中查看纪录](#)

[Google Scholar 谷歌学术](#)

[Baggen et al., 2019 Baggen等人。, 2019年 J. Baggen, H.J. Thibaut, D.L. Hurdiss, M. Wahedi, C.D. Marceau, A.L.W. van Vliet, J.E. Carette, F.J.M. van Kuppeveld](#)

Identification of the Cell-Surface Protease ADAM9 as an Entry Factor for Encephalomyocarditis Virus

MBio, 10 (2019), p. e01780-19

[View Record in Scopus](#) 在Scopus中查看纪录 [Google Scholar](#) 谷歌学术

Banerjee et al., 2020 Banerjee等人。, 2020年 A.K. Banerjee, M.R. Blanco, E.A. Bruce, D.D. Honson, L.M. Chen, A. Chow, P. Bhat, N. Ollikainen, S.A. Quinodoz, C. Loney, *et al.*

SARS-CoV-2 Disrupts Splicing, Translation, and Protein Trafficking to Suppress Host Defenses

Cell, 183 (2020), pp. 1325-1339.e21

[Article 文章](#)  [Download PDF](#) 下载PDF.

[View Record in Scopus](#) 在Scopus中查看纪录 [Google Scholar](#) 谷歌学术

Bazzone et al., 2019 Bazzone等人。, 2019年 L.E. Bazzone, M. King, C.R. MacKay, P.P. Kyaw, P. Meraner, D. Lindstrom, J. Rojas-Quintero, C.A. Owen, J.P. Wang, A.L. Brass, *et al.*

A Disintegrin and Metalloproteinase 9 Domain (ADAM9) Is a Major Susceptibility Factor in the Early Stages of Encephalomyocarditis Virus Infection

MBio, 10 (2019), p. e02734-18

[View Record in Scopus](#) 在Scopus中查看纪录 [Google Scholar](#) 谷歌学术

Carrasco-Hernandez et al., 2017 Carrasco-Hernandez等, 2017年 R. Carrasco-Hernandez, R. Jácome, Y. López Vidal, S. Ponce de León

Are RNA Viruses Candidate Agents for the Next Global Pandemic? A Review

ILAR J., 58 (2017), pp. 343-358

[CrossRef](#) 十字架 [View Record in Scopus](#) 在Scopus中查看纪录

[Google Scholar](#) 谷歌学术

Chang et al., 2014 昌等人。, 2014年 C.K. Chang, M.-H. Hou, C.-F. Chang, C.-D. Hsiao, T.H. Huang

The SARS coronavirus nucleocapsid protein--forms and functions

Antiviral Res., 103 (2014), pp. 39-50

[Article 文章](#)  [Download PDF](#) 下载PDF.

[View Record in Scopus](#) 在Scopus中查看纪录 [Google Scholar](#) 谷歌学术

Chen et al., 2018 陈等人。, 2018年 S. Chen, Y. Zhou, Y. Chen, J. Gu

fastp: an ultra-fast all-in-one FASTQ preprocessor

Bioinformatics, 34 (2018), pp. i884-i890

[CrossRef](#) 十字架 [View Record in Scopus](#) 在Scopus中查看纪录

[Google Scholar](#) 谷歌学术

Chu and Chang, 2018 楚和张, 2018年 C. Chu, H.Y. Chang

ChIRP-MS: RNA-Directed Proteomic Discovery

Methods Mol. Biol., 1861 (2018), pp. 37-45

[CrossRef 十字架](#) [View Record in Scopus 在Scopus中查看纪录](#)

[Google Scholar 谷歌学术](#)

[Chu et al., 2015](#) Chu等人。, 2015年 C. Chu, Q.C. Zhang, S.T. da Rocha, R.A. Flynn, M. Bharadwaj, J.M. Calabrese, T. Magnuson, E. Heard, H.Y. Chang

Systematic discovery of Xist RNA binding proteins

Cell, 161 (2015), pp. 404-416

[Article 文章](#)  [Download PDF 下载PDF](#)

[View Record in Scopus 在Scopus中查看纪录](#) [Google Scholar 谷歌学术](#)

[Cockrell et al., 2018](#) Cockrell等, 2018年 A.S. Cockrell, S.R. Leist, M.G. Douglas, R.S. Baric

Modeling pathogenesis of emergent and pre-emergent human coronaviruses in mice

Mamm. Genome, 29 (2018), pp. 367-383

[CrossRef 十字架](#) [View Record in Scopus 在Scopus中查看纪录](#)

[Google Scholar 谷歌学术](#)

[Eckhardt et al., 2020](#) Eckhardt等人。, 2020年 M. Eckhardt, J.F. Hultquist, R.M. Kaake, R. Hüttenhain, N.J. Krogan

A systems approach to infectious disease

Nat. Rev. Genet., 21 (2020), pp. 339-354

[CrossRef 十字架](#) [View Record in Scopus 在Scopus中查看纪录](#)

[Google Scholar 谷歌学术](#)

[Edgil et al., 2006](#) Edgil等人。, 2006年 D. Edgil, C. Polacek, E. Harris

Dengue virus utilizes a novel strategy for translation initiation when cap-dependent translation is inhibited

J. Virol., 80 (2006), pp. 2976-2986

[View Record in Scopus 在Scopus中查看纪录](#) [Google Scholar 谷歌学术](#)

[Fernandez-Garcia et al., 2009](#) Fernandez-Garcia等, 2009年 M.-D. Fernandez-Garcia, M. Mazzon, M. Jacobs, A. Amara

Pathogenesis of flavivirus infections: using and abusing the host cell

Cell Host Microbe, 5 (2009), pp. 318-328

[Article 文章](#)  [Download PDF 下载PDF](#)

[View Record in Scopus 在Scopus中查看纪录](#) [Google Scholar 谷歌学术](#)

[Finkel et al., 2020](#) Finkel等人。, 2020年 Y. Finkel, O. Mizrahi, A. Nachshon, S. Weingarten-Gabbay, D. Morgenstern, Y. Yahalom-Ronen, H. Tamir, H. Achdout, D. Stein, O. Israeli, et al.

The coding capacity of SARS-CoV-2

Nature, 589 (2020), pp. 125-130

[Google Scholar 谷歌学术](#)

[Fritzlar et al., 2019](#) Fritzlar等人。, 2019年 S. Fritzlar, T.E. Aktepe, Y.-W. Chao, N.D. Kenney, M.R. McAllaster, C.B. Wilen, P.A. White, J.M. Mackenzie

Mouse Norovirus Infection Arrests Host Cell Translation Uncoupled from the Stress Granule-PKR-eIF2 α Axis

MBio, 10 (2019), p. e00960-19

[View Record in Scopus](#) 在Scopus中查看纪录 [Google Scholar](#) 谷歌学术

Garcia-Blanco et al., 2016 Garcia-Blanco等 , 2016年 M.A. Garcia-Blanco, S.G. Vasudevan, S.S. Bradrick, C. Nicchitta

Flavivirus RNA transactions from viral entry to genome replication

Antiviral Res., 134 (2016), pp. 244-249

[Article 文章](#)  [Download PDF](#) 下载PDF.

[View Record in Scopus](#) 在Scopus中查看纪录 [Google Scholar](#) 谷歌学术

Geuens et al., 2016 Geuens等人。, 2016年 T. Geuens, D. Bouhy, V. Timmerman

The hnRNP family: insights into their role in health and disease

Hum. Genet., 135 (2016), pp. 851-867

[CrossRef](#) 十字架 [View Record in Scopus](#) 在Scopus中查看纪录

[Google Scholar](#) 谷歌学术

Gordon et al., 2020 Gordon等人。, 2020年 D.E. Gordon, G.M. Jang, M. Bouhaddou, J. Xu, K. Obernier, K.M. White, M.J. O'Meara, V.V. Rezelj, J.Z. Guo, D.L. Swaney, et al.

A SARS-CoV-2 protein interaction map reveals targets for drug repurposing

Nature, 583 (2020), pp. 459-468

[CrossRef](#) 十字架 [View Record in Scopus](#) 在Scopus中查看纪录

[Google Scholar](#) 谷歌学术

Gralinski and Baric, 2015 格罗斯基和律政 , 2015年 L.E. Gralinski, R.S. Baric

Molecular pathology of emerging coronavirus infections

J. Pathol., 235 (2015), pp. 185-195

[CrossRef](#) 十字架 [View Record in Scopus](#) 在Scopus中查看纪录

[Google Scholar](#) 谷歌学术

Harcourt et al., 2020 Harcourt等人。, 2020 J. Harcourt, A. Tamin, X. Lu, S. Kamili, S.K.

Sakthivel, J. Murray, K. Queen, Y. Tao, C.R. Paden, J. Zhang, et al.

Severe Acute Respiratory Syndrome Coronavirus 2 from Patient with Coronavirus Disease, United States

Emerg. Infect. Dis., 26 (2020), pp. 1266-1273

[CrossRef](#) 十字架 [View Record in Scopus](#) 在Scopus中查看纪录

[Google Scholar](#) 谷歌学术

Hoffmann et al., 2021 Hoffmann等人。, 2021 H.-H. Hoffmann, F.J. Sánchez-Rivera, W.M.

Schneider, J.M. Luna, Y.M. Soto-Feliciano, A.W. Ashbrook, J. Le Pen, A.A. Leal, I. Ricardo-Lax, E. Michailidis, et al.

Functional interrogation of a SARS-CoV-2 host protein interactome identifies unique and shared coronavirus host factors

Cell Host Microbe, 29 (2021), pp. 267-280.e5

[Article 文章](#)  [Download PDF 下载PDF.](#)

[View Record in Scopus 在Scopus中查看纪录](#) [Google Scholar 谷歌学术](#)

Hosmillo et al., 2019 Hosmillo等人。, 2019年 M. Hosmillo, J. Lu, M.R. McAllaster, J.B.

Eaglesham, X. Wang, E. Emmott, P. Domingues, Y. Chaudhry, T.J. Fitzmaurice, M.K. Tung, *et al.*

Noroviruses subvert the core stress granule component G3BP1 to promote viral VPg-dependent translation

eLife, 8 (2019), p. e46681

[View Record in Scopus 在Scopus中查看纪录](#) [Google Scholar 谷歌学术](#)

Hou et al., 2020 侯等人。, 2020年 Y.J. Hou, K. Okuda, C.E. Edwards, D.R. Martinez, T. Asakura,

K.H. Dinnon 3rd, T. Kato, R.E. Lee, B.L. Yount, T.M. Mascenik, *et al.*

SARS-CoV-2 Reverse Genetics Reveals a Variable Infection Gradient in the Respiratory Tract

Cell, 182 (2020), pp. 429-446.e14

[Article 文章](#)  [Download PDF 下载PDF.](#)

[View Record in Scopus 在Scopus中查看纪录](#) [Google Scholar 谷歌学术](#)

Huang et al., 2009a 黃等人。, 2009a W. Huang, B.T. Sherman, R.A. Lempicki

Bioinformatics enrichment tools: paths toward the comprehensive functional analysis of large gene lists

Nucleic Acids Res., 37 (2009), pp. 1-13

[View Record in Scopus 在Scopus中查看纪录](#) [Google Scholar 谷歌学术](#)

Huang et al., 2009b Huang等人。, 2009b W. Huang, B.T. Sherman, R.A. Lempicki

Systematic and integrative analysis of large gene lists using DAVID bioinformatics resources

Nat. Protoc., 4 (2009), pp. 44-57

[CrossRef 十字架](#) [View Record in Scopus 在Scopus中查看纪录](#)

[Google Scholar 谷歌学术](#)

Janes et al., 2018 Janes等, 2018年 J. Janes, M.E. Young, E. Chen, N.H. Rogers, S. Burgstaller-Muehlbacher, L.D. Hughes, M.S. Love, M.V. Hull, K.L. Kuhen, A.K. Woods, *et al.*

The ReFRAME library as a comprehensive drug repurposing library and its application to the treatment of cryptosporidiosis

Proc. Natl. Acad. Sci. U S A, 115 (2018), pp. 10750-10755

[CrossRef 十字架](#) [View Record in Scopus 在Scopus中查看纪录](#)

[Google Scholar 谷歌学术](#)

Jankowsky, 2011 Jankowsky, 2011年 E. Jankowsky

RNA helicases at work: binding and rearranging

Trends Biochem. Sci., 36 (2011), pp. 19-29

[Article 文章](#)  [Download PDF 下载PDF.](#)

[View Record in Scopus 在Scopus中查看纪录](#) [Google Scholar 谷歌学术](#)

Kim et al., 2019 Kim等人。, 2019年 D. Kim, J.M. Paggi, C. Park, C. Bennett, S.L. Salzberg
Graph-based genome alignment and genotyping with HISAT2 and HISAT-genotype

Nat. Biotechnol., 37 (2019), pp. 907-915

[CrossRef](#) [十字架](#) [View Record in Scopus](#) 在Scopus中查看纪录

[Google Scholar](#) 谷歌学术

Kim et al., 2020a Kim等人。, 2020A B. Kim, S. Arcos, K. Rothamel, M. Ascano

Viral crosslinking and solid-phase purification enables discovery of ribonucleoprotein complexes on incoming RNA virus genomes

Nat. Protoc., 16 (2020), pp. 516-531

[CrossRef](#) [十字架](#) [View Record in Scopus](#) 在Scopus中查看纪录

[Google Scholar](#) 谷歌学术

Kim et al., 2020b Kim等人。, 2020B D. Kim, J.-Y. Lee, J.-S. Yang, J.W. Kim, V.N. Kim, H. Chang

The Architecture of SARS-CoV-2 Transcriptome

Cell, 181 (2020), pp. 914-921.e10

[Article 文章](#)  [Download PDF](#) 下载PDF.

[View Record in Scopus](#) 在Scopus中查看纪录 [Google Scholar](#) 谷歌学术

Knott et al., 2016 knott等人。, 2016年 G.J. Knott, C.S. Bond, A.H. Fox

The DBHS proteins SFPQ, NONO and PSPC1: a multipurpose molecular scaffold

Nucleic Acids Res., 44 (2016), pp. 3989-4004

[CrossRef](#) [十字架](#) [View Record in Scopus](#) 在Scopus中查看纪录

[Google Scholar](#) 谷歌学术

Lahaye et al., 2018 拉哈伊等人。, 2018年 X. Lahaye, M. Gentili, A. Silvin, C. Conrad, L. Picard,

M. Jouve, E. Zueva, M. Maurin, F. Nadalin, G.J. Knott, *et al.*

NONO Detects the Nuclear HIV Capsid to Promote cGAS-Mediated Innate Immune Activation

Cell, 175 (2018), pp. 488-501.e22

[Article 文章](#)  [Download PDF](#) 下载PDF.

[View Record in Scopus](#) 在Scopus中查看纪录 [Google Scholar](#) 谷歌学术

Lenarcic et al., 2013 Lenarcic等人。, 2013年 E.M. Lenarcic, D.M. Landry, T.M. Greco, I.M.

Cristea, S.R. Thompson

Thiouracil cross-linking mass spectrometry: a cell-based method to identify host factors involved in viral amplification

J. Virol., 87 (2013), pp. 8697-8712

[View Record in Scopus](#) 在Scopus中查看纪录 [Google Scholar](#) 谷歌学术

Li et al., 2020 李等人。, 2020年 M. Li, H. Ramage, S. Cherry

Deciphering flavivirus-host interactions using quantitative proteomics

Curr. Opin. Immunol., 66 (2020), pp. 90-97

Article 文章  Download PDF 下载PDF.

[View Record in Scopus](#) 在Scopus中查看纪录 [Google Scholar](#) 谷歌学术

Liao et al., 2014 Liao等人。, 2014年 Y. Liao, G.K. Smyth, W. Shi

featureCounts: an efficient general purpose program for assigning sequence reads to genomic features

Bioinformatics, 30 (2014), pp. 923-930

[CrossRef](#) 十字架 [View Record in Scopus](#) 在Scopus中查看纪录

[Google Scholar](#) 谷歌学术

Lichinchi et al., 2016 Lichinchi等, 2016年 G. Lichinchi, B.S. Zhao, Y. Wu, Z. Lu, Y. Qin, C. He, T.M. Rana

Dynamics of Human and Viral RNA Methylation during Zika Virus Infection

Cell Host Microbe, 20 (2016), pp. 666-673

Article 文章  Download PDF 下载PDF.

[View Record in Scopus](#) 在Scopus中查看纪录 [Google Scholar](#) 谷歌学术

Loo and Gale, 2011 Loo和Gale, 2011 Y.-M. Loo, M. Gale Jr.

Immune signaling by RIG-I-like receptors

Immunity, 34 (2011), pp. 680-692

Article 文章  Download PDF 下载PDF.

[View Record in Scopus](#) 在Scopus中查看纪录 [Google Scholar](#) 谷歌学术

Love et al., 2014 爱等人。, 2014年 M.I. Love, W. Huber, S. Anders

Moderated estimation of fold change and dispersion for RNA-seq data with DESeq2

Genome Biol., 15 (2014), p. 550

[View Record in Scopus](#) 在Scopus中查看纪录 [Google Scholar](#) 谷歌学术

McBride et al., 2007 McBride等, 2007年 C.E. McBride, J. Li, C.E. Machamer

The cytoplasmic tail of the severe acute respiratory syndrome coronavirus spike protein contains a novel endoplasmic reticulum retrieval signal that binds COPI and promotes interaction with membrane protein

J. Virol., 81 (2007), pp. 2418-2428

[View Record in Scopus](#) 在Scopus中查看纪录 [Google Scholar](#) 谷歌学术

Meier-Stephenson et al., 2018 Meier-Stephenson等。, 2018年 V. Meier-Stephenson, T.

Mrozowich, M. Pham, T.R. Patel

DEAD-box helicases: the Yin and Yang roles in viral infections

Biotechnol. Genet. Eng. Rev., 34 (2018), pp. 3-32

[CrossRef](#) 十字架 [View Record in Scopus](#) 在Scopus中查看纪录

[Google Scholar](#) 谷歌学术

Menachery et al., 2015 Menachery等人。, 2015年 V.D. Menachery, B.L. Yount Jr., K. Debbink, S. Agnihothram, L.E. Gralinski, J.A. Plante, R.L. Graham, T. Scobey, X.-Y. Ge, E.F. Donaldson, et al.

A SARS-like cluster of circulating bat coronaviruses shows potential for human emergence

Nat. Med., 21 (2015), pp. 1508-1513

[CrossRef 十字架](#) [View Record in Scopus 在Scopus中查看纪录](#)

[Google Scholar 谷歌学术](#)

Mukhopadhyay et al., 2005 Mukhopadhyay等，2005年 S. Mukhopadhyay, R.J. Kuhn, M.G.

Rossmann

A structural perspective of the flavivirus life cycle

Nat. Rev. Microbiol., 3 (2005), pp. 13-22

[CrossRef 十字架](#) [View Record in Scopus 在Scopus中查看纪录](#)

[Google Scholar 谷歌学术](#)

Ooi et al., 2019 Ooi等，2019年 Y.S. Ooi, K. Majzoub, R.A. Flynn, M.A. Mata, J. Diep, J.K. Li, N. van Buuren, N. Rumachik, A.G. Johnson, A.S. Puschnik, et al.

An RNA-centric dissection of host complexes controlling flavivirus infection

Nat. Microbiol., 4 (2019), pp. 2369-2382

[CrossRef 十字架](#) [View Record in Scopus 在Scopus中查看纪录](#)

[Google Scholar 谷歌学术](#)

Ou et al., 1995 欧等，1995年 S.H. Ou, F. Wu, D. Harrich, L.F. García-Martínez, R.B. Gaynor

Cloning and characterization of a novel cellular protein, TDP-43, that binds to human immunodeficiency virus type 1 TAR DNA sequence motifs

J. Virol., 69 (1995), pp. 3584-3596

[CrossRef 十字架](#) [View Record in Scopus 在Scopus中查看纪录](#)

[Google Scholar 谷歌学术](#)

Phillips et al., 2016 Phillips等人。, 2016年 S.L. Phillips, E.J. Soderblom, S.S. Bradrick, M.A. Garcia-Blanco

Identification of Proteins Bound to Dengue Viral RNA In Vivo Reveals New Host Proteins Important for Virus Replication

MBio, 7 (2016), p. e01865-e15

[Google Scholar 谷歌学术](#)

Puschnik et al., 2017 Puschnik等，2017年 A.S. Puschnik, K. Majzoub, Y.S. Ooi, J.E. Carette

A CRISPR toolbox to study virus-host interactions

Nat. Rev. Microbiol., 15 (2017), pp. 351-364

[CrossRef 十字架](#) [View Record in Scopus 在Scopus中查看纪录](#)

[Google Scholar 谷歌学术](#)

Raaben et al., 2010 Raaben等人。, 2010年 M. Raaben, C.C. Posthuma, M.H. Verheij, E.G. te Linteloo, M. Kikkert, J.W. Drijfhout, E.J. Snijder, P.J.M. Rottier, C.A.M. de Haan

The ubiquitin-proteasome system plays an important role during various stages of the coronavirus infection cycle

J. Virol., 84 (2010), pp. 7869-7879

Ravindra et al., 2020 Ravindra等 , 2020年 N.G. Ravindra, M.M. Alfajaro, V. Gasque, V. Habet, J. Wei, R.B. Filler, N.C. Huston, H. Wan, K. Szigeti-Buck, B. Wang, *et al.*
Single-cell longitudinal analysis of SARS-CoV-2 infection in human airway epithelium
bioRxiv (2020), [10.1101/2020.05.06.081695](https://doi.org/10.1101/2020.05.06.081695) [10.1101 / 2020.05.06.081695](https://doi.org/10.1101/2020.05.06.081695).
[Google Scholar 谷歌学术](#)

Ringgaard et al., 2019 Ringgaard等人。, 2019年 M. Ringgaard, V. Marchand, E. Decroly, Y. Motorin, Y. Bennasser
FTSJ3 is an RNA 2¢-O-methyltransferase recruited by HIV to avoid innate immune sensing
Nature, 565 (2019), pp. 500-504
[CrossRef 十字架](#) [View Record in Scopus 在Scopus中查看纪录](#)
[Google Scholar 谷歌学术](#)

Roth et al., 2017 Roth等 , 2017年 H. Roth, V. Magg, F. Uch, P. Mutz, P. Klein, K. Haneke, V. Lohmann, R. Bartenschlager, O.T. Fackler, N. Locker, *et al.*
Flavivirus Infection Uncouples Translation Suppression from Cellular Stress Responses
MBio, 8 (2017), p. e02150-16
[CrossRef 十字架](#) [View Record in Scopus 在Scopus中查看纪录](#)
[Google Scholar 谷歌学术](#)

Salahudeen et al., 2020 Salahudeen等人。, 2020年 A.A. Salahudeen, S.S. Choi, A. Rustagi, J. Zhu, V. van Unen, S.M. de la O, R.A. Flynn, M. Margalef-Català, A.J.M. Santos, J. Ju, *et al.*
Progenitor identification and SARS-CoV-2 infection in human distal lung organoids
Nature, 588 (2020), pp. 670-675
[CrossRef 十字架](#) [View Record in Scopus 在Scopus中查看纪录](#)
[Google Scholar 谷歌学术](#)

Schmidt et al., 2021 Schmidt等人 , 2021年 N. Schmidt, C.A. Lareau, H. Keshishian, S. Ganskikh, C. Schneider, T. Hennig, R. Melanson, S. Werner, Y. Wei, M. Zimmer, *et al.*
The SARS-CoV-2 RNA–protein interactome in infected human cells
Nat. Microbiol., 6 (2021), pp. 339-353
[CrossRef 十字架](#) [View Record in Scopus 在Scopus中查看纪录](#)
[Google Scholar 谷歌学术](#)

Schoggins and Rice, 2011 Schoggins和Rice , 2011年 J.W. Schoggins, C.M. Rice
Interferon-stimulated genes and their antiviral effector functions
Curr. Opin. Virol., 1 (2011), pp. 519-525
[Article 文章](#)  [Download PDF 下载PDF](#).
[View Record in Scopus 在Scopus中查看纪录](#) [Google Scholar 谷歌学术](#)

Schubert et al., 2020 Schubert等人。, 2020年 K. Schubert, E.D. Karousis, A. Jomaa, A. Scaiola, B. Echeverria, L.-A. Gurzeler, M. Leibundgut, V. Thiel, O. Mühlemann, N. Ban
SARS-CoV-2 Nsp1 binds the ribosomal mRNA channel to inhibit translation
Nat. Struct. Mol. Biol., 27 (2020), pp. 959-966
[CrossRef 十字架](#) [View Record in Scopus 在Scopus中查看纪录](#)
[Google Scholar 谷歌学术](#)

Scobey et al., 2013 Scobey等人。, 2013年 T. Scobey, B.L. Yount, A.C. Sims, E.F. Donaldson, S.S. Agnihothram, V.D. Menachery, R.L. Graham, J. Swanstrom, P.F. Bove, J.D. Kim, et al.
Reverse genetics with a full-length infectious cDNA of the Middle East respiratory syndrome coronavirus
Proc. Natl. Acad. Sci. U S A, 110 (2013), pp. 16157-16162
[CrossRef 十字架](#) [View Record in Scopus 在Scopus中查看纪录](#)
[Google Scholar 谷歌学术](#)

Shannon et al., 2003 Shannon等人。, 2003年 P. Shannon, A. Markiel, O. Ozier, N.S. Baliga, J.T. Wang, D. Ramage, N. Amin, B. Schwikowski, T. Ideker
Cytoscape: a software environment for integrated models of biomolecular interaction networks
Genome Res., 13 (2003), pp. 2498-2504
[CrossRef 十字架](#) [View Record in Scopus 在Scopus中查看纪录](#)
[Google Scholar 谷歌学术](#)

Somasundaran et al., 1994 Somasundaran等, 1994年 M. Somasundaran, M.L. Zapp, L.K. Beattie, L. Pang, K.S. Byron, G.J. Bassell, J.L. Sullivan, R.H. Singer
Localization of HIV RNA in mitochondria of infected cells: potential role in cytopathogenicity
J. Cell Biol., 126 (1994), pp. 1353-1360
[View Record in Scopus 在Scopus中查看纪录](#) [Google Scholar 谷歌学术](#)

Sungnak et al., 2020 Sungnak等人。, 2020年 W. Sungnak, N. Huang, C. Bécavin, M. Berg, R. Queen, M. Litvinukova, C. Talavera-López, H. Maatz, D. Reichart, F. Sampaziotis, et al., HCA Lung Biological Network
SARS-CoV-2 entry factors are highly expressed in nasal epithelial cells together with innate immune genes
Nat. Med., 26 (2020), pp. 681-687
[CrossRef 十字架](#) [View Record in Scopus 在Scopus中查看纪录](#)
[Google Scholar 谷歌学术](#)

Szul and Sztul, 2011 Szul和Sztul, 2011年 T. Szul, E. Sztul
COPII and COPI traffic at the ER-Golgi interface
Physiology (Bethesda), 26 (2011), pp. 348-364
[CrossRef 十字架](#) [View Record in Scopus 在Scopus中查看纪录](#)
[Google Scholar 谷歌学术](#)

Taschuk and Cherry, 2020 Taschuk和Cherry , 2020 F. Taschuk, S. Cherry

DEAD-Box Helicases: Sensors, Regulators, and Effectors for Antiviral Defense

Viruses, 12 (2020), p. 181

[CrossRef 十字架](#) [View Record in Scopus 在Scopus中查看纪录](#)

[Google Scholar 谷歌学术](#)

Thoms et al., 2020 Thoms等 , 2020年 M. Thoms, R. Buschauer, M. Ameismeier, L. Koepke, T.

Denk, M. Hirschenberger, H. Kratzat, M. Hayn, T. Mackens-Kiani, J. Cheng, *et al.*

Structural basis for translational shutdown and immune evasion by the Nsp1 protein of SARS-CoV-2

Science, 369 (2020), pp. 1249-1255

[CrossRef 十字架](#) [Google Scholar 谷歌学术](#)

Travaglini et al., 2020 Travaglini等 , 2020年 K.J. Travaglini, A.N. Nabhan, L. Penland, R. Sinha,

A. Gillich, R.V. Sit, S. Chang, S.D. Conley, Y. Mori, J. Seita, *et al.*

A molecular cell atlas of the human lung from single-cell RNA sequencing

Nature, 587 (2020), pp. 619-625

[CrossRef 十字架](#) [View Record in Scopus 在Scopus中查看纪录](#)

[Google Scholar 谷歌学术](#)

Viktorovskaya et al., 2016 Viktorovskaya等。 , 2016年 O.V. Viktorovskaya, T.M. Greco, I.M.

Cristea, S.R. Thompson

Identification of RNA Binding Proteins Associated with Dengue Virus RNA in Infected Cells Reveals Temporally Distinct Host Factor Requirements

PLoS Negl. Trop. Dis., 10 (2016), p. e0004921

[CrossRef 十字架](#) [View Record in Scopus 在Scopus中查看纪录](#)

[Google Scholar 谷歌学术](#)

Wang et al., 2020 Wang等人。 , 2020年 R. Wang, C.R. Simoneau, J. Kulsupatrakul, M.

Bouhaddou, K. Travisano, J.M. Hayashi, J. Carlson-Stevermer, J. Oki, K. Holden, N.J.

Krogan, *et al.*

Functional genomic screens identify human host factors for SARS-CoV-2 and common cold coronaviruses

bioRxiv (2020), [10.1101/2020.09.24.312298](https://doi.org/10.1101/2020.09.24.312298) [10.1101 / 2020.09.24.312298](https://doi.org/10.1101/2020.09.24.312298)

[Google Scholar 谷歌学术](#)

Wei et al., 2021 Wei等人 , 2021年 J. Wei, M.M. Alfajaro, P.C. DeWeirdt, R.E. Hanna, W.J. Lu-

Culligan, W.L. Cai, M.S. Strine, S.-M. Zhang, V.R. Graziano, C.O. Schmitz, *et al.*

Genome-wide CRISPR Screens Reveal Host Factors Critical for SARS-CoV-2 Infection

Cell, 184 (2021), pp. 76-91.e13

[Article 文章](#)  [Download PDF 下载PDF](#)

[View Record in Scopus 在Scopus中查看纪录](#) [Google Scholar 谷歌学术](#)

White et al., 2021 White等 , 2021

K.M. White, R. Rosales, S. Yildiz, T. Kehrer, L. Miorin, E. Moreno, S. Jangra, M.B. Uccellini, R. Rathnasinghe, L. Coughlan, *et al.*

Plitidepsin has potent preclinical efficacy against SARS-CoV-2 by targeting the host protein eEF1A

Science, 371 (2021), pp. 926-931

[CrossRef 十字架](#) [View Record in Scopus 在Scopus中查看纪录](#)

[Google Scholar 谷歌学术](#)

[Wolff et al., 2020 Wolff等人。, 2020年](#) G. Wolff, R.W.A.L. Limpens, J.C. Zevenhoven-Dobbe, U. Laugks, S. Zheng, A.W.M. de Jong, R.I. Koning, D.A. Agard, K. Grünewald, A.J. Koster, *et al.*
A molecular pore spans the double membrane of the coronavirus replication organelle

Science, 369 (2020), pp. 1395-1398

[CrossRef 十字架](#) [View Record in Scopus 在Scopus中查看纪录](#)

[Google Scholar 谷歌学术](#)

[Wu et al., 2020 Wu等 , 2020年](#) K.E. Wu, F.M. Fazal, K.R. Parker, J. Zou, H.Y. Chang

RNA-GPS Predicts SARS-CoV-2 RNA Residency to Host Mitochondria and Nucleolus

Cell Syst., 11 (2020), pp. 102-108.e3

[Article 文章](#)  [Download PDF 下载PDF](#)

[View Record in Scopus 在Scopus中查看纪录](#) [Google Scholar 谷歌学术](#)

[Yang et al., 2021 杨等人。, 2021](#) S.L. Yang, L. DeFalco, D.E. Anderson, Y. Zhang, A.J. Aw, S.Y. Lim, L.X. Ni, K.Y. Tan, T. Zhang, T. Chawla, *et al.*

Comprehensive mapping of SARS-CoV-2 interactions in vivo reveals functional virus-host interactions

bioRxiv (2021), [10.1101/2021.01.17.427000](https://doi.org/10.1101/2021.01.17.427000) [10.1101 / 2021.01.17.427000](https://doi.org/10.1101/2021.01.17.427000)

[Google Scholar 谷歌学术](#)

[Yue et al., 2015 岳等人。, 2015年](#) Y. Yue, J. Liu, C. He

RNA N6-methyladenosine methylation in post-transcriptional gene expression regulation

Genes Dev., 29 (2015), pp. 1343-1355

[CrossRef 十字架](#) [View Record in Scopus 在Scopus中查看纪录](#)

[Google Scholar 谷歌学术](#)

[Zaccara et al., 2019 Zaccara等人。, 2019年](#) S. Zaccara, R.J. Ries, S.R. Jaffrey

Reading, writing and erasing mRNA methylation

Nat. Rev. Mol. Cell Biol., 20 (2019), pp. 608-624

[CrossRef 十字架](#) [View Record in Scopus 在Scopus中查看纪录](#)

[Google Scholar 谷歌学术](#)

[Zhou et al., 2020 周等人。, 2020年](#) P. Zhou, X.-L. Yang, X.-G. Wang, B. Hu, L. Zhang, W. Zhang, H.-R. Si, Y. Zhu, B. Li, C.-L. Huang, *et al.*

A pneumonia outbreak associated with a new coronavirus of probable bat origin

Nature, 579 (2020), pp. 270-273

[CrossRef 十字架](#) [View Record in Scopus 在Scopus中查看纪录](#)

[Google Scholar 谷歌学术](#)

¹²

These authors contributed equally

这些作者同样贡献

¹³

Present address: Stem Cell Program, Boston Children's Hospital, Boston, MA, USA

目前地址：美国马士顿波士顿儿童医院干细胞计划

¹⁴

Department of Stem Cell and Regenerative Biology, Harvard University, Cambridge, MA, USA

哈佛大学干细胞和再生生物学系，剑桥，马，美国

¹⁵

Lead contact

铅接触

© 2021 The Author(s). Published by Elsevier Inc.
